NASA Contract Report 165792

Test Progress on the Electrostatic Membrane Reflector

D.J. Mihora
Technical Staff

General Research Corporation

CONTRACT NAS1-16133
June 29, 1981

National Aeronautics and
Space Administration

Langley Research Center
Hampton, Virginia 23665

The technical monitor for this program at NASA, Langley Research Center, is Mr. J. W. Goslee. Through his direction, the test program was initiated and undertaken.

CONTENTS

LIST OF TABLES

LIST OF FIGURES

LIST OF FIGURES (CONTINUED)

LIST OF FIGURES (CONTINUED)

1 INTRODUCTION

1.1 THE REFLECTOR CONCEPT

The electrostatic membrane reflector (EMR) is essentially an electrically charged capacitor with a very thin deformable surface as one of its electrodes. Figure 1.1 is a schematic view of a base-line test bed, built and tested at NASA Langley Research Center. When a voltage is applied between the flat circular membrane and the control electrode rings, the electrostatic attractive force (Coulomb's force) draws the membrane inward. High-voltage supplies are used to generate high field strength between the supported back electrodes and the deformable membrane electrode. A membrane, acted upon by such a pressure loading, forms a concave surface of the sort required for antenna reflectors. The fixed control-electrode surface is segmented into electrically isolated rings, each supplied with a different control voltage and thus exerting a different field strength and pressure on the membrane. Like pneumatic pressure applied to a deformed balloon, the electrostatic force is always normal to the (conducting) membrane; but unlike pneumatic pressure, the electrostatic loading can vary from point to point. The ability to change pressure at different points on the membrane allows the forming of different reflector geometries.

Achieving and controlling the membrane tension requires a spatially and temporally controllable pressure field on the membrane. Electrostatic pressures are very attractive because (1) they are readily controllable by voltage changes with negligible current flow, (2) they can be an integral part of a closed-loop control system that locks the membrane into the desired shape, (3) they can provide enough pressure to contour commercial polymer membranes thick enough to be reasonably manufactured and handled, and (4) they can be maintained with very little power consumption and thus allow the use of microweight solid-state power supplies.

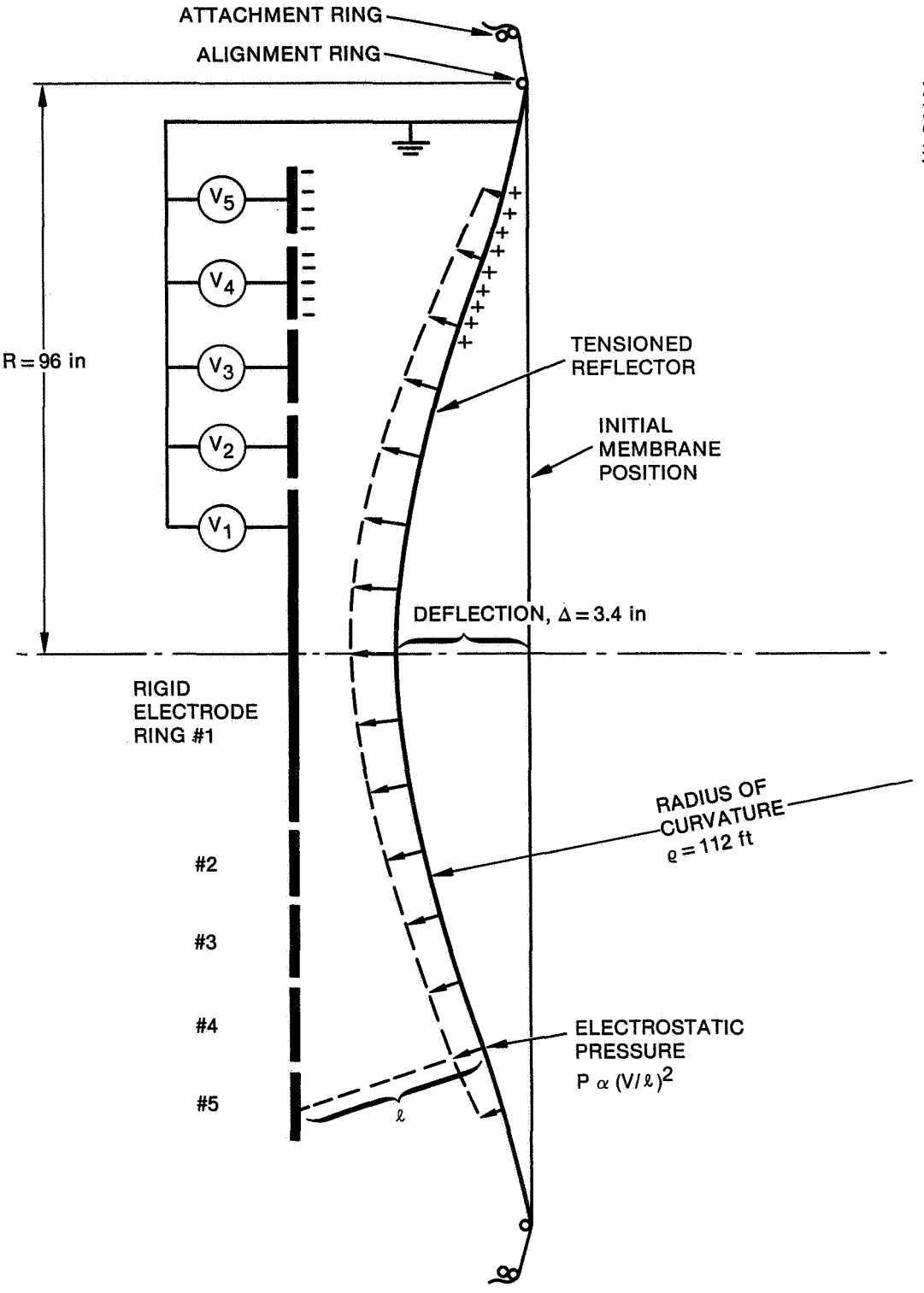

Figure 1.1. Electrostatic Membrane Reflector (EMR)

The design philosophy embodied in the EMR follows.

1. The membrane reflector can be an insulator such as a polymer, provided a conducting surface is bonded to it. The reflection of electromagnetic waves even at frequencies as low as 1 GHz requires an aluminum coating only 500 A thick to achieve greater than 99 percent reflectivity. The metal surfaces can be very light, but must be smooth to a fraction of the operating wavelength.

2. Bending stiffness is achieved by the tensioned thin membrane rather than a thick (heavy) supporting structure. The membrane has a high stiffness because of the extensional strain imposed by the electrostatic pressure. A very efficient, stiff structure is achieved without the mass penalty of conventional bending-stiffened structures.

3. To achieve and control the membrane tension requires a spatially and temporally controllable pressure field, which electrostatic force provides.

4. The reflector can be aligned with respect to a surface sensor that measures its contour and provides position error signals when the membrane reflector deviates from its desired shape. A controller then converts the error signals to voltage adjustments. The mechanical accuracy of the surface is governed by the accuracy of the surface sensor.

5. Accurate shape--high "figure quality"--is maintained by a closed-loop control circuit which readjusts the shape in the presence of on-board or external disturbances. The closed-loop circuit would provide surface stability for ground and Earth-orbiting antennas.

The electrostatic membrane reflector concept has the largest payoff for space applications where very large, low mass, precision reflectors are required. In Earth orbit, this concept appears to have considerable merit for antennas of 30-m to 150-m diameter, operating in the 1- to 10-GHz frequency regime, such as have been proposed for radiometer and radar missions. Even higher surface quality is possible for millimeter and sub-millimeter radiotelescopes operating as high as 600 to 1000 GHz.

Several electrostatic membrane reflector concepts that would be automatically deployable (jack-in-the-box) from the Space Shuttle bay are undergoing system and subsystem design integration studies by the Martin Marietta Corporation. The supporting structure that holds the control electrodes and the membrane reflector is also the deployment structure for unfurling the antenna. Three structures are being investigated: a radial-rib design, a continuous space truss (box or tetrahedron), and a 3- or 4-longeron compression rim. A 100-meter-diameter aperture deployed from the Space Shuttle represents a reasonable goal. Figure 1.2 illustrates the Martin Marietta concept of the 100 meter antenna, using the compression-rim structure.

The conceptual electrostatic membrane reflector shown in Fig. 1.3, also using the compression rim, is unique among reflector antennas in that it has no rigid support structure behind it. The support structure, hinges, and mechanisms used to deploy the antenna are part of the compression rim. Very few mechanical actuators are required to deploy the reflector. The concept incorporates a tension field structure (surfaces (2) and (3)) to fashion the control electrode surface, (2). The accuracy requirement on this "billowed" control surface is quite relaxed. The membrane reflector surface (1) can be designed to be 10^2 to 10^3 times more accurate than the control surface. This higher accuracy is achieved by adjusting the voltages on surface (2) and by the favorable smoothing that occurs when the reflector surface (1) is under stress. There is a minimal acceptable gap between (1) and (2) to achieve the improvement in surface quality.

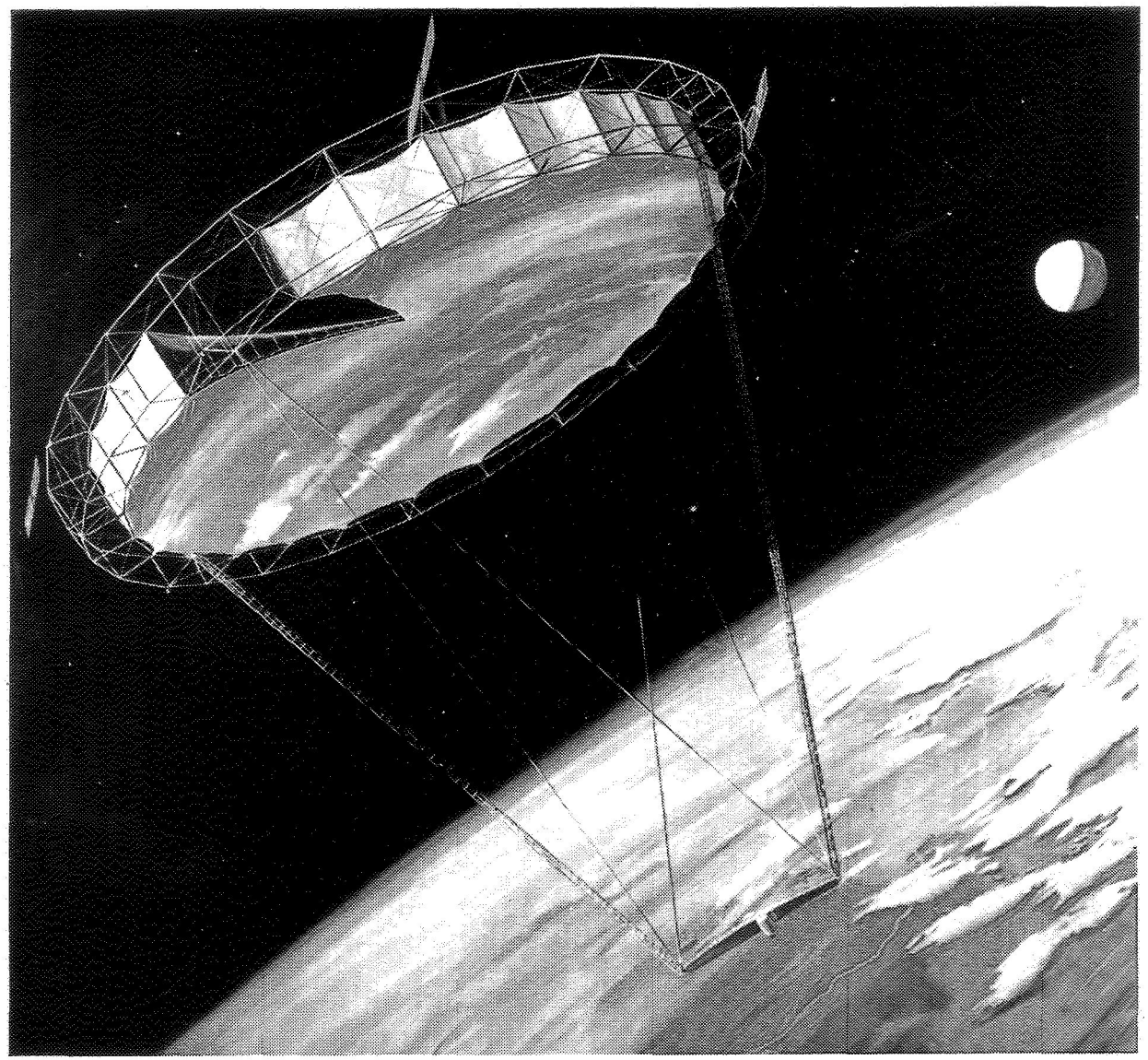

Figure 1.2. Martin Marietta Antenna Concept--100 Meter Diameter EMR

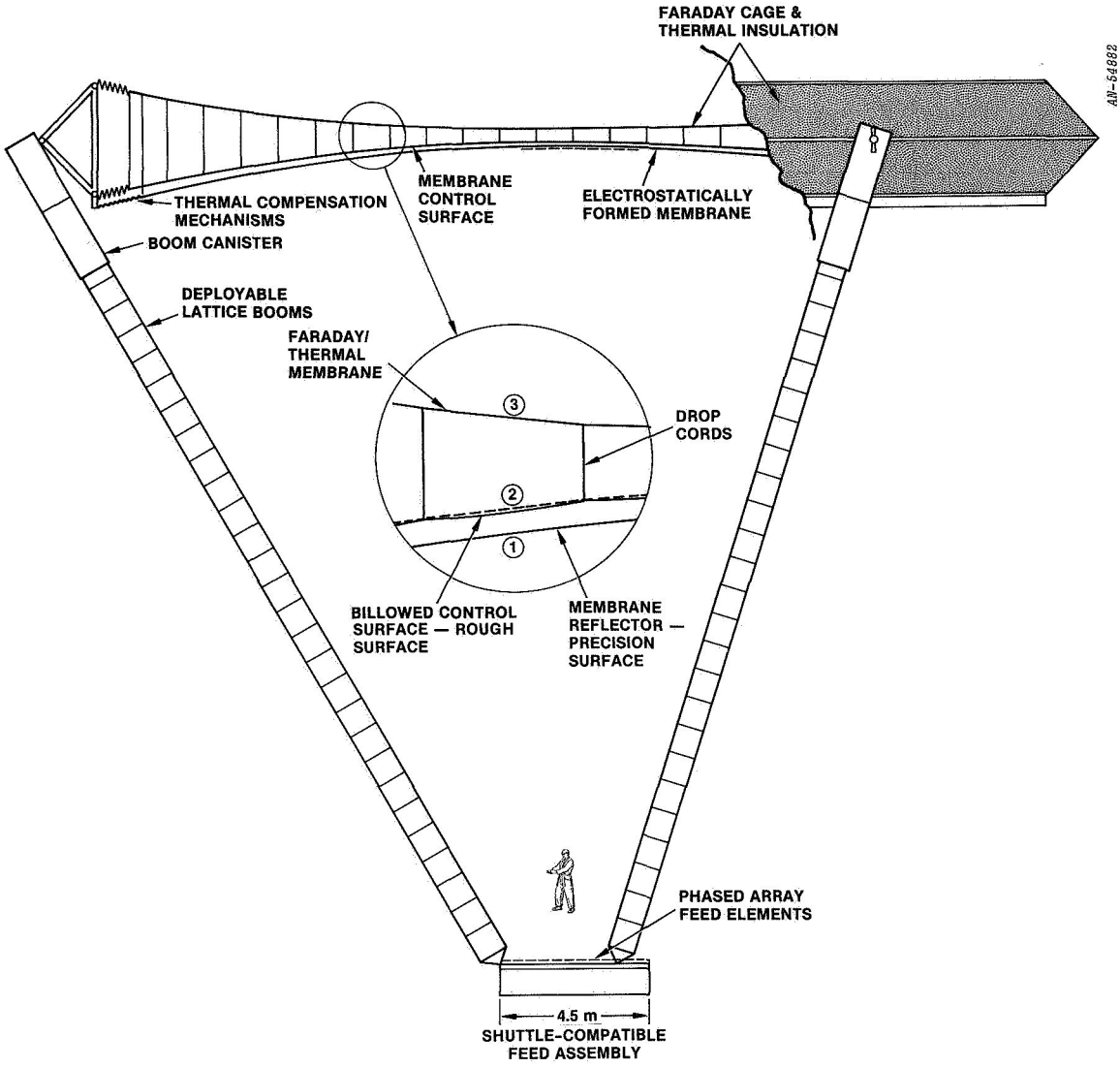

Figure 1.3. Conceptual Electrostatic Membrane Reflector Schematic Layout

1.2 SUBSCALE GROUND TEST ARTICLE

Preliminary test results from the electrostatic membrane subscale test fixture at NASA Langley Research Center are the subject of this report. The test fixture was designed and built in 1980 by NASA. The components, including the membrane reflector, are commercially available items. The 16-foot aperture diameter represented a size that was not too large to handle manually but not too small to obtain data over a reasonable area. It was decided that an axisymmetric surface had many advantages for a preliminary model. One such advantage was the simplicity of the control electrodes, which are concentric rings. Figure 1.4 is a photograph of the five control electrodes to which five separate power supplies are connected. The outer rim to which the membrane is attached is the ground reference for the five power supplies. The widths of the flat control electrodes were selected to provide the best shape control when deforming a flat (untensioned) membrane surface to a sphere (tensioned).

Figure 1.5 shows the 0.3 mil Kapton test membrane installed on the test fixture, with electrostatic force applied. Voltages up to 70 kV have been used in tests. Since the membrane reflector and rim are grounded (the exterior of a satellite could also be construed as the ground reference), one can safely touch the membrane reflector surface. Proper design of ground-based electrostatic membrane reflectors can eliminate corona and air discharge so that low-power, high-voltage supplies (e.g., CRT solid-state power supplies) can be used.

The membrane shown in Fig. 1.5 is aluminized Kapton with the aluminized side facing the control electrodes and the diffuse Kapton surface facing the camera. Four seams are evident. The seams provide a practical test of fabricating and manufacturing quality membrane-reflector surfaces. To achieve the model's designed radius of curvature of 34.14 m (112 ft), the membrane's center point moves about 87 mm (3.4 inches). This relatively small deflection induces a stress that is about 6 percent of yield stress or 626 psi in the membrane, which eliminates most visible

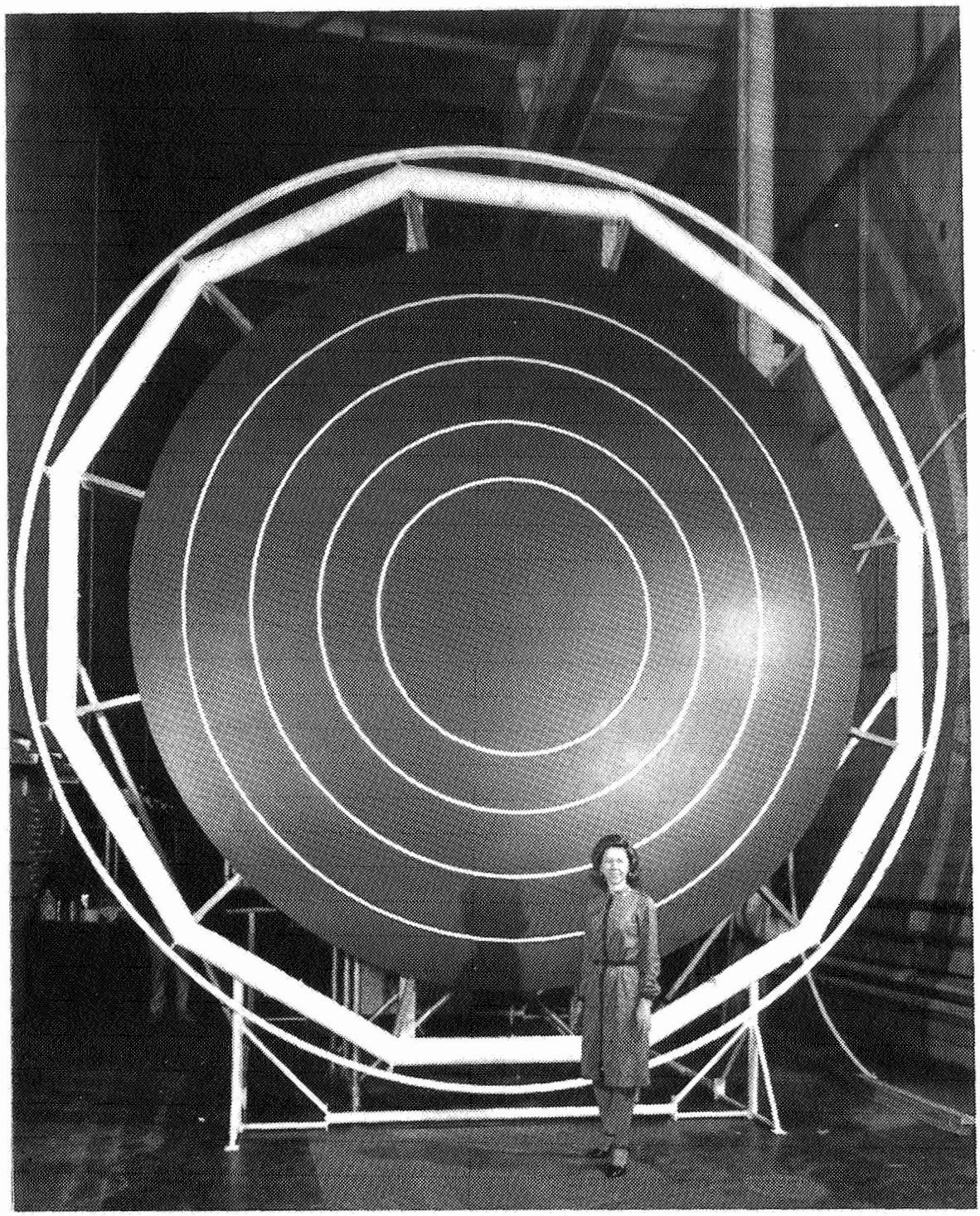

Figure 1.4. Support Ring for Membrane Reflector and Concentric Ring Electrodes

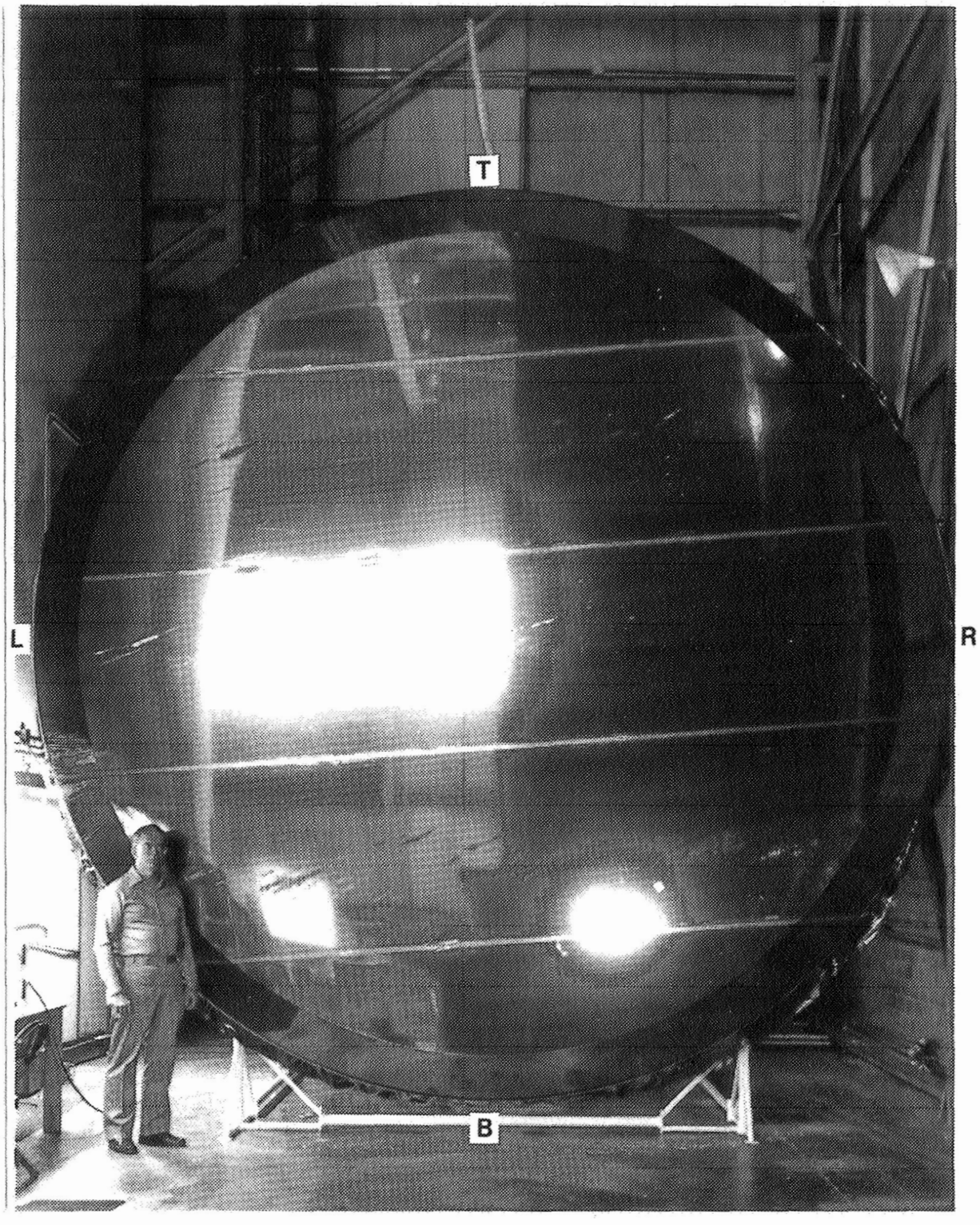

Figure 1.5. Electrostatic Membrane Reflector at NASA, Langley

wrinkles and imperfections in the membrane. The focal length-to-diameter ratio, $f_n = 3.5$, is larger than desirable for full-scale orbital reflectors, but provides a good initial test bed for experimentation.

Various factors are associated with the selection of the baseline, $f_n = 3.5$. Much smaller focal ratios would require the fabrication of a preformed-dished membrane, which was ruled out until more experience is gained in fabricating flat membrane panels.

1.3 INITIAL MEASUREMENTS

Model tests at NASA have been open-loop; i.e., the power supply voltages were set and the resulting shape was determined. Refinement of the shape by mechanical perimeter adjustments and vernier voltage adjustments will be performed in the latter part of 1981. The reflector's shape was measured by three types of figure sensors: a laser scan technique that measures surface slope, a pair of theodolites that triangulate for range, and photogrammetry that reconstructs position from three photographic plates.

The laser measuring system is a modified Foucault or knife-edge test (Fig. 1.6). The aperture of a 3-milliwatt HeNe laser is placed at the estimated center of curvature of the reflector with its beam directed toward the reflector. A projection screen attached to the laser and normal to the emerging laser beam shows the position of the reflected beam as the laser scans the surface of the reflector. If the concave surface is a true spherical surface, the reflected beam always returns to the laser aperture in the center of the screen. For a nonspherical surface, the reflected beam falls on the screen some distance from the laser aperture. From geometry, the reflector surface deviations from a true spherical surface are related to this distance. The reflector contour is calculated by summing the incremental deviations over the incremental span.

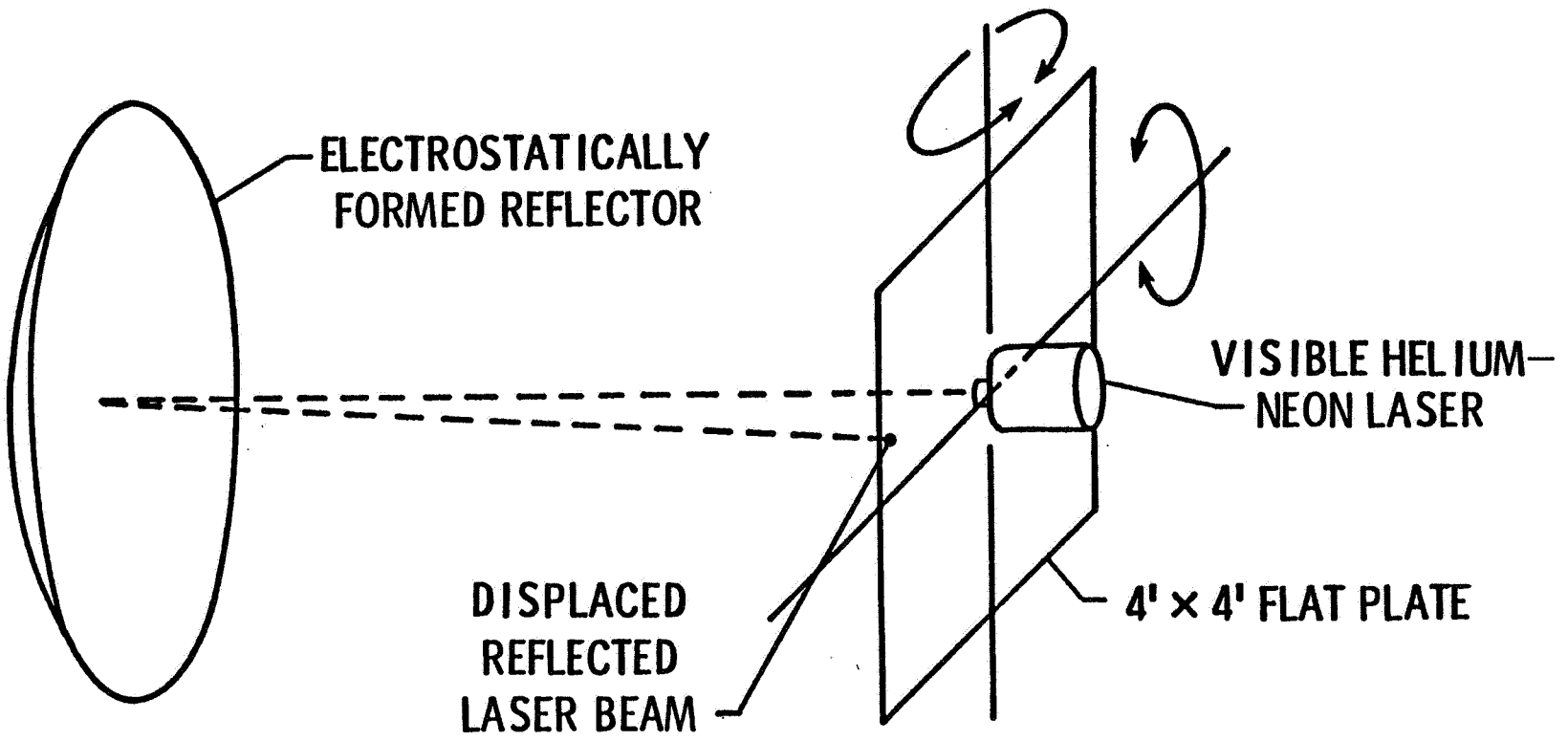

Figure 1.6. Laser Surface Measurement System

Another technique (Fig. 1.7) used two digital theodolites (K&E Vectrons) which were set up to input the horizontal and vertical angles of 61 points on the concave surface to a desktop computer (HP-85) which was programmed to produce the X, Y, Z coordinates of the points and their deviation from a spherical surface. The coordinates were related to the plane of the 16-foot diameter ring.

Still-camera photogrammetry (Fig. 1.8) was also used to develop the X, Y, Z coordinates of the 61 points on the surface as related to the plane of the 16-foot diameter ring. Three negatives were exposed at each test voltage condition and used as the basis for developing the coordinates and deviation from a spherical surface.

The three methods were tried in order to evaluate their relative merits. It became apparent that each technique had its advantages and disadvantages. For example: (a) The laser system could give a quick analysis of the surface characteristics along horizontal, vertical, and diagonal diameters as long as the selected point on the surface was smooth enough to return the beam. Wrinkles or large distortions would cause the return beam to disperse and distort the integration process, particularly toward the edges of the 16-foot ring. (b) The theodolite system could give accurate readings of the 61 points on the surface; however, even with the digital theodolites, the process was a time-consuming one. The hygroscopic characteristics of the Kapton film caused changes in the points being read over a 3- to 4-hour time period. This was particularly noticeable during a very humid period encountered during the testing. (c) The photogrammetry technique was good in that the data were taken at a specific point in time and preserved for future analysis; however, the data analysis was time-consuming and the coordinates of the points were not available until five to seven days after the photographs were taken.

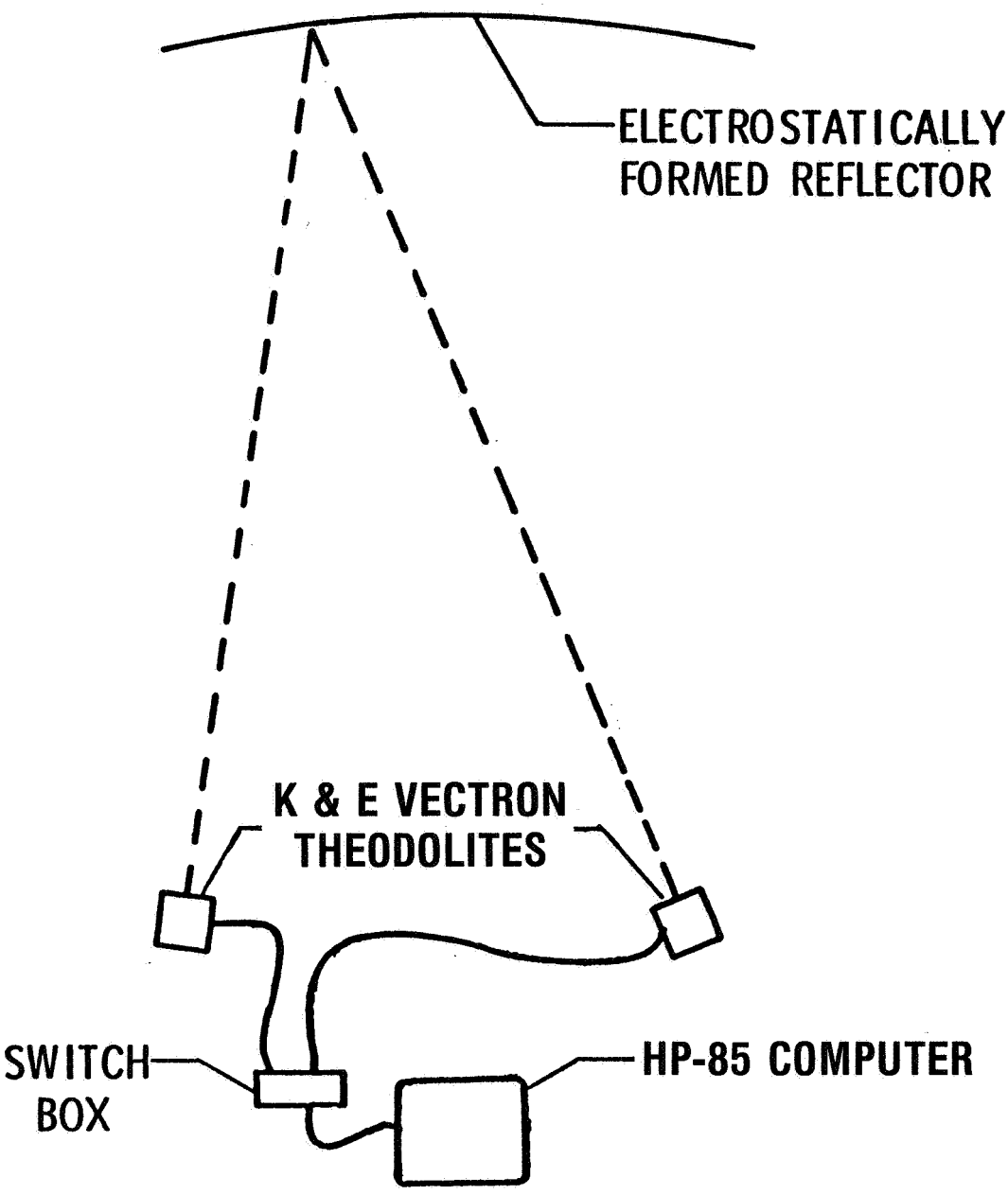

Figure 1.7. Digital Theodolite Surface Measurement System

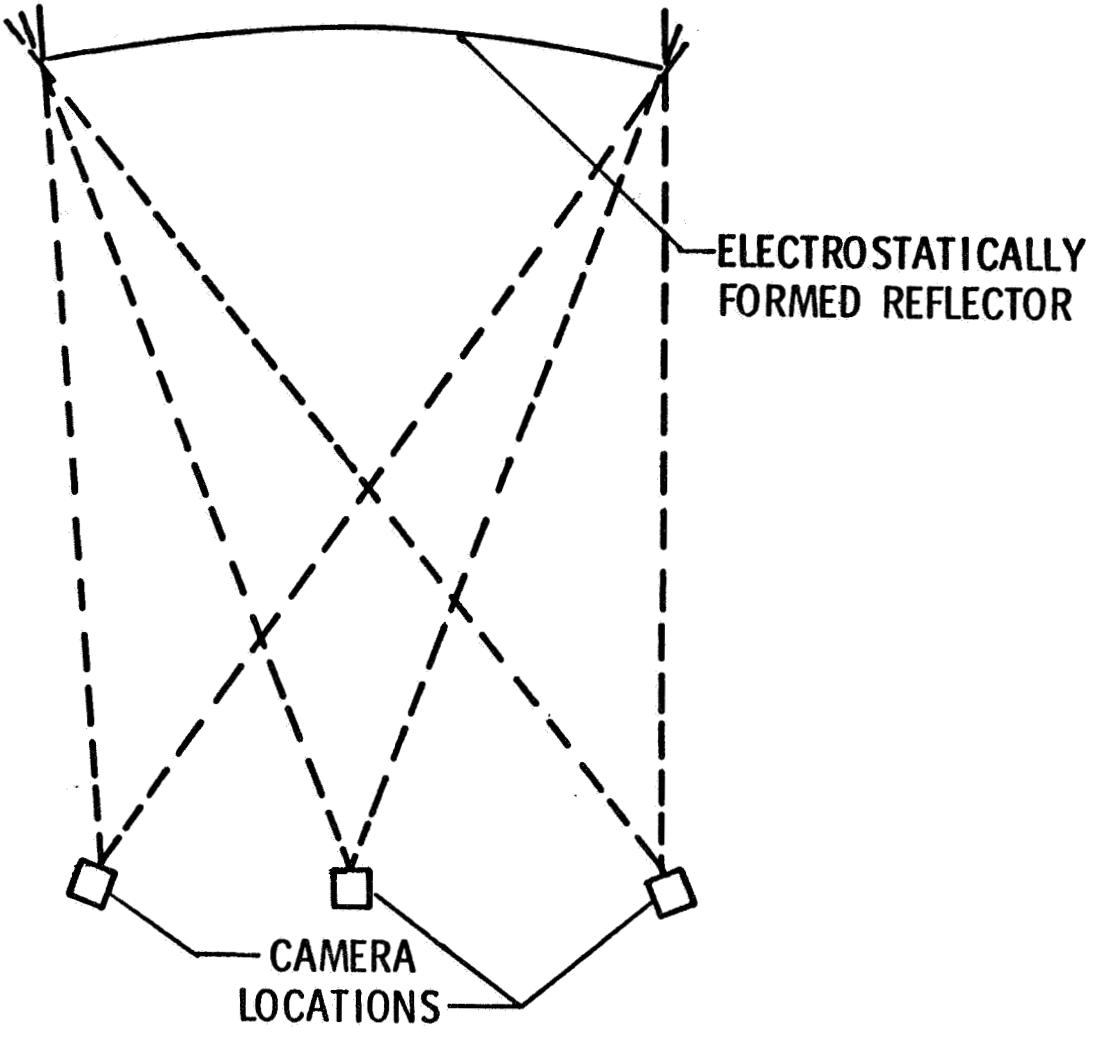

Figure 1.8. Photogrammetric Surface Measurement System

This report discusses the test results and insights learned on EMR operation. The data represents the initial analytic measurements of the 4.88 m aperture. In 1978 GRC prescribed the basic parameters of this antenna. Detailed design, fabrication, and check-out were carried out in 1979 by NASA Langley staff and their on-site subcontractors. Test results discussed in this report were obtained from June 1980 to July 1981. During this period the measurement techniques and the model components were being adjusted. Limitations in this period allowed for only simple tests and minor modifications of hardware. Six different planar membranes[1] were fabricated and tested. The latest membrane, together with adjustments of the support ring, provided the best results. Significant progress has been made in understanding the behavior of an EMR in a model of reasonably large size.

[1] Use of commercial products or names of manufacturers in this report does not constitute official endorsement of such products or manufacturers, either expressed or implied, by the National Aeronautics and Space Administration.

2 SUMMARY

The simple layout of the 4.88 m electrostatic membrane reflector provides a basic testbed for many experiments in membrane response and electrostatic shape control. Its simplicity makes it easy to mount and test different membranes. Both the electrode surface and the untensioned membrane are flat; proper choice of electrode voltages leads to a spherical tensioned surface, which is easy to measure. The flat membranes are made from sheet Kapton, which is commercially available in a maximum width of 1.3 m. Allowing material for seams and edge attachment, four seams across the membrane are necessary.

The simple layout does have disadvantages. It requires rather high voltages, particularly near the rim where the reflector-to-electrode gap is the largest. The geometry of the set-up and material properties limited the peak stress in the membrane to about 6 percent of yield. The associated strain eliminates most but not all of the wrinkles. The nominal membrane deflection of 87.3 mm is large in comparison to the membrane thickness of 7.6 μm but it is small compared to the diameter of 4.88 m.

All the tests were performed open-loop. Numerous voltages were tried on the five concentric control electrodes, but both the maximum voltage and the voltage difference between adjacent electrodes had to be limited because of electrical discharge, especially on humid days. On some days, the voltages could not be adjusted to form a better reflector surface but had to be adjusted simply to achieve the desired deflection at the center of the membrane. This limitation will be corrected on the next model. Achieving the 87.3 mm deflection with Kapton was hampered by the stiffness (Young's modulus) of the material, which was higher than anticipated. Also, Kapton is hygroscopic, and the membrane tightened whenever the humidity went down.

The instrumentation used to measure the membrane surface is accurate to a fraction of a millimeter. However, the time to survey the entire surface and then compare it to the ideal surface is long. Near-real-time adjustment of the voltages to converge on a better shape was not designed into these tests.

The early test results dictated modifications that produced a factor of 10 improvement in membrane reflector surface quality. The tests proceeded to yield satisfactory answers in many areas.

Improvements in surface quality during this test program were associated with the removal of residual errors. The improvement in surface quality is evident on comparing an early test (4-1) with the most recent test (5-1). Figure 2.1 shows the errors or residuals of the reflector shape, defined as the measured shape minus the ideal (spherical) shape. The vertical direction is proportional to the deflection errors. The upper frame defines the plane of zero errors. The measurements using the photogrammetry technique were used to reconstruct these surface error distributions. In the early tests (e.g., 4-1), the error distribution had the following distinct traits: (1) The perimeter of the membrane is distorted. The membrane is pulled against an alignment rim and transmits the surface quality of this rim. Near the center of the membrane, the perimeter errors are somewhat averaged. In test 4-1, the surface reflector quality is better than the quality of the rim. (2) A low-amplitude undulation over the surface matches the direction of the seams and the five horizontally aligned panels used to form this surface. This error source is a combination of fabrication deficiencies, material anisotropy, and double-thickness seams. Note that in test 5-1 the seam errors are virtually non-existent. (3) Just inside the perimeter attachment, the membrane displays a slight annular bulge. The electrostatic pressure near the rim is lower than it should be because the outermost electrode does not extend to the rim.

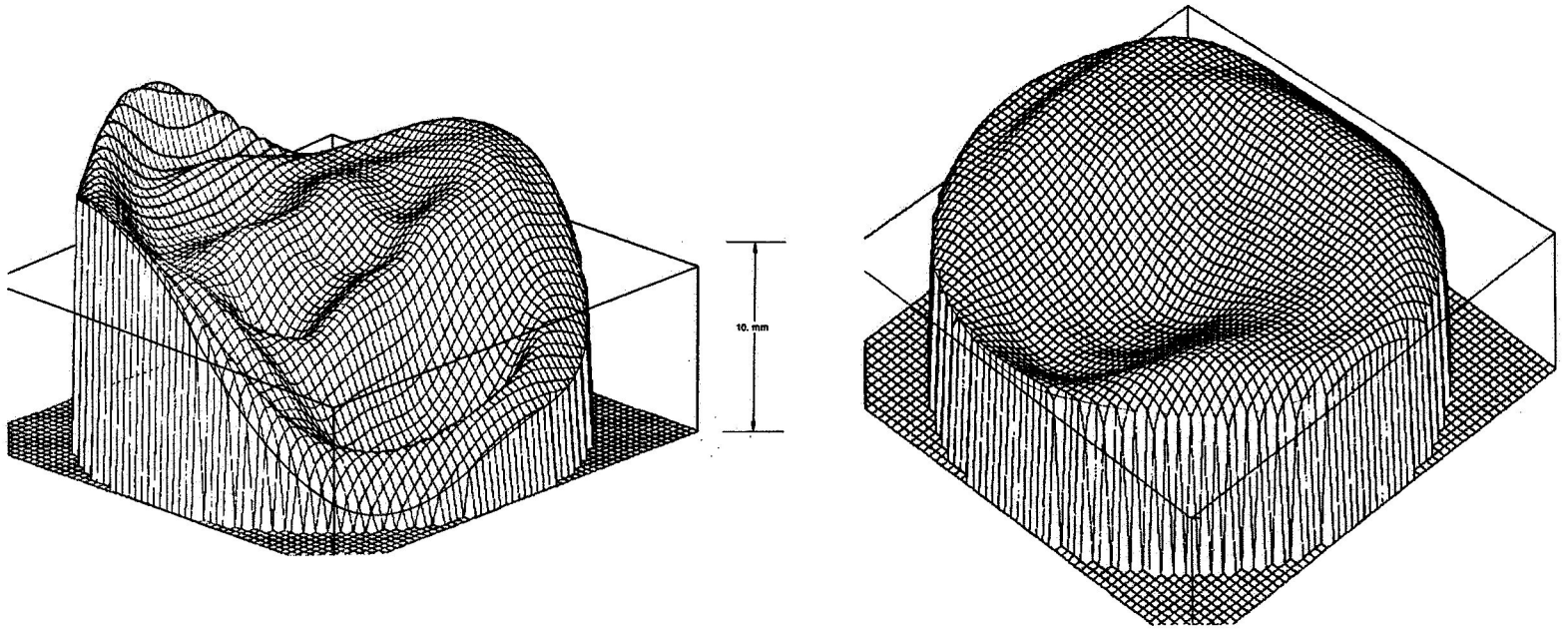

Figure 2.1. Improvements Made in EMR

Surface quality was much improved in test 5-1. The rim flatness was improved to about $\pm$ 1.0 mm. The membrane quality--particularly the flatness of the procured raw material--increased substantially. Wrinkles were reduced with an improved seam joining technique. The planar electrode surface was aligned more accurately parallel to the plane of the rim to remove a tilt error that had propagated into the membrane reflector. The principal remaining error is the annular bulge along the perimeter. An increase in pressure near the rim is still required to eliminate the bulge.

The extent of each single electrode's influence on the membrane was determined from experiment and compared to theory. Each electrode influences the reflector shape well beyond the edge of the electrode. The control effectiveness of each electrode was determined. Linear static control over a wide range was shown to be feasible. Small shape adjustments are linearly related to voltage. Several control matrices were constructed which specify the voltage adjustments on m control electrodes to eliminate m deflections on the reflector surface. The groundwork is set for the development of an automated closed-loop system which automatically minimizes surface errors.

There are several directions for improving the simple model. The proposed design changes presented here are a consequence of this test program. The aluminized Kapton membranes are substantially stiffer than indicated by data sheets. Lower-stiffness membranes such as polyethylene would allow operation at lower voltages. A lower voltage can also be used by pre-forming the membrane and electrode surfaces instead of having them both flat. The gap between electrodes and membrane could then be made much smaller than the present values (6.5 cm at the center and 15.2 cm near the rim). The electrode surface should also be extended closer to the rim.

The original goal of a focal length-to-diameter ratio $f_n = 3.5$ was barely achievable in air using the flat Kapton membrane. A lower focal length can be achieved by pre-forming the membrane. A lower focal length using a flat membrane would require operating in a vacuum chamber where higher electric field strengths are achievable.

The Kapton membranes exhibit a rather large hygroscopic expansion coefficient. As the humidity increases, water absorption expands the membrane. In space, humidity would not be a problem but thermal changes would affect the membrane in the same way. The thermal expansion coefficient for Kapton is $\alpha_T = 2.0 \times 10^{-5}$ m/m/°K while the hygroscopic expansion coefficient is $\alpha_H = 1.7 \times 10^{-5}$ m/m/% . Large strains or deflections are generated by moderate humidity or temperature changes. The current test fixture often requires adjustment to correct for excessive perimeter tension or slack. Improved perimeter compensation techniques should be developed on subsequent models to minimize the environmental effects. With perimeter compensation, a much smaller level of electrostatic shape maintenance will be required. A future expectation is to incorporate perimeter compensation utilizing catenary cords and discrete attachment points rather than a continuous hoop attachment. At each apex point of the catenary rim would be a passive spring system, rather like a circular trampoline. Like prior models, the system can be built to operate in an open-loop stable manner.

The next step in electrode design is control of both the radial and the azimuthal shape. The implications of size and geometry of single electrodes are now well understood and specific layouts can be prescribed for a particular goal.

The major advantage of the EMR is its tolerance for a high level of random or periodic roughness of the electrode surface. The electrode surface is allowed to be two to three orders of magnitude less accurate than the membrane. Without this trait, the value of the EMR would be

severely diminished. The improvement in quality from electrode to membrane is not achieved automatically. It depends principally upon the membrane stress and the gap between the membrane and the electrodes.

The EMR can be scaled to much larger sizes while maintaining the same stresses and surface quality as the 4.88 m model. A 100 m aperture[1] was designed using the same approximate stresses and voltages as the 4.88 m layout. The electrode size is associated with control requirements to achieve a particular surface quality. On the 100 m configuration, approximately 40 electrodes are required for a 1 cm (RMS) surface quality and 220 electrodes for a 1 mm (RMS) surface quality.

By limiting the membrane stress on future models to the level of the current baseline, almost all testing can continue to be performed on the ground without a vacuum chamber. Higher membrane stress would require the use of a vacuum chamber which allows higher field strengths and voltages without breakdown.

---

[1] D.J. Mihora, R.R. Chase, and M. Mortz, The Electrostatic Membrane Reflector - Conceptual Designs, General Research Corporation CR-1-1035, May 1981.

3 DISCUSSION

The design parameters of the 4.88 m EMR were calculated several years ago.[1] Experimental values for most of them have now been measured or derived from the tests made between June 1980 and July 1981. Table 3.1 summarizes the important parameters and gives the calculated values.

Figures 3.1 and 3.2 summarize the calculated state of the baseline spherical reflector surface. To form this surface from a flat membrane, an electrostatic pressure equal to 1.9 N/m^2 at the center is required. The required pressure distribution is shown in Fig. 3.1. The pressure at the rim is about half the center value. The electric field strength varies as the square root of pressure, and thus decreases at the rim to about 0.7 of the centerline value.

The voltage distribution on the control electrodes can increase or decrease with distance from the center, depending on the gap between the membrane and the electrodes. For design simplicity, a flat electrode surface was prescribed. Near the rim the gap is 15.3 cm, which is 2.33 times larger than the central value of 6.5 cm. Equal voltages on each of the electrodes would thus produce a factor of 5.3 reduction in electrostatic pressure from center to rim. One would then expect an excessive curvature near the center (too small radius of curvature) and too shallow a curve (too large radius of curvature) near the rim. This has been observed in tests. To achieve the factor of two pressure reduction from the center to the rim, the voltage must be increased outward to compensate for the gap which increases by a factor of 1.6. The original design specified a voltage of 43 kV at the center and 68 kV at the rim electrode. Substantially lower voltages could be used if the electrode surface were curved and positioned closer to the membrane.

---

[1] D.J. Mihora, P.J. Redmond, et al., Electrostatically Formed Antennas (Test Concept), General Research Corporation NASA CR-159068, April 1979.

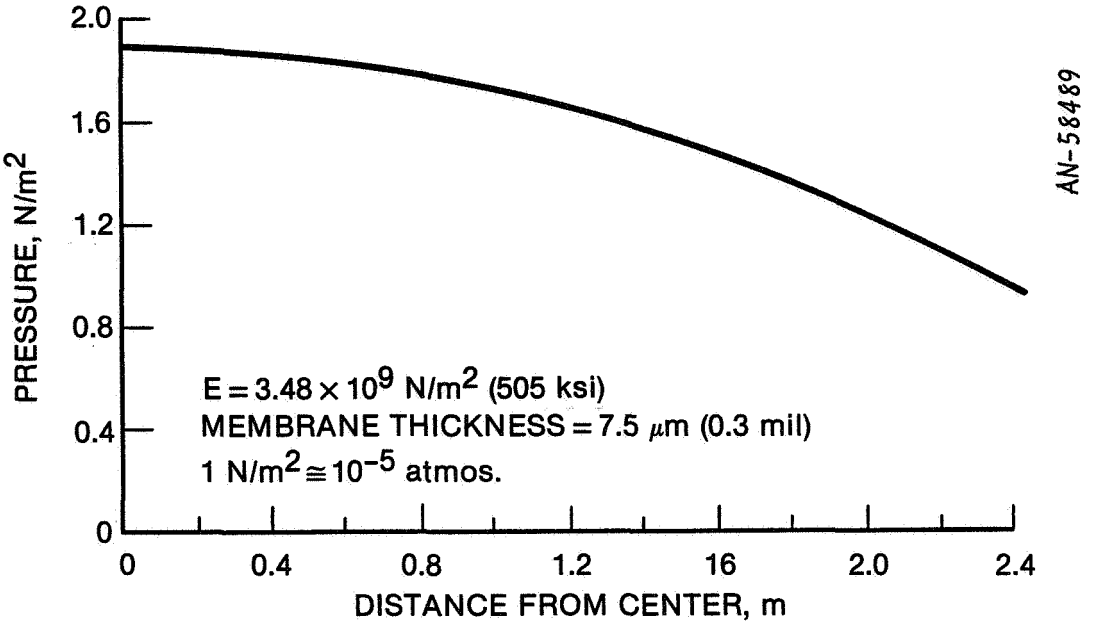

Figure 3.1. Calculated Pressure Distribution to Form Sphere of Focal Ratio 3.5 from Flat Membrane

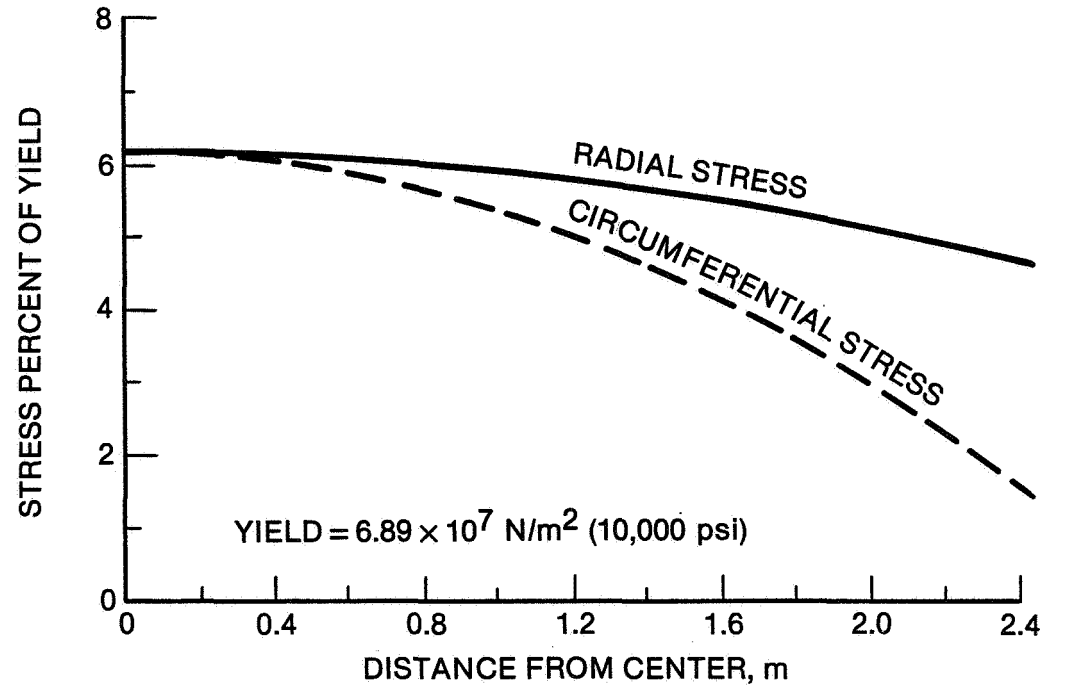

Figure 3.2. Calculated Stress Distribution in Baseline f_N = 3.5 Reflector

Associated with the pressure loading (Fig. 3.1) is a reacted stress in the tensioned membrane. Figure 3.2 shows the radial and circumferential stresses. The peak stress is at the center. Like the pressure distribution, the stresses decrease radially outward. At the rim the ratio of radial to circumferential stress is Poisson's ratio for the membrane.

The maximum stress in the membrane is about 6 percent of yield stress (yield = 6.89×10^7 N/m^2 [10,000 psi]) . The electric field required to produce this is near the onset of corona discharge in one-atmosphere air. In the vacuum of space, the electrostatic pressure and membrane stress could conceivably be an order of magnitude larger. For ground testing, however, operation in air is much preferred because of accessibility. Important parameters of the ground test model are summarized in Table 3.1. The originally calculated values of some of these parameters have changed over the last year. The subsequent sections will discuss several variables such as humidity, pre-tension, and materials properties that have altered the baseline characteristics listed in Table 3.1.

TABLE 3.1

DESIGN PARAMETERS OF THE 4.88 m
DIAMETER ELECTROSTATIC MEMBRANE REFLECTOR

$f_N = 3.5$	This focal-length-to-diameter ratio is for a spherical reflector with a radius of curvature $\rho = 34.16$ m (112 ft) and depth of 87.3 mm (3.44 in).
$\Delta Z = 87.3$ mm	The membrane's central deflection is very large when compared to the membrane thickness, i.e., $\Delta Z/h = 11{,}480$. Large geometric rotations are present but small (linear) strain of the membrane occurs.
gap = $0.75\Delta Z = 65.3$ mm	The closest spacing between the control electrode and the membrane reflector is three-fourths of the membrane deflection.
$E = 3.48 \quad 10^9$ N/m^2 (505 KSI)	Modulus of elasticity of (0.3 mil) Mylar coated with 500 A of aluminun.
$h = 7.6$ μm	Membrane thickness. Resistivity should be less than 1 Ω/square. The conductive aluminum coating should be at least 500 A thick when used as a 10-GHz reflector. The membrane should be very flat over correlation lengths in the centimeter-to-meter region. Narrow creases or folds are acceptable.
$P(0) = 1.9$ N/m^2	The maximum electrostatic pressure (at center of reflector) is large by one comparison (200,000 times solar pressure) but small by another (1/50,000 atmosphere). The electric field strength necessary to generate this pressure is $E = 6.6 \times 10^5$ V/m (16,500 V/inch). This level is below a corona condition in dry air and well below air breakdown and discharge. Required pressure for given displacement is proportional to the thickness-modulus product, Eh.

TABLE 3.1 (Continued)

δ_G = 34 mm (1.34 in)	Gravity sag of membrane with rim horizontal and no tension other than that due to gravity. Gravity sag is proportional to $E^{-1/3}$.
V(0) = 43 kV V(R) = 68 kV	Voltages to form the sphere. Notice that voltage increases from center [V(0)] to perimeter [V(R)].
$\sigma(0) = 4.3 \times 10^6$ N/m^2 (626 psi)	Membrane stress at the center is approximately 6 percent of yield stress, $\sigma_y = 6.895 \times 10^7$ N/m^2 (10 KSI).
$\sigma_r(R) = 0.74\sigma(0)$	The radial stress at the perimeter is nearly as large as at the center.
$\sigma_\theta(R) = 0.22\sigma(0)$	The circumferential stress near the perimeter is much less than at the center. The rim attachment must be carefully managed to prevent radial wrinkles.
$C = 1.4 \times 10^{-9}$ farads	Capacitance, $C = \varepsilon_v \varepsilon_r A/Z$ where $\varepsilon_v = 8.84 \times 10^{-12}$ farad/meter ε_r = dielectric constant A = flat plate area Z = average electrode separation The capacitance is very small because the dielectric constant for air is minimum ($\varepsilon_r = 1$) and the electrode separation is large.
W = 2.52 J	W = 1/2 CV^2. The energy storage is small since the capacitance is small. By comparison, a typical automotive battery stores over a million joules of energy.

3.1 PERIMETER BOUNDARY CONDITIONS

As a mechanism, the membrane reflector has a large "leverage". A small strain of the membrane will result in a large (normal) deflection. The membrane reflector achieves a central deflection, $\Delta Z = 87.3$ mm (3.44 inches) with a strain at the center of only $\varepsilon_r = 0.00086$. This strain is analogous to a radial expansion

$$\Delta\bar{r} = r\varepsilon = 2.44\ (0.00086) = .0021\ \text{m} = 2.1\ \text{mm}$$

The "leverage" of the tensioned membrane is $\frac{\Delta Z}{\Delta r} = 41.6$. Thus, small radial strain equates to a substantial shape change. Conversely, large pressure changes are required to compensate for small changes in the perimeter boundary conditions.

Figure 3.3 indicates the electrostatic pressure required to form the $f_n = 3.5$ surface for different degrees of pre-tension in the membrane. The curve for zero perimeter pre-tension (baseline) is the same as Fig. 3.3 and is denoted as $\Delta r = 0$. With pre-tension corresponding to a 2 mm strain ($\Delta r = 0.002$ m), the pressure requirement doubles and the maximum stress (strain) is twice the baseline value. The pressure distribution is altered, too, so that the loading at the rim is a larger fraction of that at the center. The opposite is true for a perimeter condition with Δr negative--i.e., a slack membrane.

These important results emphasize an important design consideration--radial pre-tension can dramatically alter overall results. Additional insight on the significance of the perimeter condition is shown in Fig. 3.4. It shows the relation between a radial expansion, Δr, and the central deflection, ΔZ, that would produce the same stress in the membrane. From Fig. 3.4, a 0.014 inch radial pre-tension, Δr, produces the same stress as a $\Delta Z = 1.4$ inch central deflection. This latter value is the amount of sag due to gravity when the perimeter ring is horizontal. It was recommended that the membrane reflector be

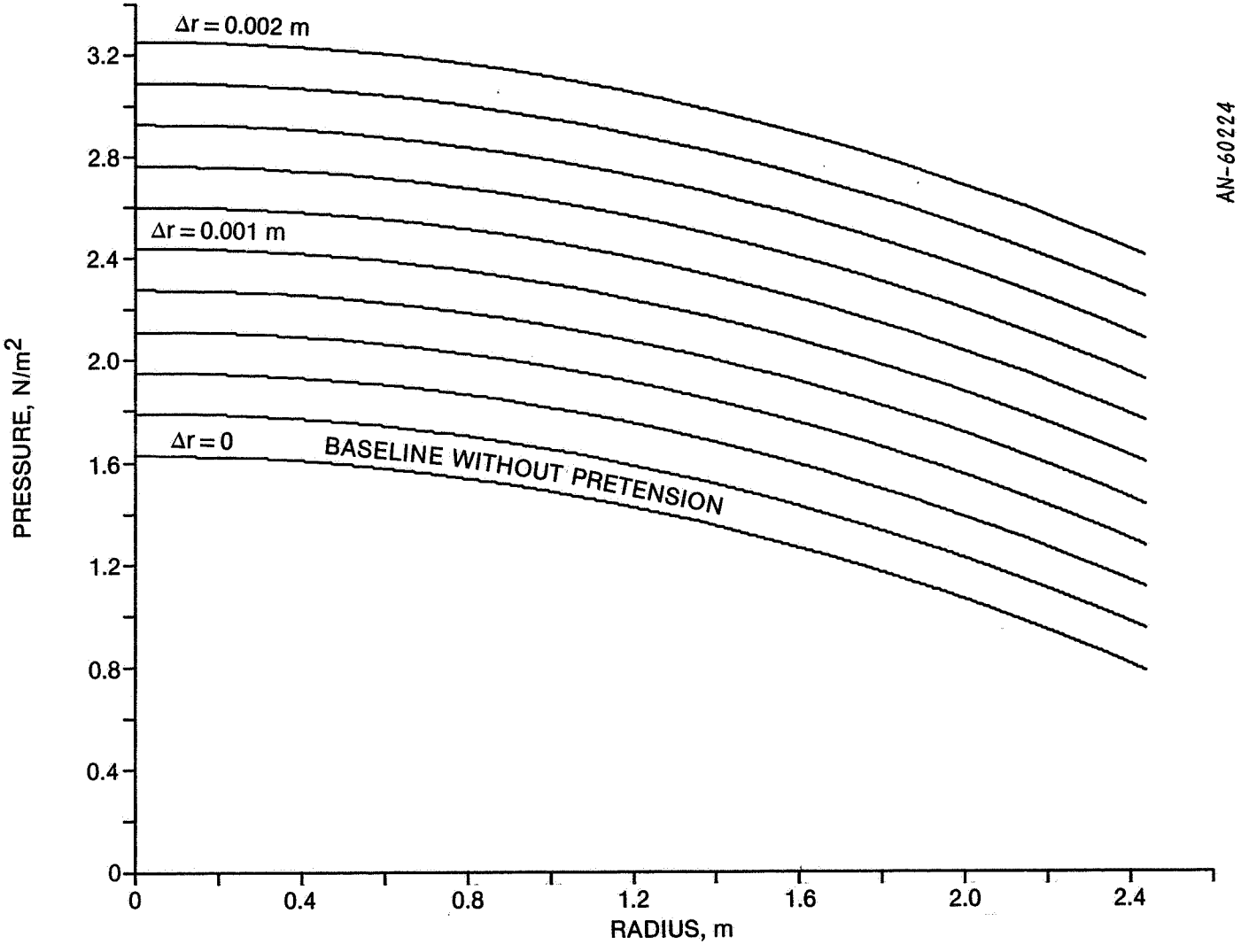

Figure 3.3. NASA 1980 Membrane with Pre-Tension

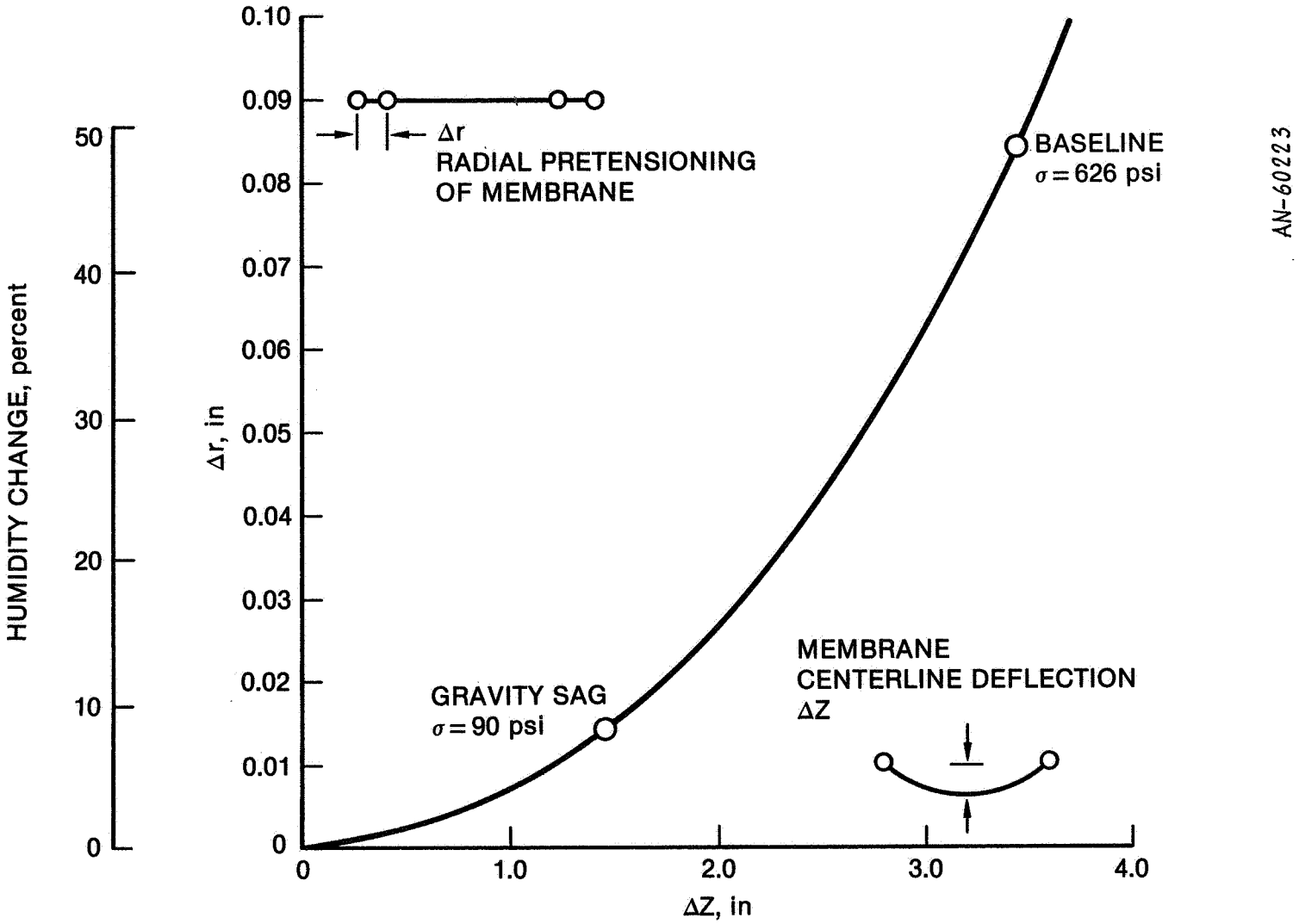

Figure 3.4. Conditions Producing the Same Stress

adjusted to this amount of gravity sag as an indication of zero average pre-tension. This adjustment is somewhat difficult, considering it is equivalent to a 0.35 mm (0.014 inch) adjustment in radial position.

Assuming a clamped horizontal membrane perimeter without pre-stress and a uniform pressure loading due to gravity, the central deflection is

$$\delta = 0.6535 \left(\frac{R^4 P}{Eh} \right)^{1/3}$$

where the gravitational pressure, $P = \rho g h$.
Substituting

$R = 2.44$ m ; radius
$\rho = 1400$ kg/m^3; density
$g = 9.8$ m/s^2; gravity

one obtains

$$\delta = 51.4\ E^{-1/3}$$

which is plotted in Fig. 3.5 over a range of stiffness, E.

This method of adjusting tension by sag measurement obviously leaves much to be desired, because the sag could be correct with unequal tensions around the rim.

Once the pre-tension adjustment is made, its accuracy can unfortunately be lost with a change in the humidity of the air. In the next section, which discusses material properties, data will be presented on the hygroscopic linear expansion coefficient of Kapton. This polymer swells as it absorbs water vapor. The expansion coefficient is quite large. For example, a 50% humidity change imparts a change in stress equal to that needed to form the $f_N = 3.5$ spherical surface from a flat membrane.

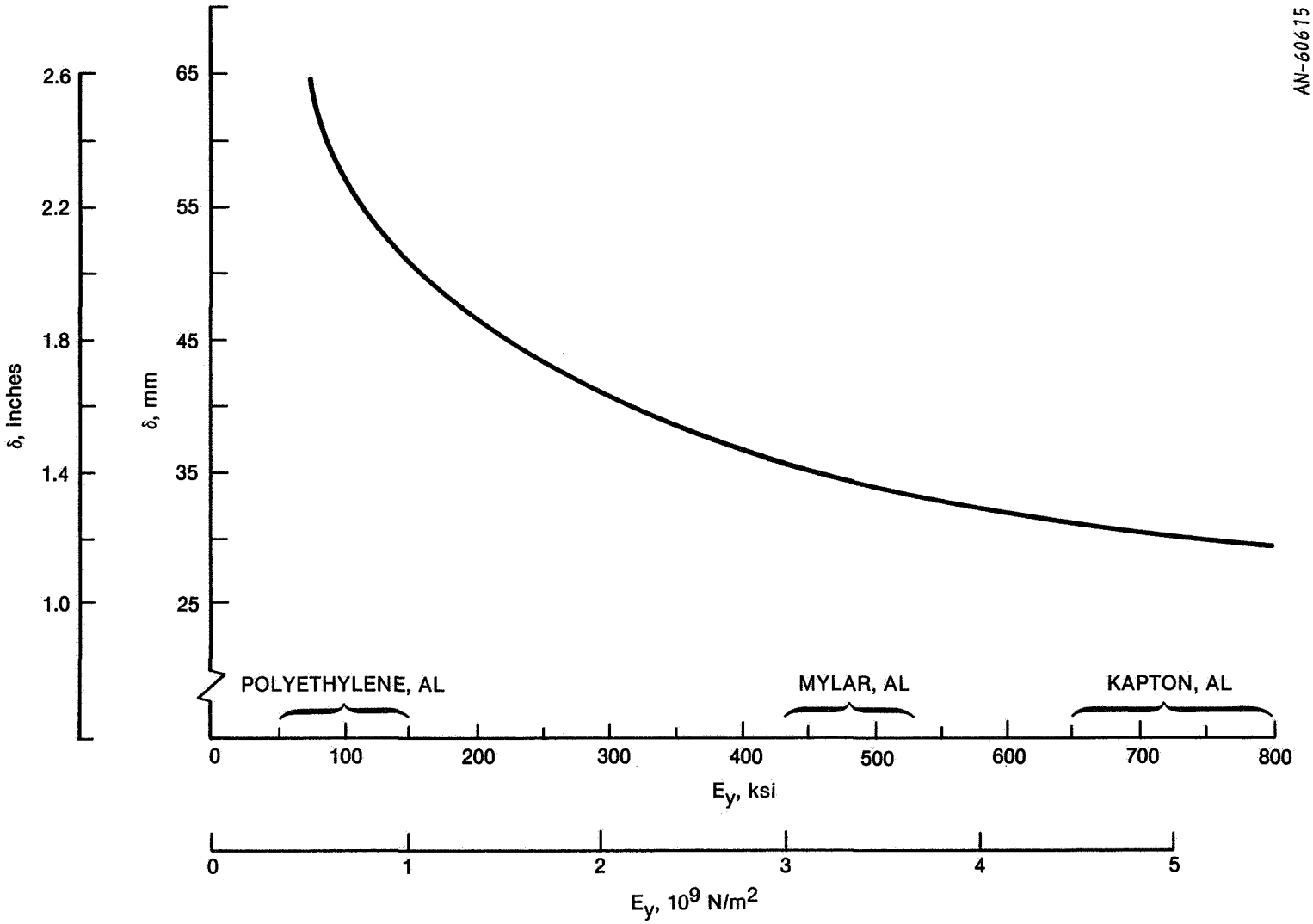

Figure 3.5. Zero Pre-Tension State Based upon a Prescribed Gravity Sag

It is quite clear that some form of perimeter adjustment would be highly advantageous. Perimeter control can be used to compensate for geometric errors of the rim (flatness and radius), eliminate radial pre-tension, and compensate for thermal and hygroscopic expansion. It appears that a catenary perimeter and a linear spring mechanism may satisfy the kinematic requirements. The catenary also provides techniques for measuring radial stresses. Large non-symmetric perimeter anomalies could be measured and eliminated with the catenaries. Electrostatic forces could also be used to bias out these errors, but without perimeter compensation, the voltages and stresses might be very large.

3.2 MATERIAL PROPERTIES

Prediction of membrane performance with the 4.88 m model requires knowledge of material properties. Information from biaxial stress-strain tests would be preferred but such data is virtually non-existent. Several uniaxial tests were performed on aluminized Kapton in 1980-81 at NASA and the results are noteworthy. The stiffness for the 7.6 μm (0.3 mil) membrane was significantly higher than reported in the literature. In the original design layout of the EMR baseline, the value of Young's modulus assumed was the manufacturer's quoted value (with a factor for aluminization). These values now appear to be in error, and a new set of baseline parameters have been developed.

The average modulus of elasticity for the aluminized membrane is

$$\bar{E} = E_1 h_1/\bar{h} + E_2 h_2/\bar{h}$$

where $\bar{h} = h_1 + h_2$ and h_1, h_2 are the thicknesses of the polymer and the aluminum. Assuming room-temperature properties, the (brochure) modulus of Kapton is

$$E_1 = 2.96 \times 10^9 \text{ N/m}^2 \text{ (430 KSI)}$$

and that of aluminum is

$$E_2 = 6.89 \times 10^{10} \text{ N/m}^2 \text{ (10,000 KSI)}$$

To provide adequate conductivity, the aluminum needs to be at least 500 Å thick. The latest membranes have had both sides vacuum-deposited with aluminum as would be required on real space configurations. The expected membrane stiffness is as follows:

Aluminum Thickness, (h_2), Å	Composite Stiffness ($\overline{E}$), N/m^2 (KSI)
0	2.96×10^9 (430)
500	3.42×10^9 (496)
1000	3.87×10^9 (562)
1500	4.32×10^9 (627)

Figure 3.6 indicates the NASA Instron measurements on December 28, 1980, of 0.3 mil Kapton with 1000 Å aluminum. Results are shown to ultimate with substantial stress and elogation. For the 4.88 m model, the maximum operating stress of 4.3×10^6 N/m^2 (626 psi) is far down on the curves. The modulus is shown for two measurement directions--along and across the strip. Dupont has indicated that Kapton is generally more uniform in stiffness than Mylar because of its manufacturing process. Additional Instron tests on February 3, 1981, were made to verify earlier results. Five sets of data were averaged to yield the following results:

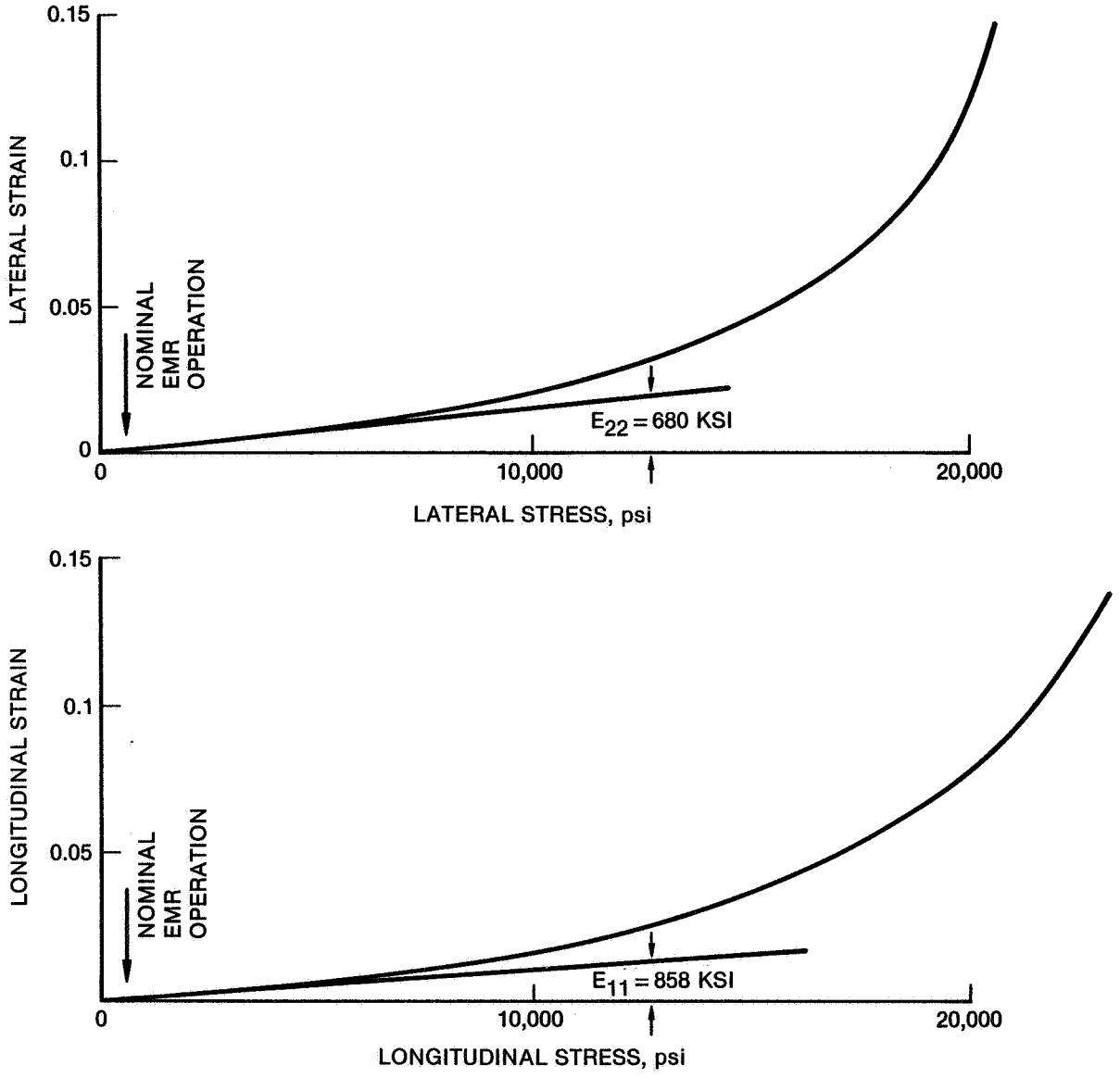

Figure 3.6. Uniaxial Kapton Stress-Strain Tests (12/28/80)

Aluminum Thickness, Å	Stiffness, N/m^2 (KSI)	
1000	$E_{11} = 5.74 \times 10^9$	(833)
	$E_{22} = 5.31 \times 10^9$	(770)
	$\bar{E} = 5.52 \times 10^9$	(801)
430	$E_{11} = 5 \times 10^9$	(725)
	$E_{22} = 4.6 \times 10^9$	(667)
	$\bar{E} = 4.8 \times 10^9$	(696)

Assuming the aluminum stiffness of 6.89×10^{10} N/m^2, the stiffness of the uncoated Kapton from the above tests is determined to be 4.5×10^9 N/m^2 (655 KSI). This value is 52 percent larger than the quoted value from the manufacturer. The higher stiffness is not advantageous. It necessitates a higher voltage (and field strength) to achieve the $f_n = 3.5$ aperture.

The electrode voltages are related to the membrane thickness-modulus product, Eh (i.e., the membrane stiffness). A stiffer membrane requires higher pressures and voltages to generate the desired shape. The substantial difference in measured properties of tested membranes has altered the voltage requirements. Table 3.2 compares several EMR characteristics using different membranes. The original baseline assumed a Mylar/aluminum membrane with a modulus of elasticity of 3.45×10^9 N/m^2 (500 KSI). With the latest measurements, an average modulus of 5.52×10^9 (800 KSI) would require an increased electrostatic pressure from 1.9 to 3 N/m^2. Test data from test 5-1 shown in column 3 indicate substantial agreement in terms of the central pressure. Of course, the level of pre-tension as measured by the gravity sag can by itself significantly influence the voltage requirements.

TABLE 3.2

VOLTAGE CONTROL RELATED TO MEMBRANE STIFFNESS

	ORIGINAL LAYOUT CR-159068	CORRECTED MATERIALS PARAMETERS	TEST 5-1	POLYETHYLENE MEMBRANE
MODULUS, (E), KSI	500	800	--	75
POISSON'S RATIO (ν)	0.3	0.3	--	--
THICKNESS, (h), mils	0.3	0.3	0.3	0.5
ALUMINUM THICKNESS, Å	500	1000	1000	500
P_o, N/m^2	1.9	3.0	3.2	.475
E_o, kV/cm (kV/in)	6.6 (16.7)	8.35 (21.2)	8.52 (21.6)	3.3 (8.38)
S_{GRAV}, mm (in)	35.0 (1.4)	29.0 (1.18)		65.0 (2.6)
V(0), kV	43.0	54.0	60.0	21.5
V(R), kV	68.0	86.0	66.0	34.0
ΔZ, mm	87.3	87.3	82.0	87.3

The outermost electrode voltage V(R) = 60 kV of test 5-1 is substantially less than the recommended value. One would expect the reduced voltage (and pressure) to yield inadequate deflection near the rim. This is observed in the test results discussed in Section 4. Large voltage changes are required near the rim to produce the required shape improvements to test 5-1. Unfortunately, higher voltage was not achievable at the rim, apparently because of current flow between electrodes. Modification of the electrode surface on subsequent models is expected to allow the full range of voltage control.

Also included in Table 3.2 are the voltage requirements using an aluminized polyethylene membrane. This polymer is unsuitable for use in space because of its thermal characteristics and UV degradation. However, for ground tests it could be quite useful. The pressure and voltage required to form the membrane is substantially less than with most membrane materials. Alternatively, the membrane could be stretched tighter or a much thicker membrane could be used. An 81 μm (3.2 mil) polyethylene membrane would have the same stiffness as the 0.3 mil Kapton membrane used in test 5-1.

3.3 CONTROL

Active adjustment of a reflector surface can introduce a substantial performance improvement over passive antennas. Some other reflector concepts control shape by using servo motors to pull strings and move support structures. With the EMR, however, shape control is an intrinsic part of the basic layout. Electrostatic pressure and consequently the membrane reflector shape are altered by simple voltage adjustments. The EMR incorporates a uniquely simple and effective servo with the membrane surface as the only moving part. Open-loop tests have been performed to gain specific insight on membrane shape control which will be presented in this section.

The membrane's shape is controlled by a complicated summation of the effects of all the electrodes. The influence of a single electrode must be understood in the development of shape adjustments. Several experiments have been performed to determine the influence of a single electrode on the membrane. The results are in general agreement with predictions. With these results, important insights on the EMR are emerging. Techniques may now be prescribed for convergence to the best overall shape. The optimum voltage distribution can now be developed to compensate for daily variations in membrane hygroscopic expansion as well as perimeter pre-tension. Several control algorithms to achieve a static shape improvement are very straightforward and can be implemented on small mini-computers. Finally, the electrode layout can be revised now that the shape-influence relationships are understood.

For small deflections about the operating condition, the load-deflection relationships are essentially linear. This is true for most structural systems. The EMR behavior is shown in Fig. 3.7. The structural response from the unstressed state ($\Delta Z = 0$) to the operating condition, $\Delta Z = 87.3$ mm (3.44 inch), is nonlinear. Deflections are proportional to the cube root of the load: $\Delta Z \propto P^{1/3}$. The linearization shown by the straight line in Fig. 3.7 indicates reasonable accuracy provided one is near the operating point. Even if one isn't close to the operating point, the linearized solutions provide an estimate of the proper "order-of-magnitude" adjustments. Test data to be presented later in this section will confirm that linearity is reasonable over a large voltage excursion.

The linearized solution to membrane response as predicted by theory[1] is shown in Fig. 3.8. The membrane deflection response is

[1] D.J. Mihora, P.J. Redmond and P.K. Abbey, Candidate Mirror Studies--Electrostatically Controlled Membrane Mirrors (ECMM), General Research Corporation CR-2-740, September 1977, pp. 5-1 through 5-20.

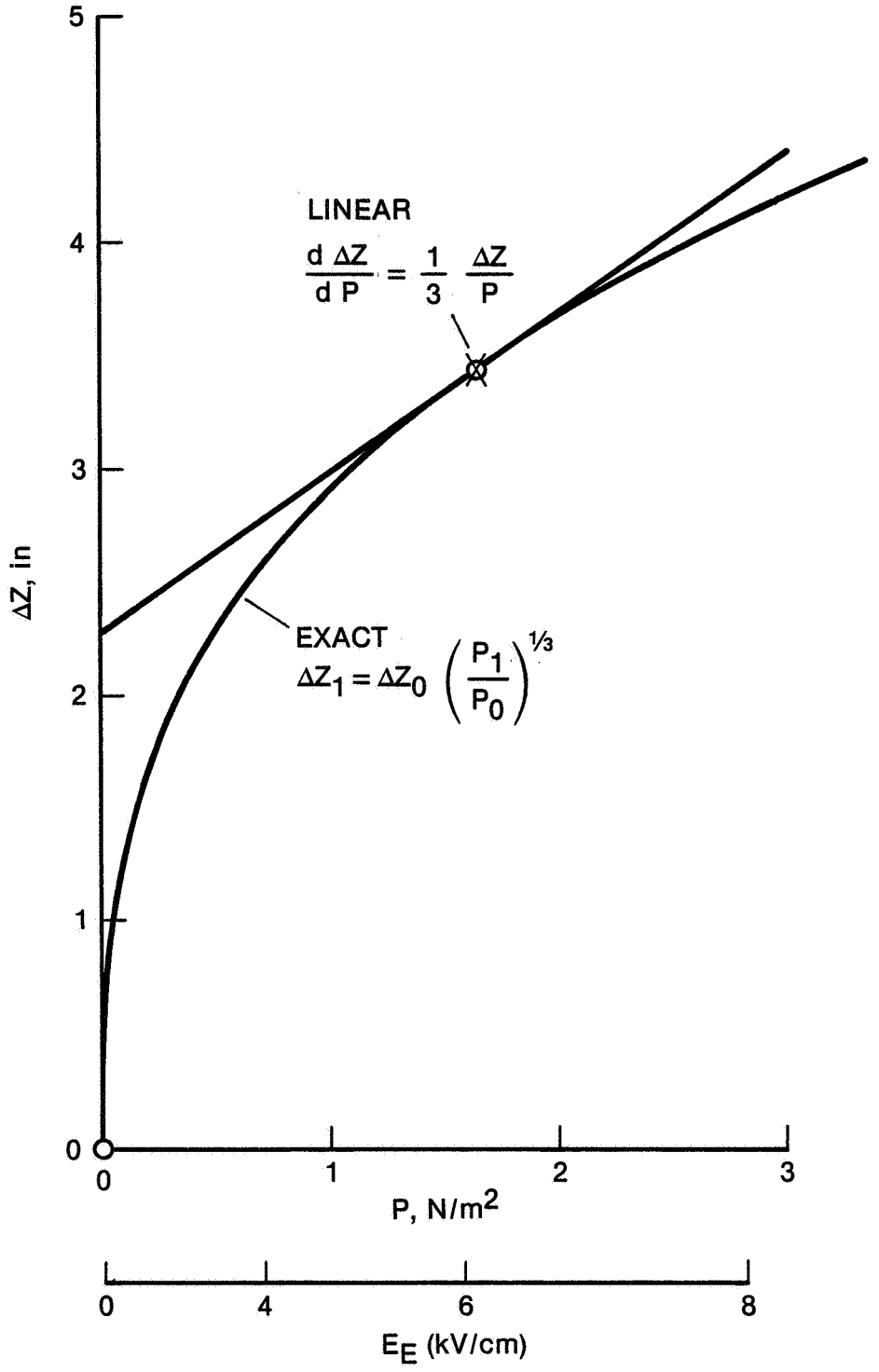

AN-60222

Figure 3.7. Linearity Near the Operating Condition

normalized to a unit pressure loading applied from single electrodes. The membrane deflection is

$$\Delta Z = \frac{dZ}{dP}\frac{dP}{dV}\Delta V$$

The pressure-voltage relation depends upon the spacing geometry between the membrane and electrode. The membrane behavior is present in the $\frac{dZ}{dP}$ term. Figure 3.8 indicates that the center electrode (No. 1) produces the largest deflection response. The smallest response is generated with the outermost ring (No. 5). The peak in each response occurs directly above the individual control electrode. The electrode locations were originally prescribed to minimize pressure errors from the five electrodes.[1] The five electrodes cannot exactly generate the ideal loading necessary to form a perfect sphere. Finite numbers of electrodes introduce small surface errors. The maximum error due to the use of only five electrodes is about 15 μm. For the NASA missions requiring a surface quality of 1 mm, two electrode rings would be adequate for shape control of a 16 ft membrane. Thus, the five electrodes provide substantially more than the minimum in spatial resolution. Even with the relatively small electrode width, each electrode produces a substantial membrane deflection along the entire radius from center to rim. The combined response is the summation of the contribution of five different "influence functions". Before the summation, each influence function is multiplied by a constant. The five constants can be selected to minimize the deflection errors, ΔZ_i, over the surface. Note that it is much easier to remove deflection errors near the center of the membrane than out near the rim. The higher "control power" of the center electrode is obvious during testing.

---

[1] D.J. Mihora, et al., Electrostatically Formed Antennas (Test Concept), General Research Corporation NASA CR-159068, April 1979, p. 76.

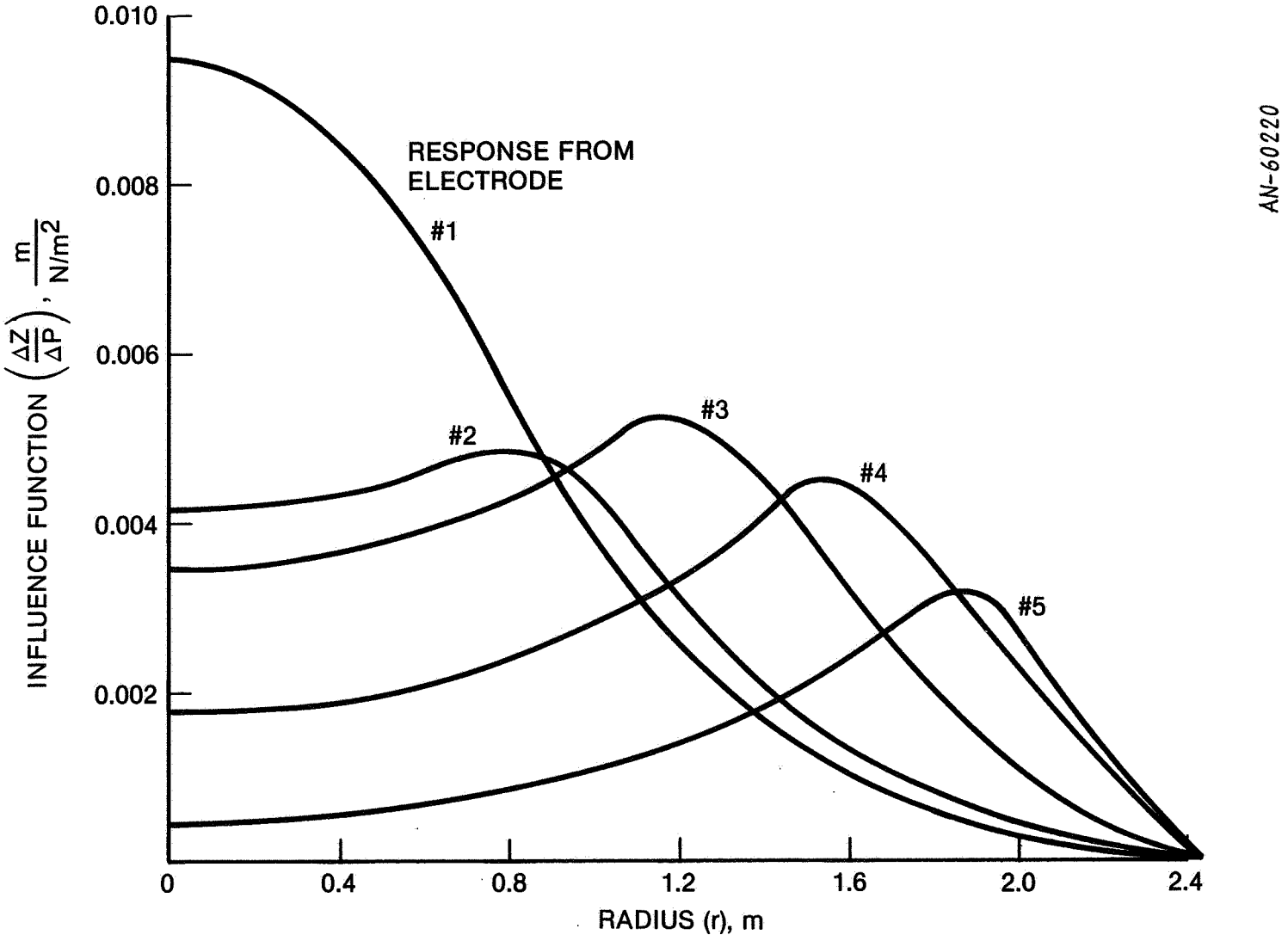

Figure 3.8. Membrane Deflection Associated with an Incremental Pressure Change (Theoretical)

A test series was run in April 1981 to determine the electrode influence functions experimentally. One set of results is shown in Fig. 3.9. In this test, the voltage on each electrode individually was reduced by 8 kV and the change in deflection was recorded. Initially, all the electrodes were at 48 kV. In these results, the deflections are directly related to voltage. (In Fig. 3.8, deflections were related to a unit pressure change.) There is a qualitative agreement in the shape of these influence functions. There are also differences, particularly out near the rim. A detailed comparison of theory with experiment is probably not warranted; humidity, perimeter pre-tension, and the constant voltage distribution produced a basic membrane shape substantially different from the spherical surface modeled in theory. The following observations, however, can be made: First, the center electrode has the largest influence on the membrane. Second, the deflection response function is quite broad for each of the five electrodes. Third, the peak response is usually at some point above the electrode that is being altered.

Additional insight into the membrane control characteristics is seen in Fig. 3.10, a plot of the peak deflection as the voltage is changed on each electrode (except No. 5). These results show that control is linear--i.e., deflection, Z, is proportional to voltage, V. The slopes of of the curves, $\frac{\Delta Z}{\Delta V}$, quantify the control power of each electrode.

Very simple static control techniques can be constructed using the linear influence functions. The deformation of the membrane may be expressed as a function of the applied loads, i.e.,

$$\Delta Z_1 = A_{11}\,\Delta P_1 + A_{12}\,\Delta P_2 + A_{13}\,\Delta P_3 + A_{14}\,\Delta P_4 + A_{15}\,\Delta P_5$$

$$\Delta Z_2 = A_{21}\,\Delta P_1 + A_{22}\,\Delta P_2 + A_{23}\,\Delta P_3 + A_{24}\,\Delta P_4 + A_{25}\,\Delta P_5$$

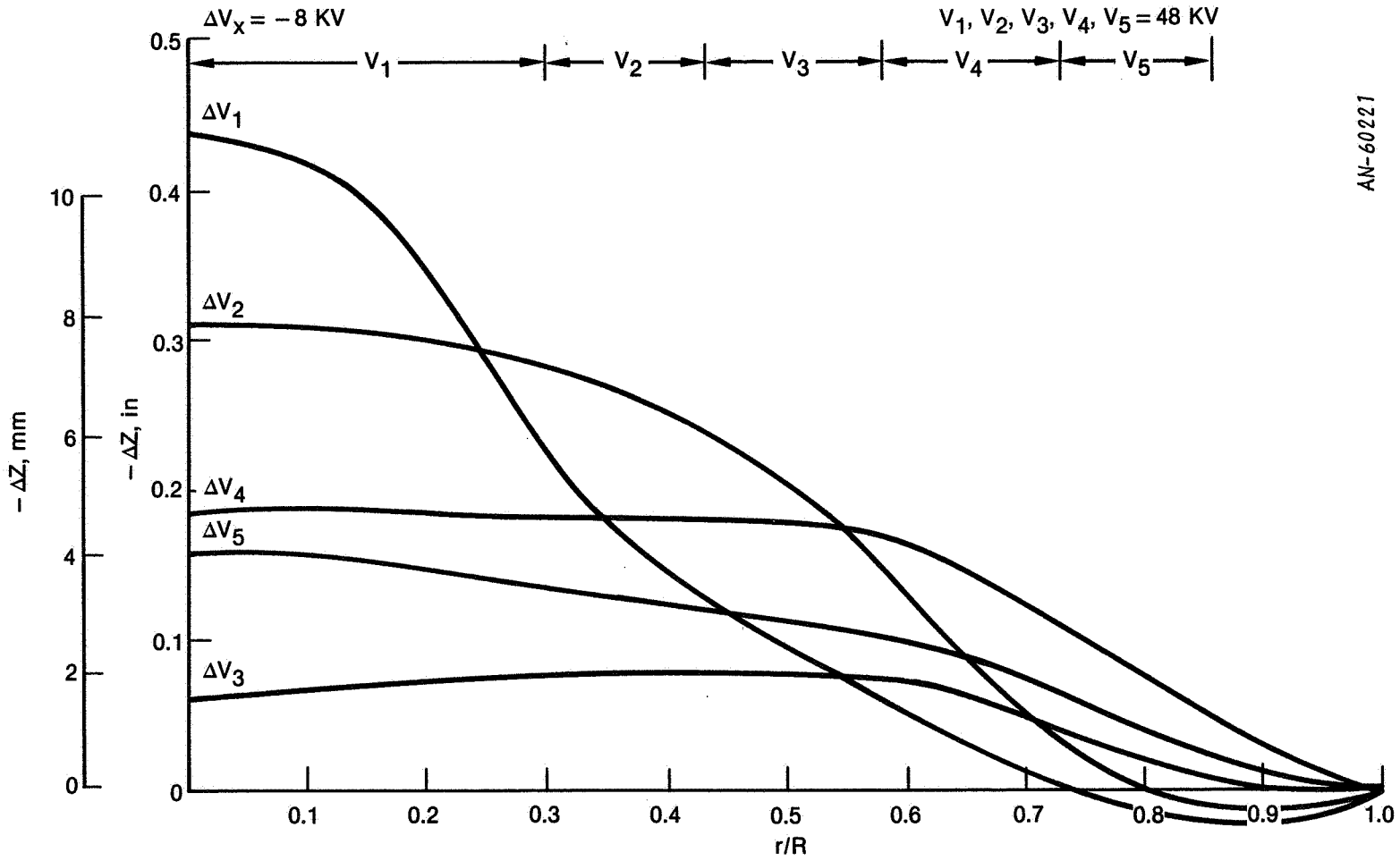

Figure 3.9. Single-Electrode Influence Functions (Test Data)

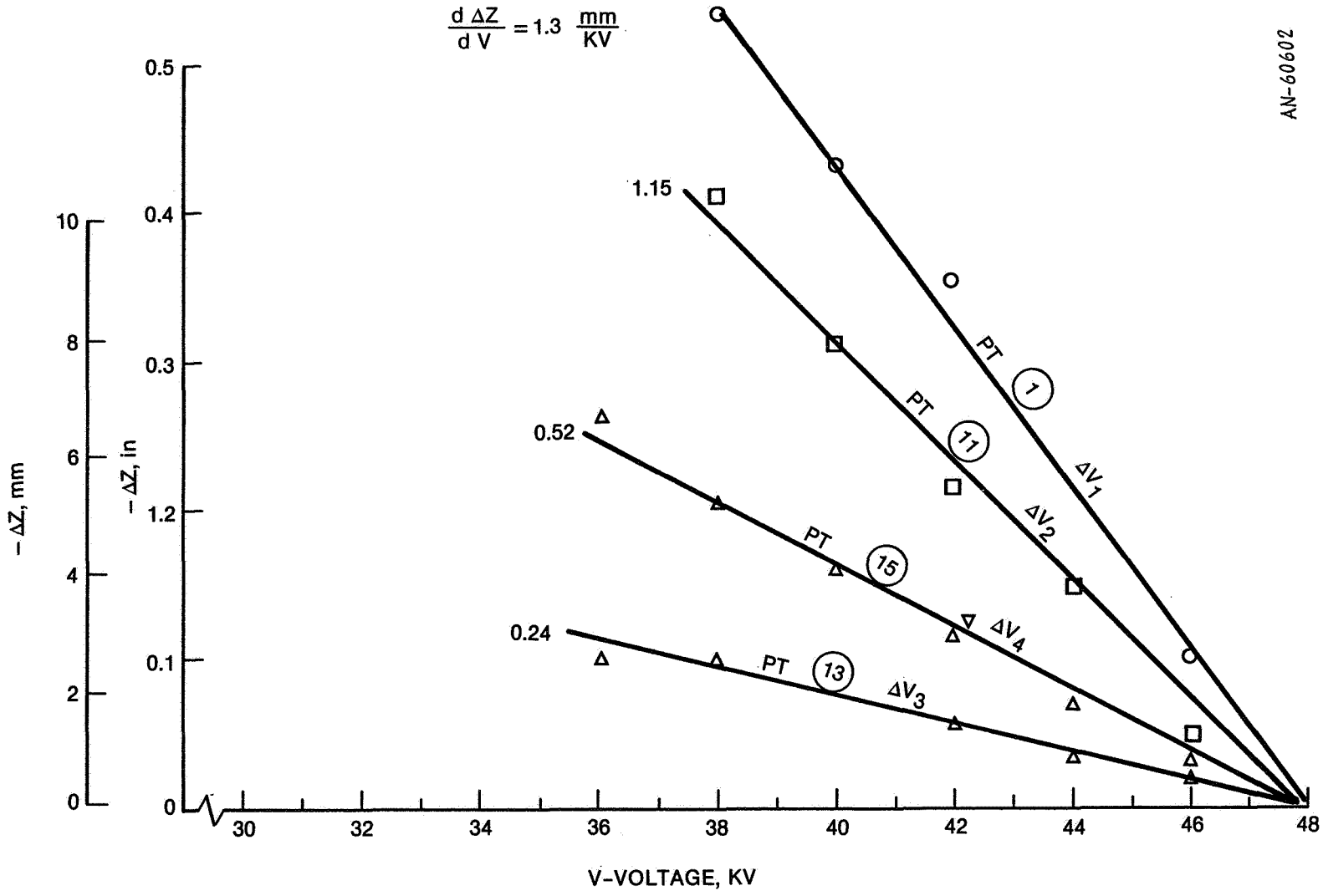

Figure 3.10. Linearity of Shape Control

$$\Delta Z_3 = A_{31}\,\Delta P_1 + A_{32}\,\Delta P_2 + A_{33}\,\Delta P_3 + A_{34}\,\Delta P_4 + A_{35}\,\Delta P_5$$

$$\Delta Z_4 = A_{41}\,\Delta P_1 + A_{42}\,\Delta P_2 + A_{43}\,\Delta P_3 + A_{44}\,\Delta P_4 + A_{45}\,\Delta P_5$$

$$\Delta Z_5 = A_{51}\,\Delta P_1 + A_{52}\,\Delta P_2 + A_{53}\,\Delta P_3 + A_{54}\,\Delta P_4 + A_{55}\,\Delta P_5$$

or written simply

$$\{\Delta Z\} = [A]\,\{\Delta P\}$$

The A_{ij} influence coefficients specify the contribution to the deflection at each measurement point, ΔZ_i, of a pressure increment, ΔP_j, applied at electrode j. The radial location of the ΔZ_i measurement points is rather arbitrary. We will discuss the significance of the radial measurement locations. Three sets of radial positions were used in constructing control matrices. The [A] matrix for each case is constructed directly from the influence functions shown in Fig. 3.8.

The required pressure adjustments to the membrane reflector are determined from

$$\{\Delta P\} = [B]\,\{\Delta Z\}$$

where

$$[B] = [A]^{-1}$$

Insights can be obtained on membrane control by examining the numbers in the [B] matrix. This matrix was constructed for the following three cases (Table 3.3):

TABLE 3.3

CONTROL MATRICES, [B], ASSOCIATED WITH THE MEMBRANE DEFLECTION FUNCTION

UNITS: $\frac{N/m^2}{m}$

CASE 1 EQUAL Δr INCREMENTS

r/R						
0			737	711	8	9	17
.19			- 6688	8901	-2178	9	17
.38	$[B_{ij}]$ =		-11447	-15778	5001	- 626	17
.57			-11937	16773	5838	1490	-366
.76			6113	- 9045	3507	-1122	743

CASE 2 FOR RANDOM (GAUSSIAN) ERRORS

r/R						
.19			330	-364	648	- 3475	7935
.42			-401	811	-3236	17780	-40374
.62	$[B_{ij}]$ =		148	- 99	2930	-18156	41335
.8			- 79	-141	-1095	10276	24210
.922			35	61	130	2851	8106

CASE 3 FOR PEAK IN INFLUENCE FUNCTIONS

r/R						
0			279	-240	10	5	17
.325	$[B_{ij}]$ =		-419	994	-568	43	14
.466			142	-597	909	-445	58
.627			- 44	203	-586	952	-469
.766			19	- 61	219	-698	840

Case 1: Deflection measurements are taken at equal Δr increments. A disadvantage of this choice is that the outer points represent a disproportionately large fraction of the surface. Radial measurement locations are r/R = 0, .19, .38, .57, and .76. See Table 3.3.

Case 2: Radial locations were selected from a numerical algorithm which attempts to minimize the RMS deflection errors. An integral can be written which relates the RMS surface error in terms of the influence functions. If the deflection errors are assumed to be random, the minimum RMS errors are associated with a Gaussian integration scheme. For a five-point Gaussian integration, the ideal radial measuring points can be shown to be r/R = .19, .42, .62, .8, .922. The measuring points are more uniformly distributed over the aperture than in Case 1.

Case 3: Radial locations were selected at the points of peak membrane deflection in the influence functions shown in Fig. 3.8. The radial positions are at r/R = 0.0, .325, .466, .627, .766.

Table 3.3 shows the control matrices for these three cases. Only 5 x 5 matrices were constructed. Algorithms can be developed for adjusting the j electrodes with measurements of ΔZ_{ji}'s at locations i = 1 to n. The diagonal elements in Table 3.3 are all necessarily positive. Although the matrices were developed from linear considerations, the matrices are not symmetric. In Case 1 and Case 2, the off-diagonal elements vary dramatically in magnitude. The matrix in Case 3 appears "balanced"; however, this may not be the preferred asset in selecting the control matrix. Two principal aspects in matrix selection are conflicting. The radial measurement locations should be selected to provide the best overall control. The matrix should not be over-

sensitive to the deflections (or measurement errors) far from the diagonal elements. Control experiments should be performed to aid in developing measurement location preferences.

In most situations, shape control need only correct for slow drift of the membrane reflector. The dynamics of the membrane reflector are not part of the static control system. Real-time dynamic control of the EMR is far more complex than "static" control and in most situations it is unnecessary. Dynamic control is an involved discipline that requires significant discussion that is not part of this current effort. However, it is straightforward to describe the structural dynamics of the EMR in an open-loop sense.

Subsequent to the structural modeling to generate influence coefficients, the same code was used to determine the modal vibrations. Figure 3.11 indicates the first 12 eigenvalues and eigenfunctions. Unlike most structures, the EMR eigenvalues are not defined independent of applied loads. The electrostatic field reduces the frequency and alters the shape of the structure as compared to a "free-vibration" model. Development of the eigenvalues is complicated by the addition of electrostatic pressure to the "free-vibration" model. (The electrostatic pressure varies with the membrane reflector vibration). All the mode shapes are shown as a function of radius. Unlike a drumhead membrane, the EMR is not flat (although it is quite shallow) and has a varying stress distribution. The aperture is axisymmetric. Traversing in an azimuthal direction (θ), the modal amplitude varies with cos $m\theta$ where m = azimuthal mode number. The lowest mode frequency (in a vacuum) is $\omega_{00} = 79.9\ s^{-1}$ (f = 12.7 Hz) using the baseline[1] EMR. This mode shape is similar but not identical to that of a drumhead membrane. Some eigenvalues are quite close to one another. The eigenvalues associated with the azimuthal modes grow considerably more slowly than the radial modes. Tests in the air have not been performed to validate these results. Future tests in a vacuum would be much more meaningful.

[1] NASA CR-159068.

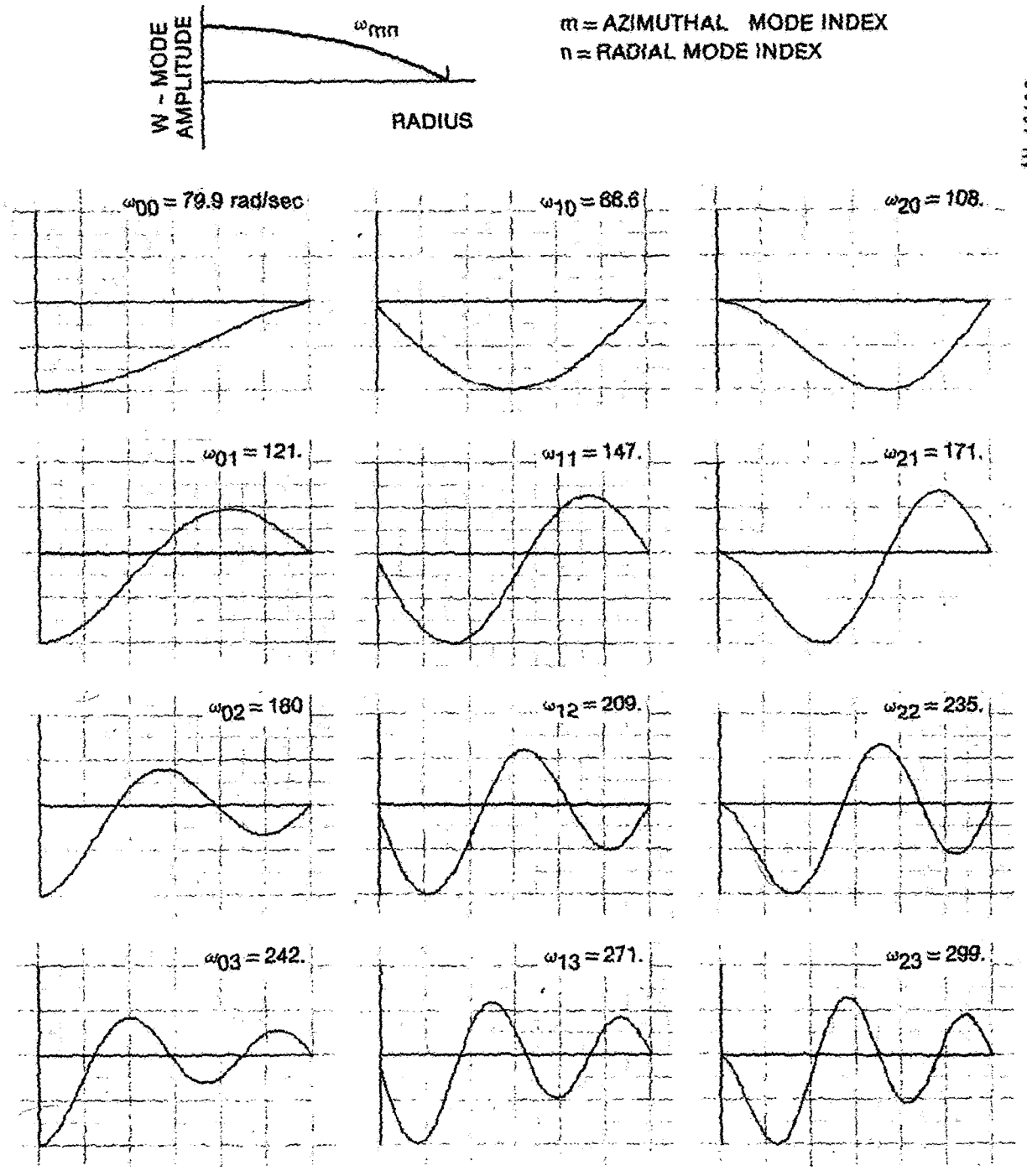

Figure 3.11. Lowest Vibration Modes of 4.88 m EMR

4 2-D PLOTS

During the eight-month period October 1980 through May 1981, 20 sets of data were examined. Some of the data was used in a qualitative manner to recommend test fixture modifications. Principal design adjustments included the following: First, elimination of perimeter pre-tension by gravity sag measurement; second, reduction of the rim deflection errors to the order of $\pm$ 1.0 mm; third, alignment of the back electrode surface with respect to the rim. This sequence of improvements led to an order-of-magnitude improvement in the membrane reflector quality.

Analyses were conducted on 13 tests. Table 4.1 shows the voltages on the five electrodes in each test. As mentioned previously in this report, humidity and perimeter pre-tension caused havoc by daily altering the dimensions of the membrane. Also, the surprisingly high stiffness of the Kapton membranes necessitated higher voltages than the design values to achieve the desired deflections.

The analyses included 2-D regressions which yielded insights on membrane waviness over short distances and 3-D error projection plots indicating overall behavior. Section 5 presents the 3-D results. This section gives the 2-D representation of the membrane shape.

The shape of the baseline spherical surface can be represnted by a power series:

$$Z = 1/2 \frac{R^2}{\rho}\left(\frac{r}{R}\right)^2 + 1/8 \frac{R^4}{\rho^3}\left(\frac{r}{R}\right)^4 + 1/16 \frac{R^6}{\rho^5}\left(\frac{r}{R}\right)^6 + \cdots$$

where X is the membrane deflection at radius r , and R = 2.44 m, ρ = 34.1 m , yielding

$$Z(mm) = 87.2\left(\frac{r}{R}\right)^2 + 0.11\left(\frac{r}{R}\right)^4 + \cdots$$

TABLE 4.1

VOLTAGES IN MEMBRANE TESTS

TEST	DATE	V_1	V_2	V_3	V_4	V_5
1-1	10-06-80	40	42	48	54	58
2-1	10-15-80	62	68	68	68	70
3-1	10-17-80	68	68	68	68	68
3-2	10-17-80	70	66	66	68	60
3-3	10-17-80	67	68	67	66	60
3-4	10-17-80	68	70	70	69	60
4-1	10-24-80	41	45	48	55	57
4-2	10-31-80	46	51	57	63	68
4-3	11-03-80	40	40	40	40	40
4-4	4-08-81	52	52	52	52	52
4-5	4-08-81	50	52	54	60	60
4-6	4-08-81	40	44	48	52	55
5-1	5-22-81	60	62	64	66	66
DESIGN CONDITIONS*		45	50	56	63	67

* ZERO PRE-TENSION, E = 500 KSI

It is seen from this result that the spherical surface is very close to a parabola (for which only the quadratic term would be nonzero). It is instructive to formulate the test results into the form:

$$Z = A_1(r/R) + A_2(r/R)^2 + A_3(r/R)^3 + \ldots$$

The non-symmetric terms A_1, A_3, ... are retained because of a non-symmetric rim. A regression analysis was used to provide the best fit (RMS) of the test data to the power series. The important output of the curve fitting is the coefficients A_i and the residuals or roughness of test data.

A summary of the 2-D modeling is shown in Table 4.2 for tests 1-1 through 4-3. Data is given for horizontal, vertical, and diagonal traces across the aperture. The curve fit used the fourth-order polynomial. The non-symmetric terms, A_1 and A_3, are significant. From the 3-D plots one can identify these non-symmetric terms with the rim non-symmetry. The largest anomaly is not in the non-symmetric terms but rather in the large negative values of A_4. This term becomes significant as one approaches the rim. The deformed shape becomes less curved near the rim. (The A_4 terms subtract from the A_1 terms). The deformed membrane does not retain a constant radius of curvature but rather displays an increasing radius of curvature near the rim. The reason for this "flatness" near the rim is easily explained. The pressure loading is not adequate near the rim. The largest deviations from the desired shapes are generally those for tests with equal voltages on all electrodes. The analytic prediction for the desired spherical surface dictated voltages of 45, 50, 56, 63, and 67 kV. This ideal voltage distribution is associated with a membrane stiffness, $E = 3.44 \times 10^9$ N/m^2 (500 KSI) and zero initial pre-tension. Despite differences caused by humidity and material properties, the general form of the voltage distribution has been validated in the tests.

A significant parameter listed in Table 4.2 is the roughness, σ_H, of the membrane reflector. It is defined as the RMS error of the surface (compared to the power series representation obtained from the regression

TABLE 4.2

OPEN LOOP REFLECTOR SHAPES

ANALYTIC REPRESENTATION OF SURFACE

$$z \text{ (mm)} = A_1(r/R) + A_2(r/R)^2 + A_3(r/R)^3 + A_4(r/R)^4$$

Test No.	A_1	A_2	A_3	A_4	Roughness (Waviness) about Generated Shape σ_H (mm) RMS
Ideal	0	87.2 mm	0	.11	0
HORIZONTAL					
1-1	-1.27	95.4	9.2	- 2.2	0.3
2-1	-1.9	102.0	-3.7	-18.1	0.3
3-1	- .91	113.8	-5.6	-30.9	0.15
3-2	- .5	118.8	-5.7	-37.2	0.3
3-3	-1.22	110.1	-5.3	-29.7	0.18
3-4	- .79	112.8	-5.7	-26.6	0.18
4-1	5.84	97.4	-6.4	- 4.8	0.5
4-2	4.98	139.7	-5.68	-24.2	0.46
4-3	5.99	112.8	-6.25	-22.3	0.58
VERTICAL					
1-1	.9	77.3	4.7	8.07	0.9
2-1	-2.5	88.7	2.2	-9.63	0.4
4-1	-7.4	80.6	3.9	5.63	1.4
4-2	-8.4	118.5	5.1	-10.2	1.3
4-3	-5.5	97.4	3.1	-13.3	1.7
DIAGONAL					
4-1(+45°)	-6.9	92.9	-6.1	- 4.6	.69
4-2(+45°)	- .9	132.0	-4.4	-21.1	1.35
4-3(+45°)	-1.9	106.7	-4.7	-21.2	.84
4-2(-45°)	8.5	129.8	-5.3	-24.4	.61
4-3(-45°)	8.9	103.6	-6.4	-22.3	.56

equations). It is a measure of the inability of the best-fit curve to be placed through the test data. It indicates the localized roughness and irregularity in the membrane. Principal error sources contributing to σ_H are material irregularity and seams. The roughness varies from 0.15 to 1.7 mm. The roughness in the vertical direction is three to six times larger than in the horizontal direction. The seams are aligned horizontally. Crossing the seams (vertically) rather than traversing the seams produces the largest irregularity. However, the seam errors are substantially smaller than the errors associated with the A_1, A_3, and A_4 terms. The errors associated with A_1, A_3, and A_4 can be eliminated by voltage adjustment and improved rim symmetry. The residual roughness, σ_H, provides an estimate of EMR potential when using off-the-shelf commercial materials. In these early tests, the average residual roughness was about 1.0 mm. In subsequent tests (e.g., 5-1) the residual roughness was substantially less, although not evaluated as part of this contract.

Membrane surface quality can be better understood by examining regression results. Figures 4.1 and 4.2 (pp. 57, 58) show the development of the regression curves for test 1-1. Plotted in these figures is the deviation of the membrane from the reference power series. In Figs. 4.1 and 4.2, three power series are best fit through the test data. Increasing numbers of terms are used to eliminate the low frequency distortions. The final curves use four terms (A_1, A_2, A_3, A_4) to define the shape. In each case, the variance σ is given.

In these earliest tests, a rim error in terms of an out-of-flatness can be seen in the data. In Fig. 4.1-a and Fig. 4.2-a, the residual errors approaching the rim are evident. Tilt errors of the rim are removed in Figs. 4.1-b and 4.2-b by including the A_1 term. Finally, the third-order asymmetry is removed in the lower figure. The residual membrane errors have a high-frequency content. The waviness attributed to the seams is clearly evident in Fig. 4.2. In these tests, the smallest correlated errors are attributed to the materials and the seams. The

largest errors are attributed to a non-symmetric rim (see 3-D plots in Sec. 5), hygroscopic effects, differential perimeter pre-tension, and non-optimum voltages.

The effects of electrostatics are dramatically displayed using the radius of curvature rather than the shape. This occurs because the radius of curvature involves the second derivative of shape. Figure 4.3 indicates a radius of curvature comparison using a voltage distribution similar to theory. The horizontal and vertical radii are close to expectations out to $r/R = 0.85$. Beyond that point the shape diverges. In the test model, the outermost electrode did not extend beyond $r/R = 0.85$.

A significant departure in the measured radius of curvature is seen in Fig. 4.4. In tests 3-1 and 3-4 the voltage distribution was nearly constant. Excessive voltage and loads at the center produce a radius of curvature distribution far from the desired value. The theoretical voltage distribution introduces a pressure distribution that varies by 2.0 from the rim to the center; the constant voltage distribution results in a pressure varying by a factor of 5.3 from rim to center. The excessive pressure at the center as compared to the rim produces the small radius of curvature at the center and a much larger value toward the rim.

A round balloon requires a constant pressure to form a spherical surface. A flat membrane attached to a rigid ring requires a varying pressure to form a spherical surface. Both theory and prior EMR tests have confirmed that the pressure at the center of the membrane should be approximately twice as large as that at the rim. Understanding the spatial results for these tests is tedious because the overall response has been masked by the various error sources. Tests 1-1 and 4-1 display the best overall shapes, which use a voltage/pressure distribution similar to the recommended form.

A thorough analysis was made of the data from tests 4-1 through 4-3 which was obtained from photogrammetry measurements. For each test 61 points

on horizontal, vertical, and diagonal lines on the membrane reflector surface defined the shape. Regression results using this data are shown in Figs. 4.5 through 4.16. The power series coefficients and residual errors are shown for each radial line. Line A is a horizontal radial ($\theta = 0°$) that does not cross a seam. The other lines, B, C, D, are at 45° increments (standard coordinate notation).

The following observations can be made concerning the 2-D test data.

Line C shows the waviness across the seams. It is conjectured that the waviness is caused principally by the anisotropic nature of the membrane material and not by the membrane overlap in the seam area.

It is important to remove the low-order tilt and asymmetry (A_1, A_3 terms) introduced by the perimeter attachment. The perimeter-introduced errors are substantially larger than the residual errors.

As expected, the same residual errors exist for Cases 4-1 through 4-3 despite changes in voltage. Using an "off-the-shelf" commercial membrane, the residual error is approximately 0.5 to 1.5 mm at a stress of about 5 percent of yield. Further reduction in the residuals would be obtained by alternate seaming patterns, select orientation of the anisotropic membranes, improved manufacturing of the seams, and increased membrane stress.

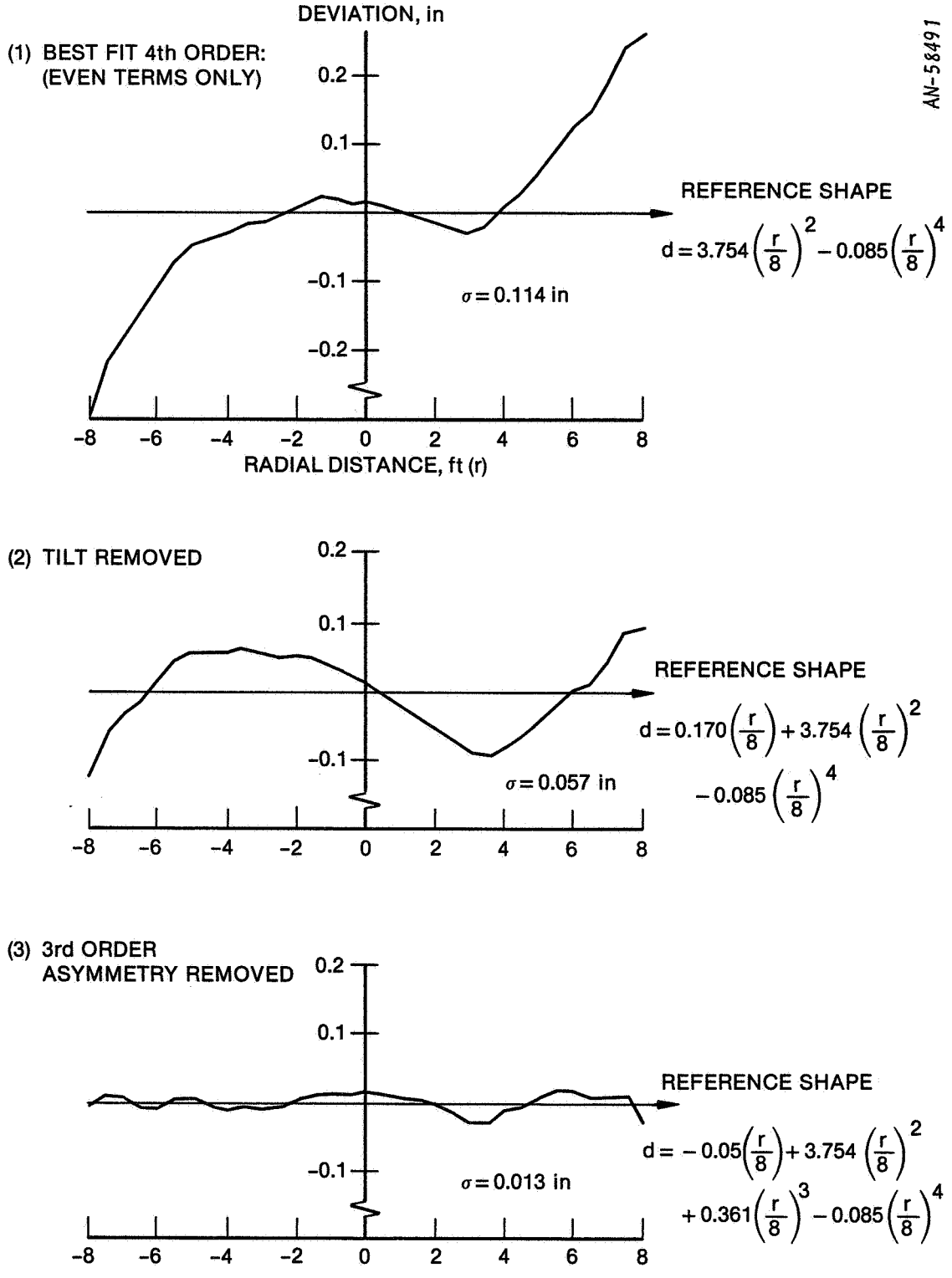

Figure 4.1. Regression Results, Test 1-1 (Horizontal)

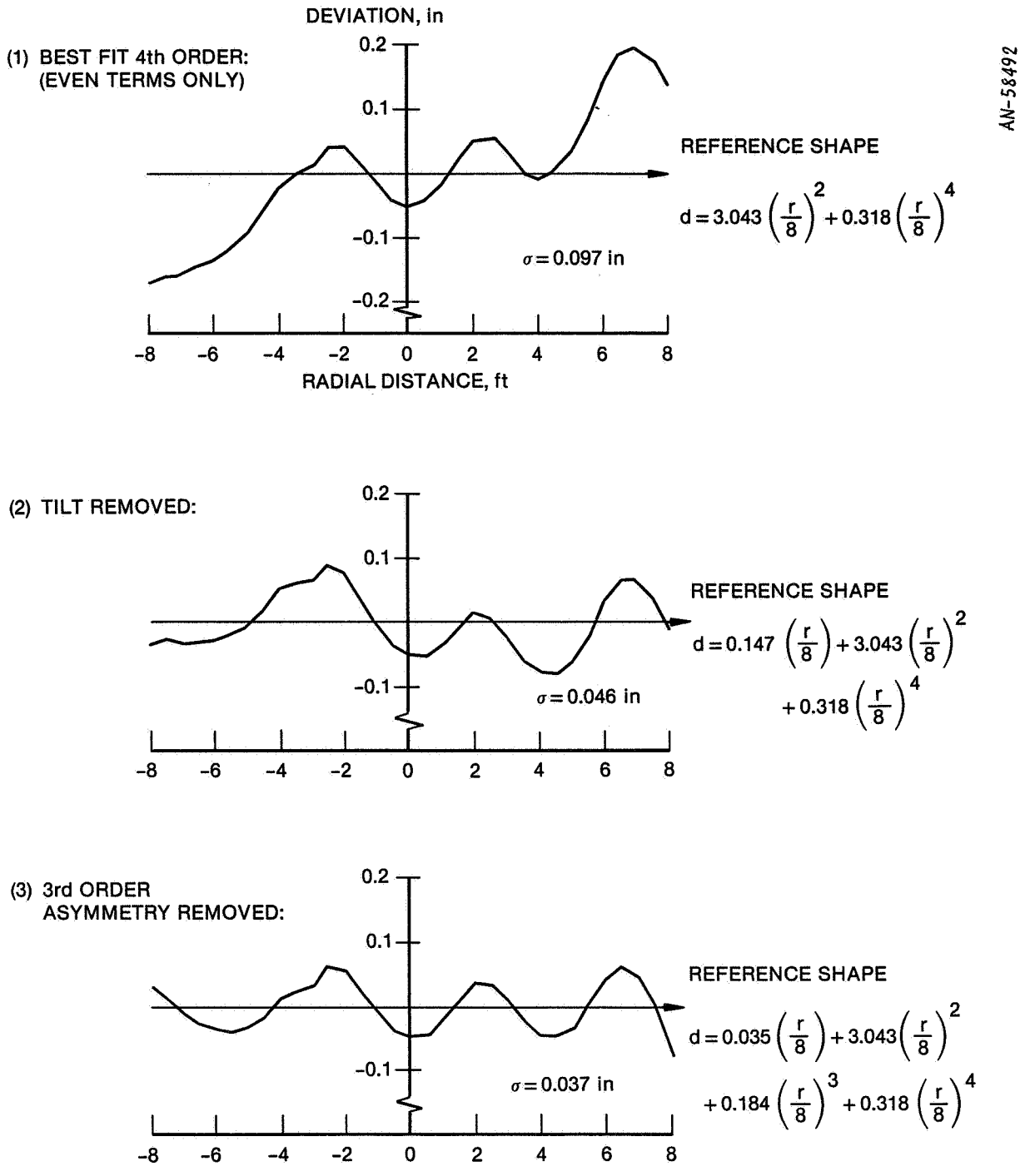

AN-58492

Figure 4.2. Regression Results, Test 1-1 (Vertical)

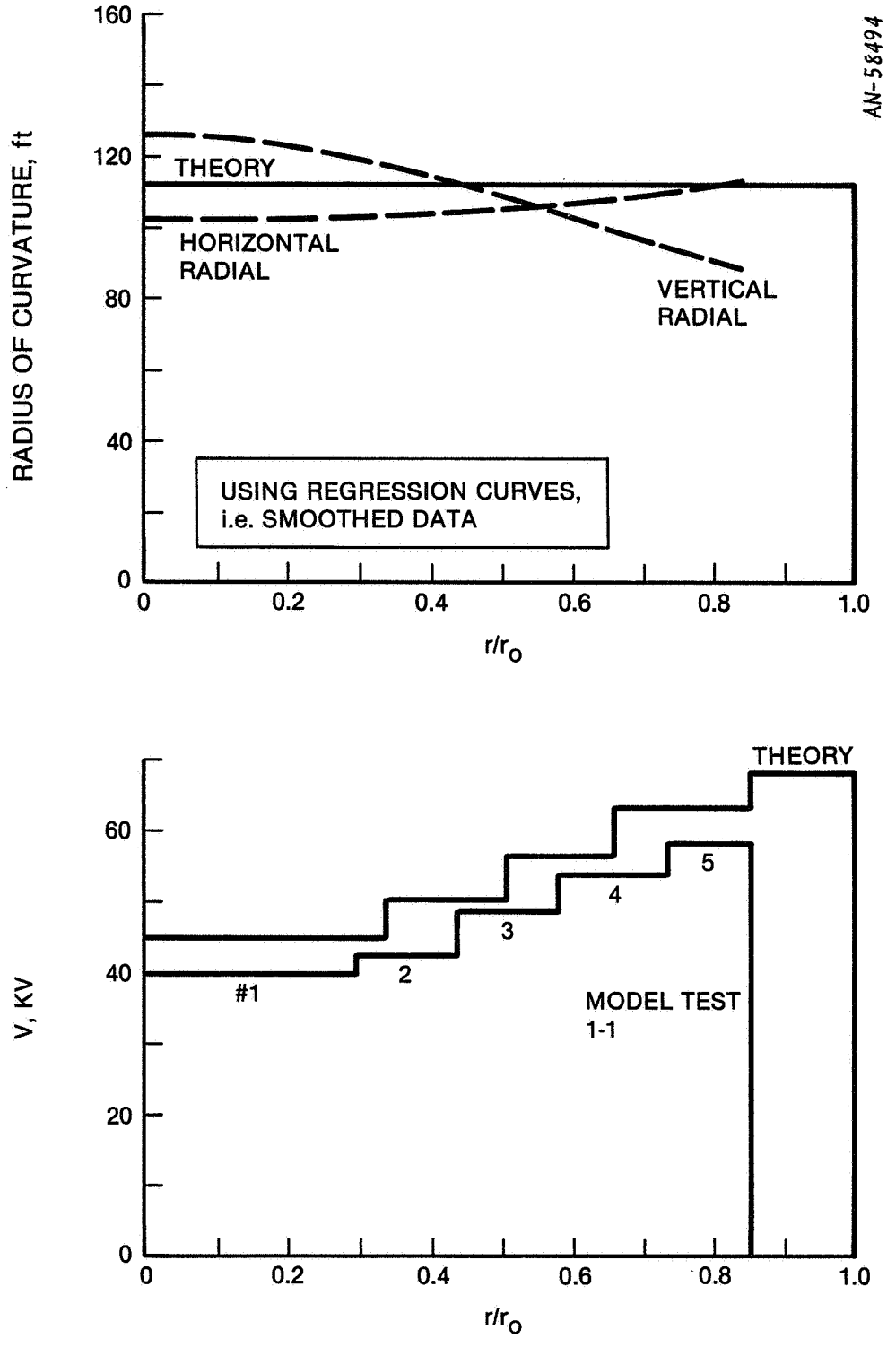

Figure 4.3. Radii of Curvature and Voltage Distributions, Test 1-1

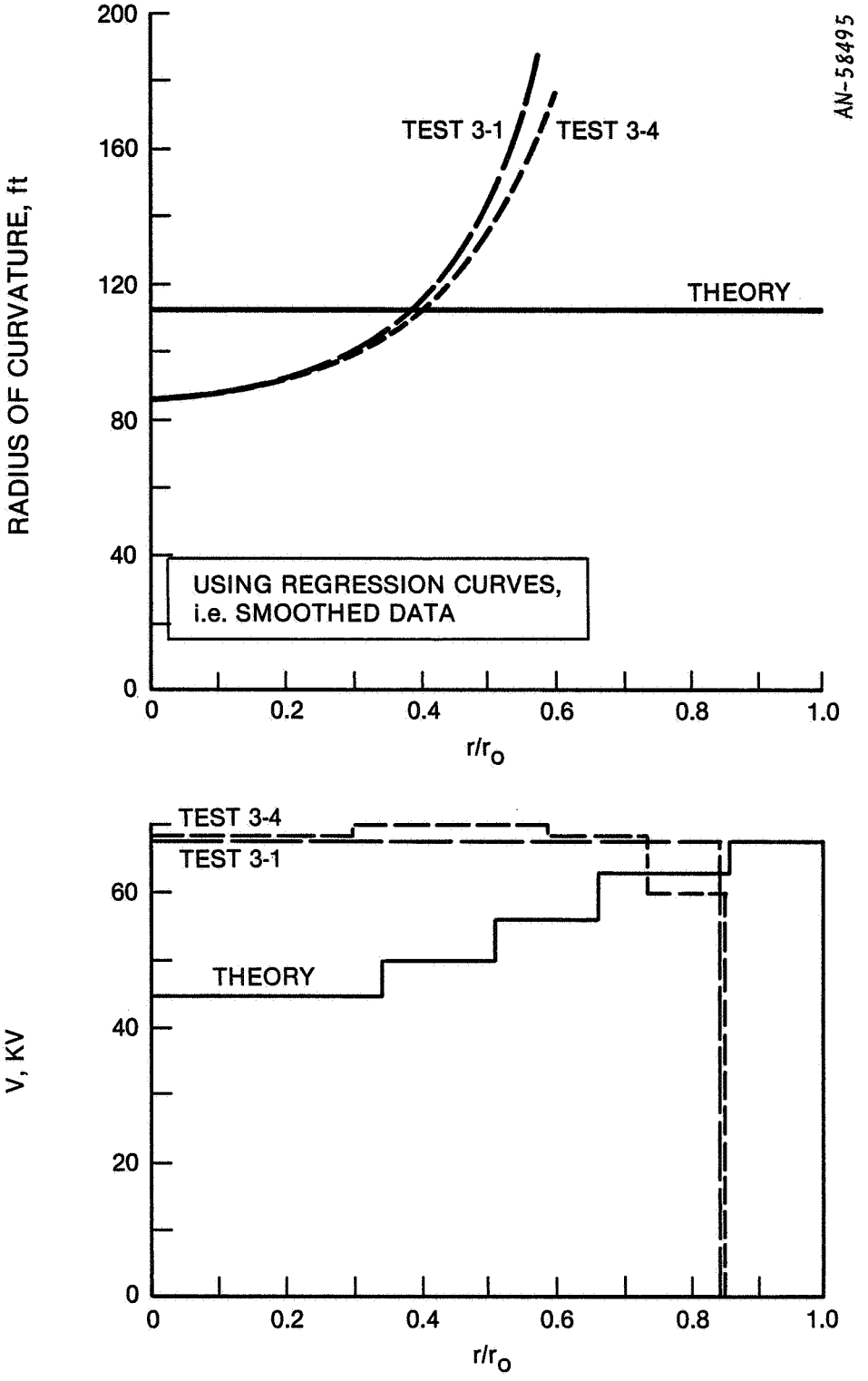

Figure 4.4. Radii of Curvature and Voltage Distributions, Tests 3-1 and 3-4

REGRESSION RESULTS

TEST 4-1

OCT 24, 1980

VOLTAGES = 41, 45, 48, 55, 57 KV

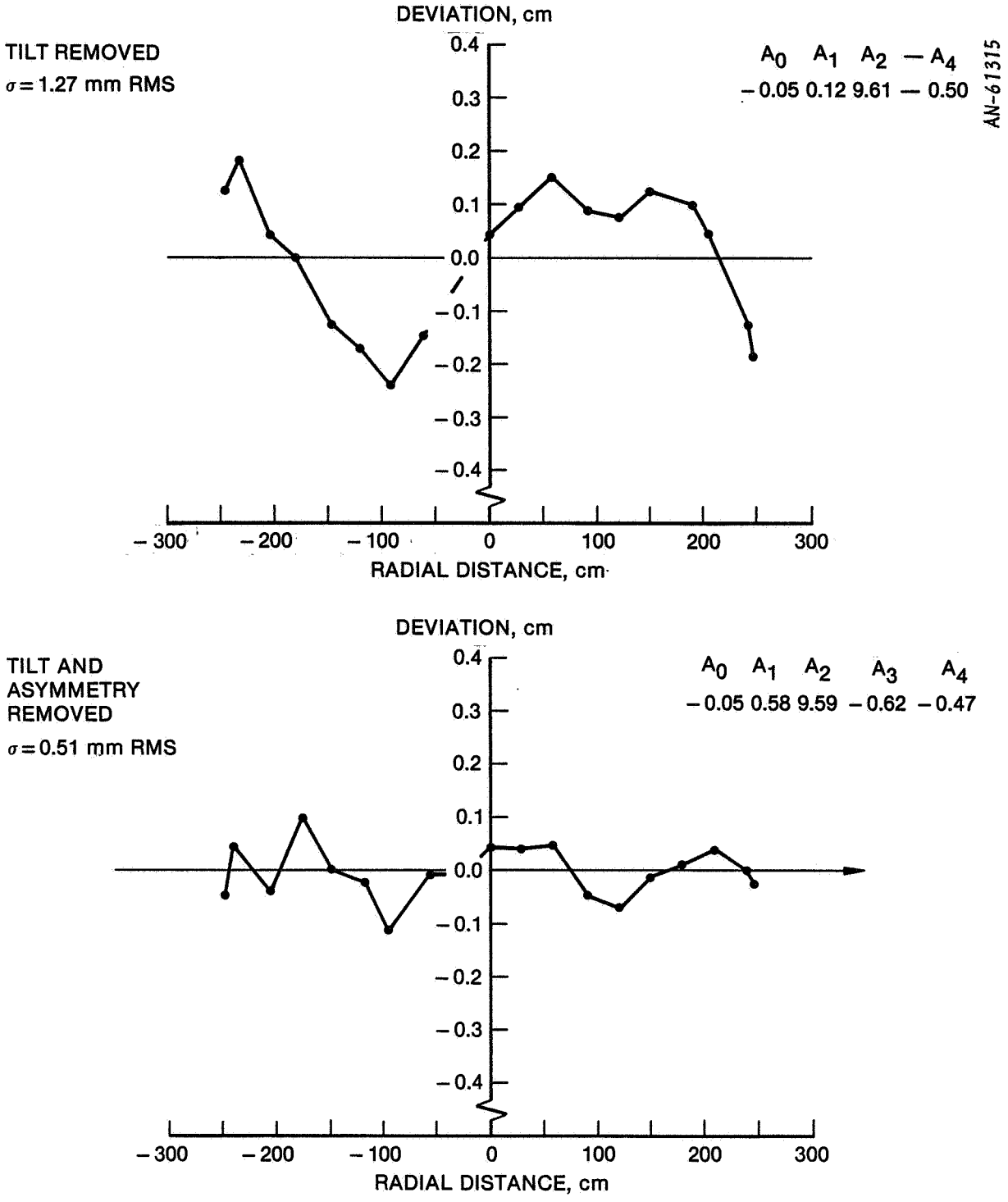

Figure 4.5. NASA Test 4-1, Line A (0°)

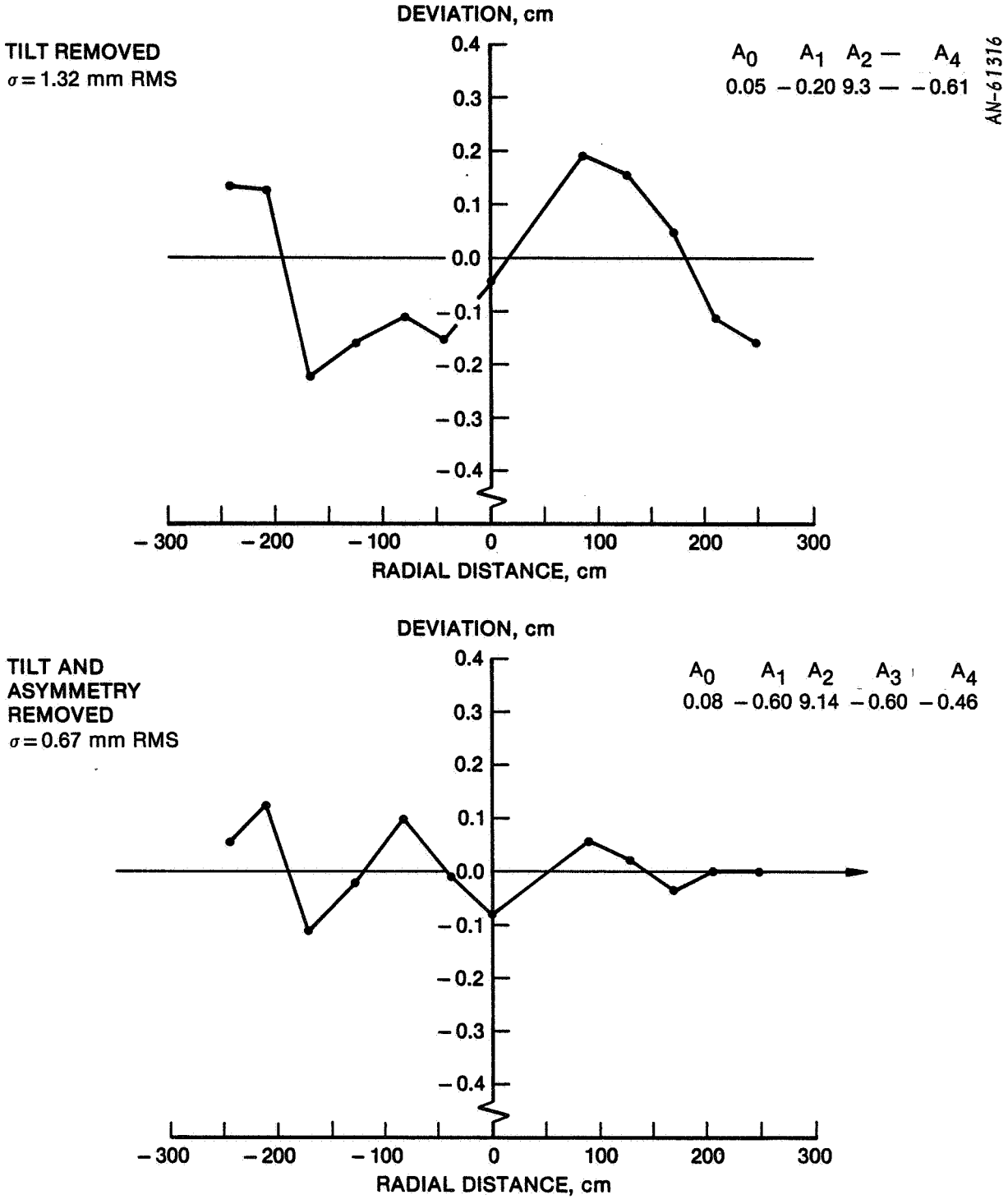

Figure 4.6. NASA Test 4-1, Line B (45°)

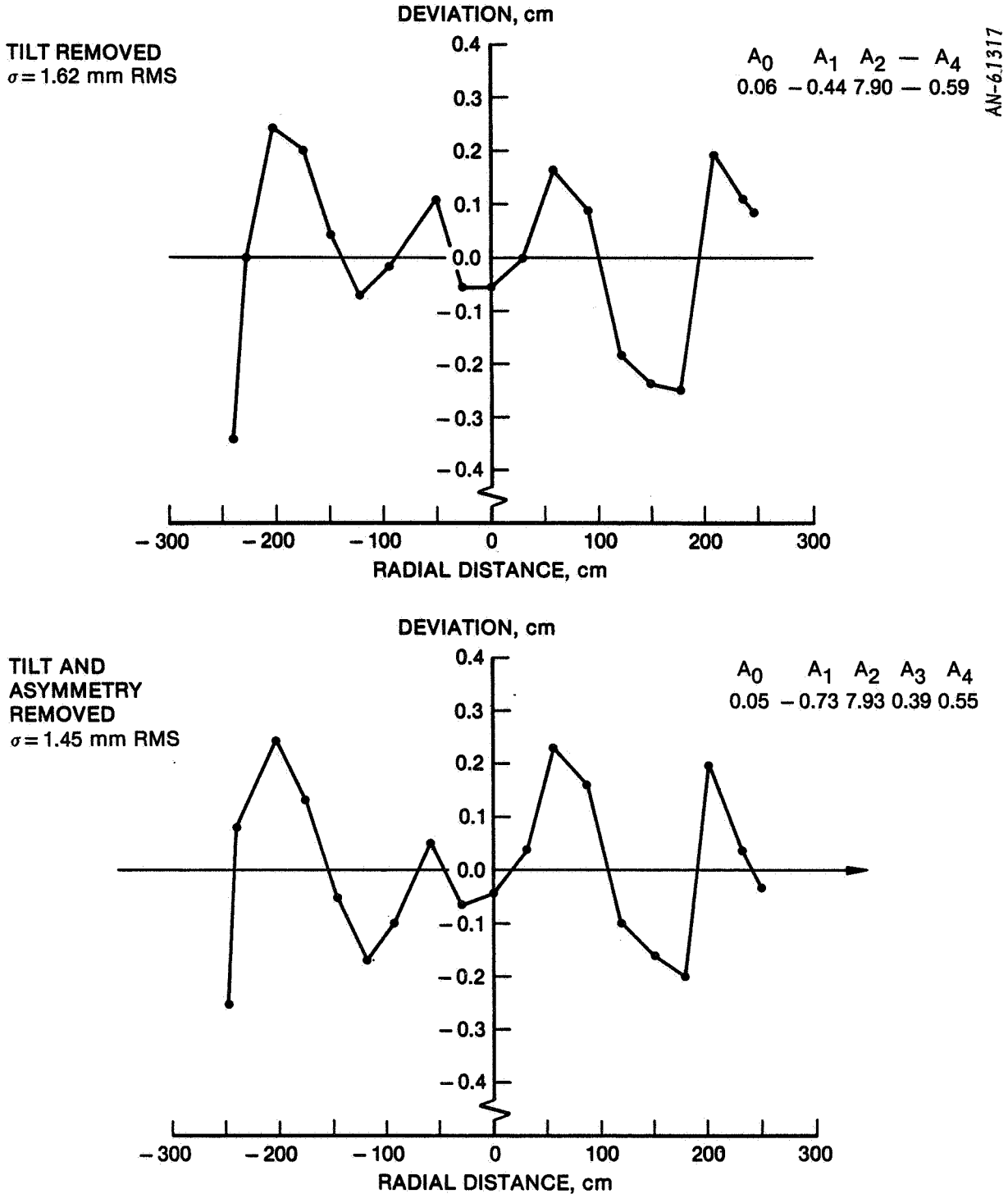

Figure 4.7. NASA Test 4-1, Line C (90°)

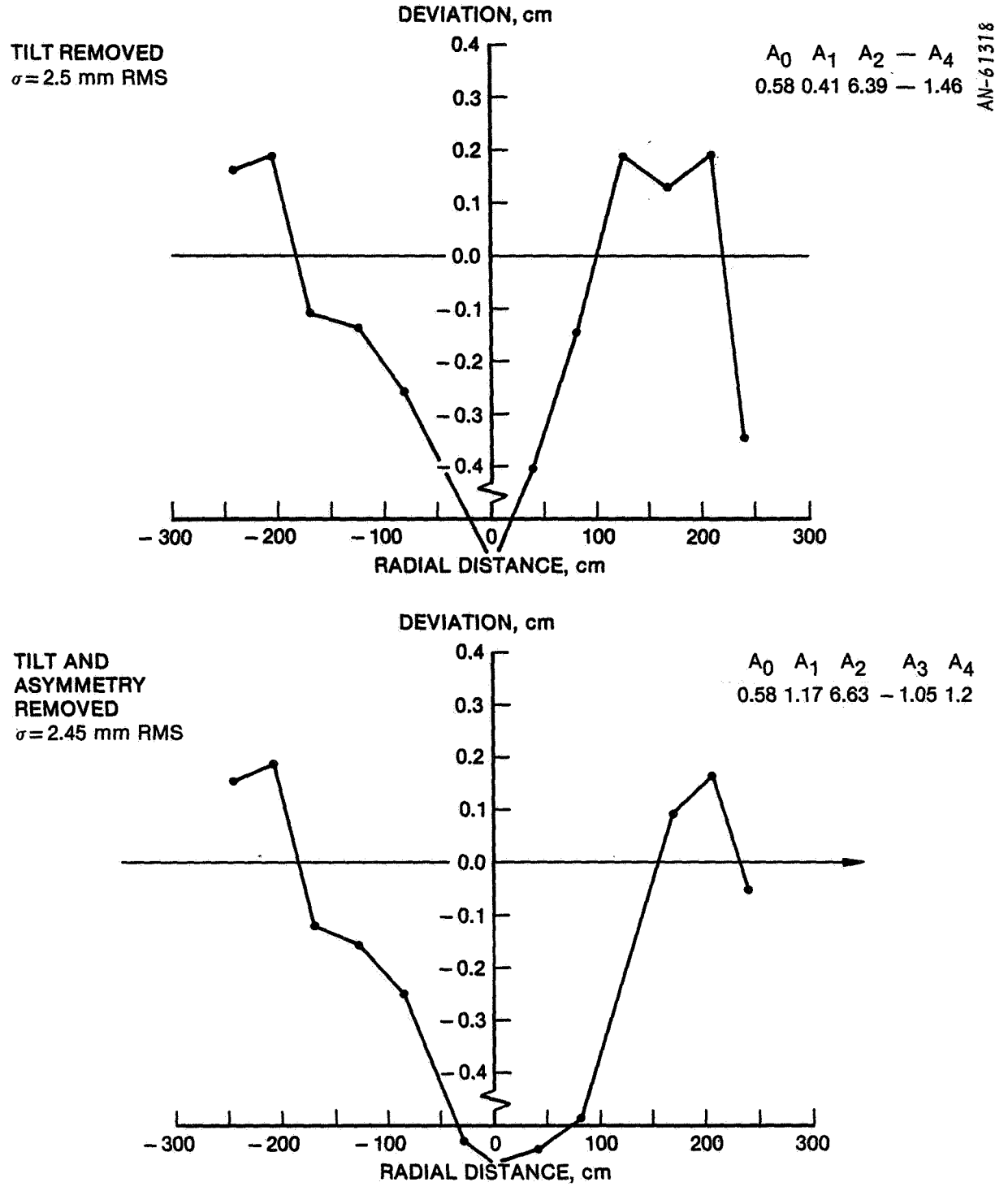

Figure 4.8. NASA Test 4-1, Line D (-45°)

REGRESSION RESULTS

TEST 4-2

OCT. 31, 1980

VOLTAGES = 46, 51, 57, 63, 68 KV

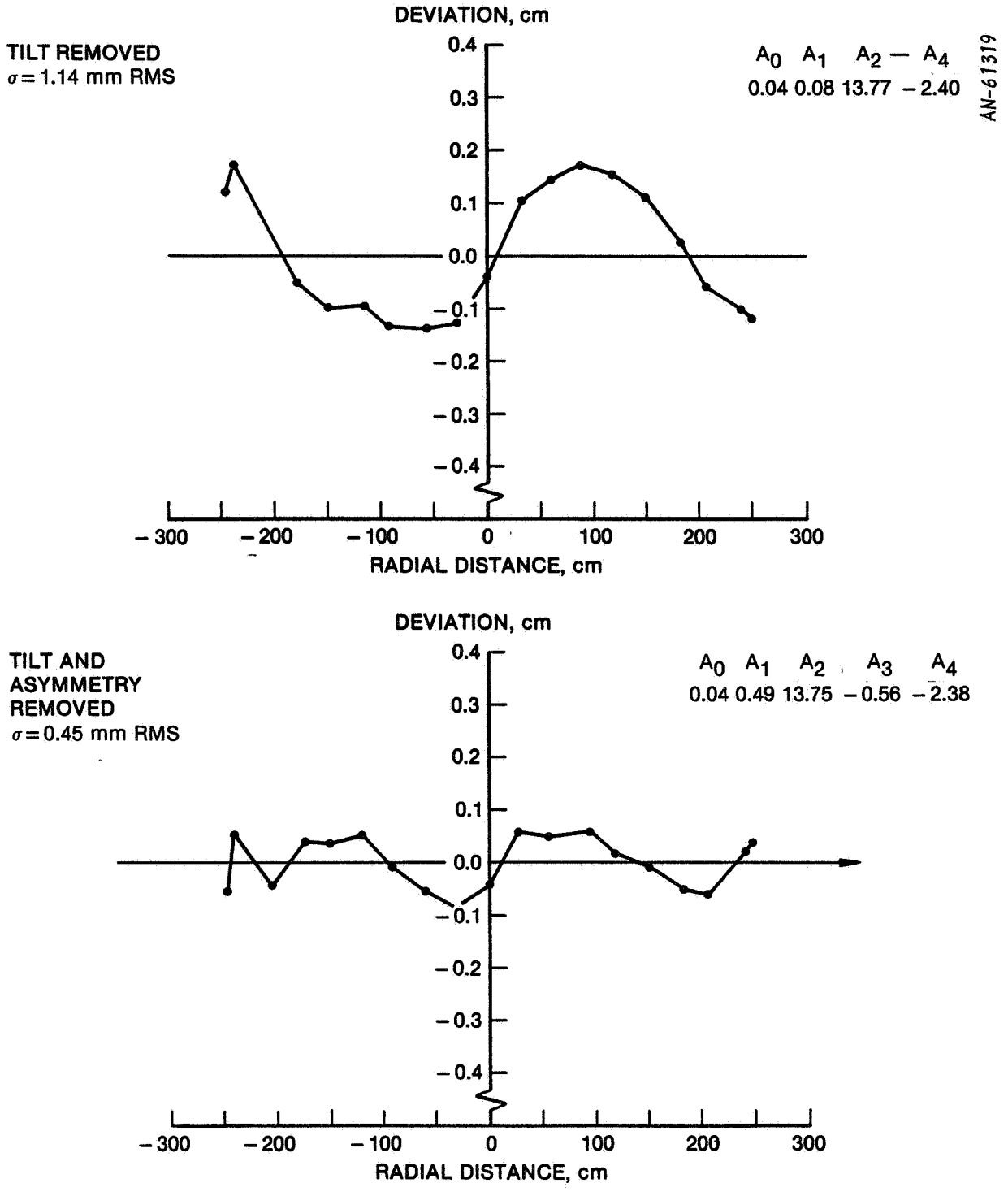

Figure 4.9. NASA Test 4-2, Line A (0°)

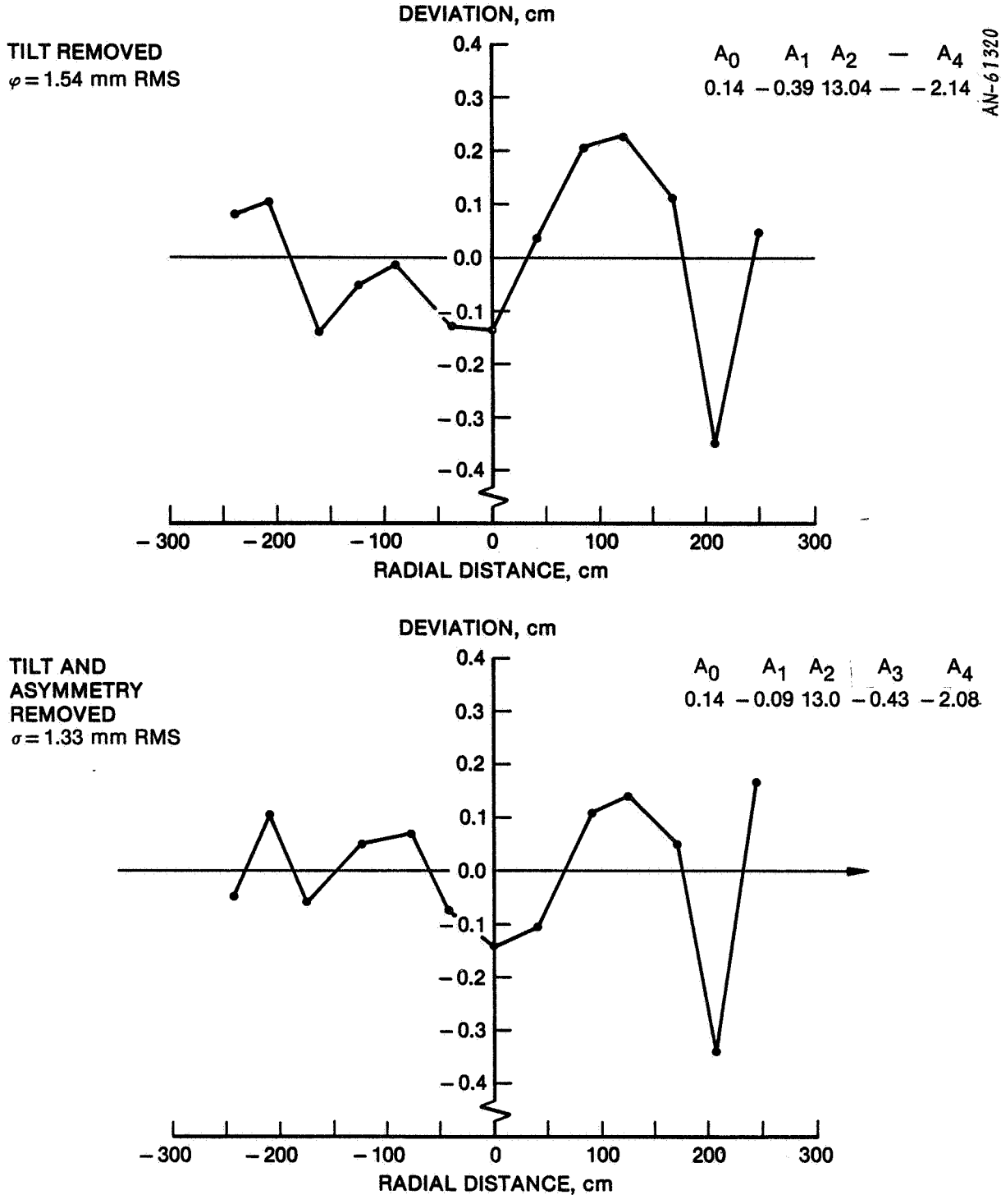

Figure 4.10. NASA Test 4-2, Line B (45°)

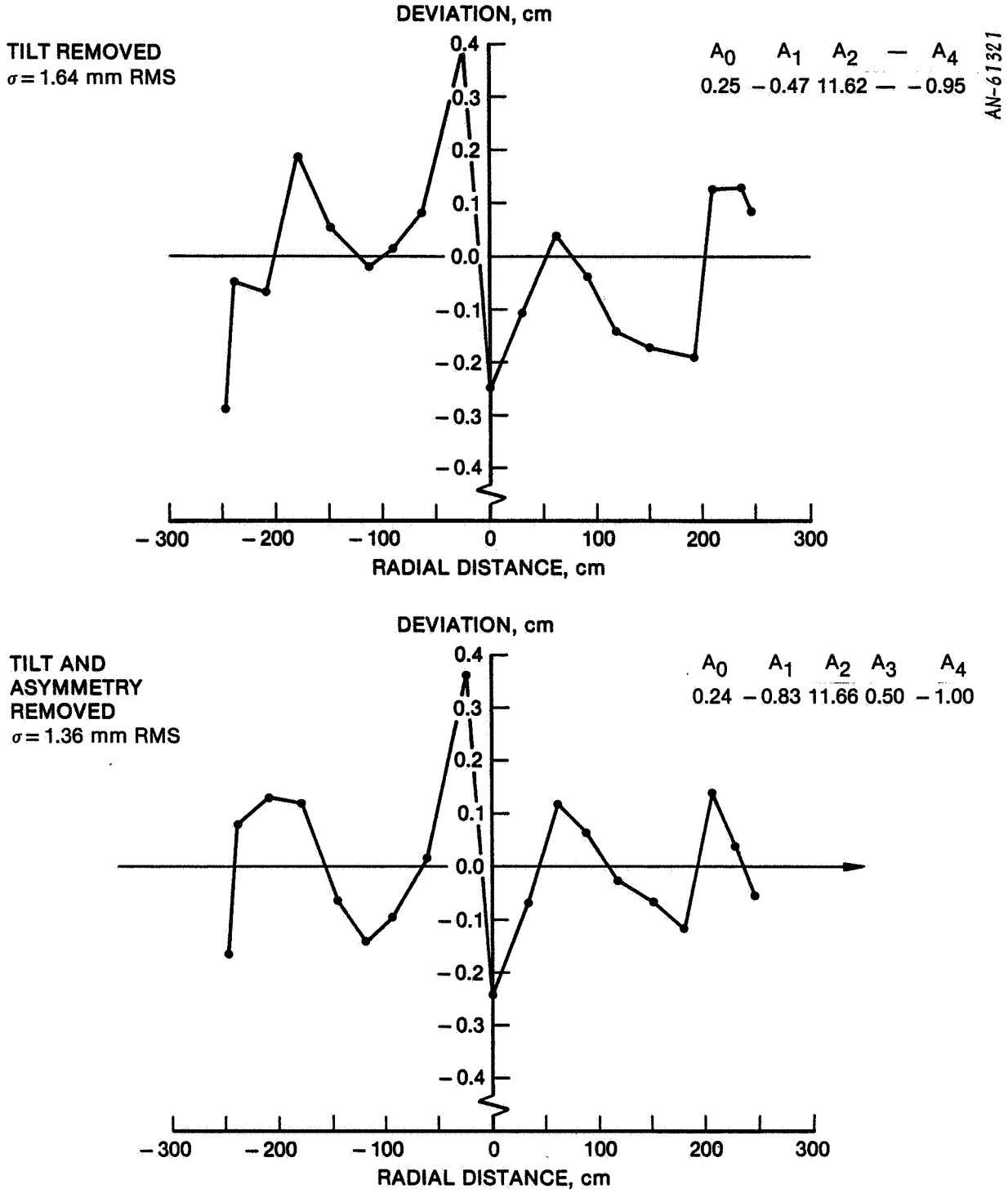

Figure 4.11. NASA Test 4-2, Line C (90°)

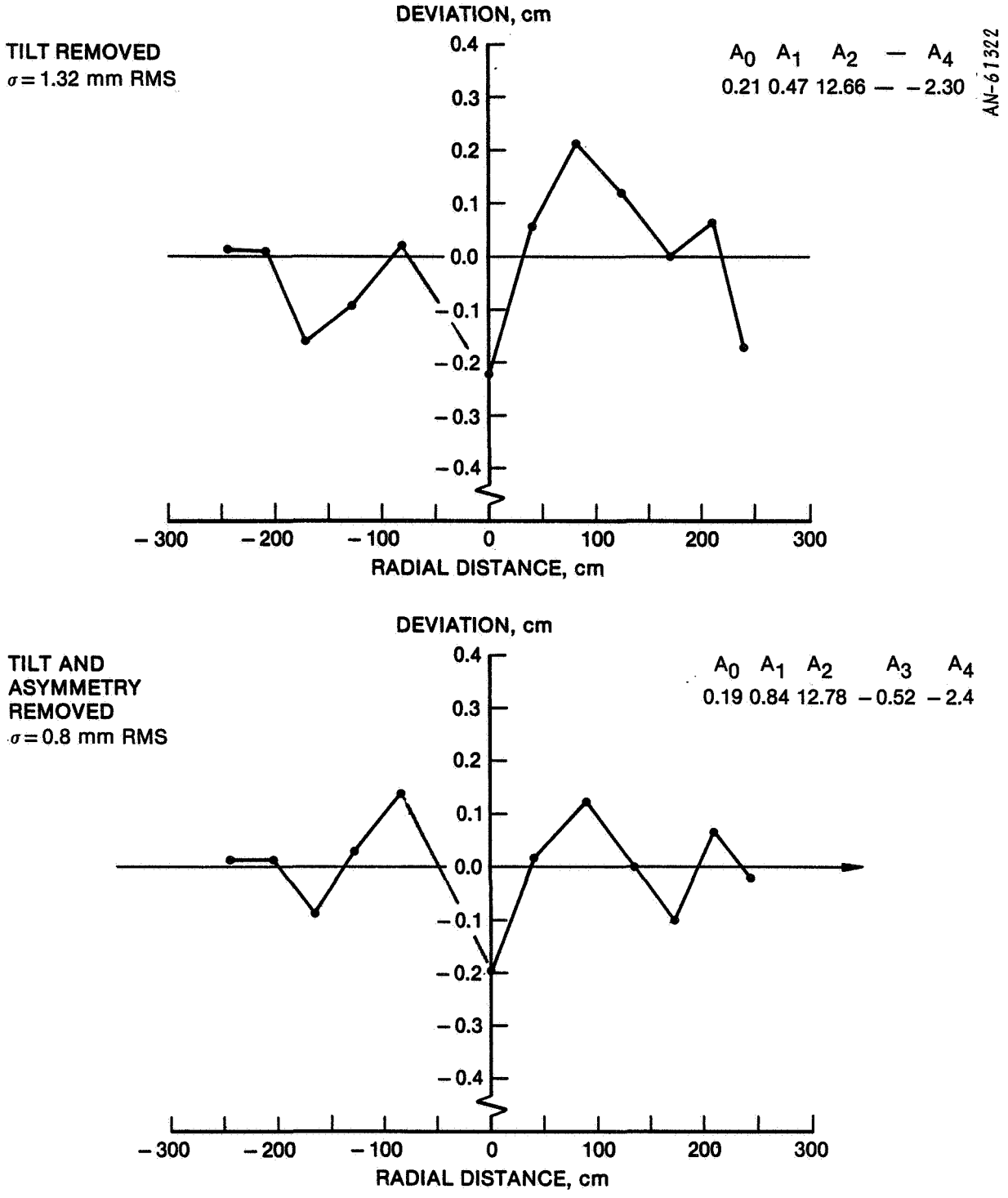

Figure 4.12. NASA Test 4-2, Line D (-45°)

REGRESSION RESULTS

TEST 4-3

NOV. 3, 1980

VOLTAGES = 40, 40, 40, 40, 40 KV

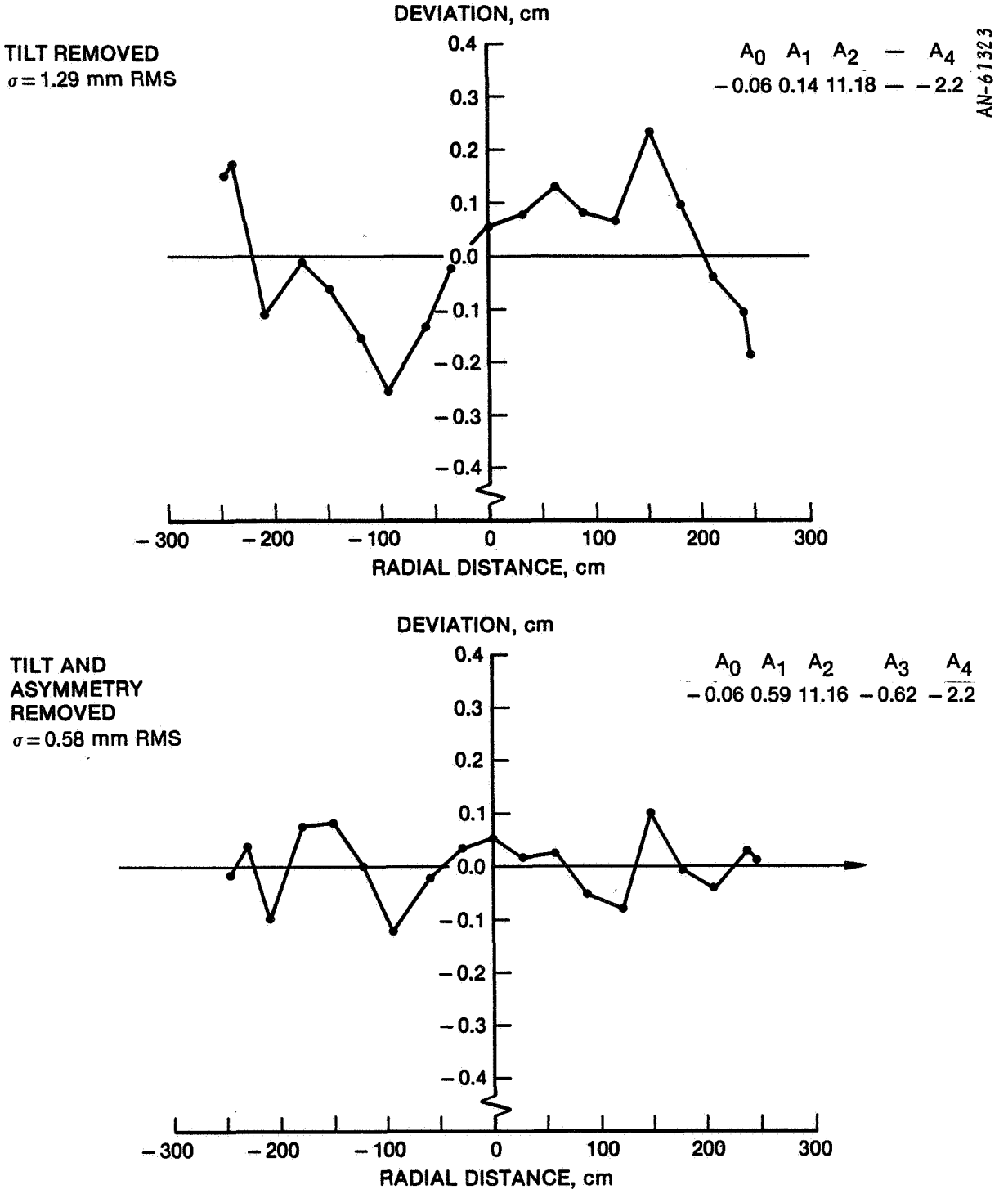

Figure 4.13. NASA Test 4-3, Line A (0°)

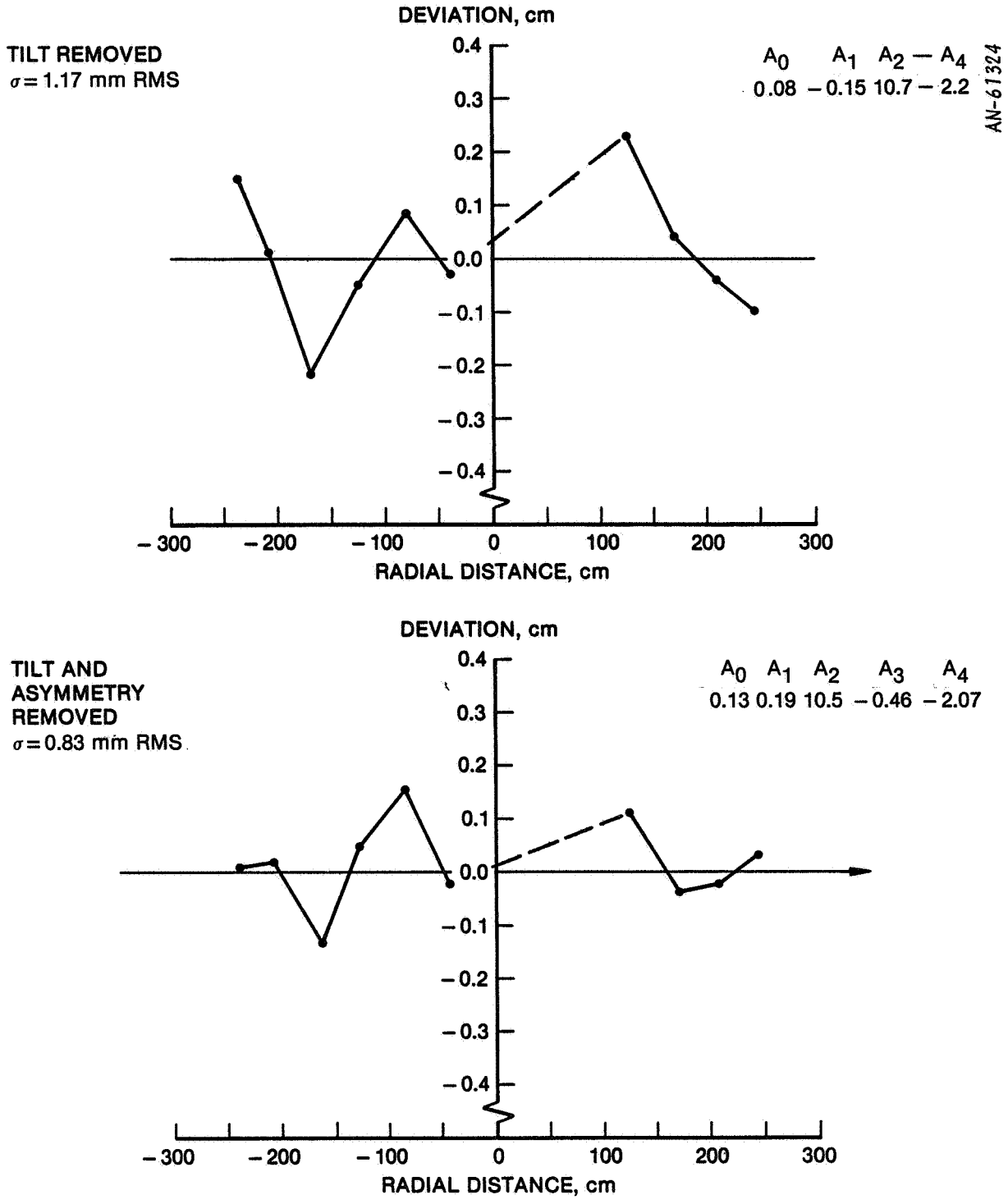

Figure 4.14. NASA Test 4-3, Line B (45°)

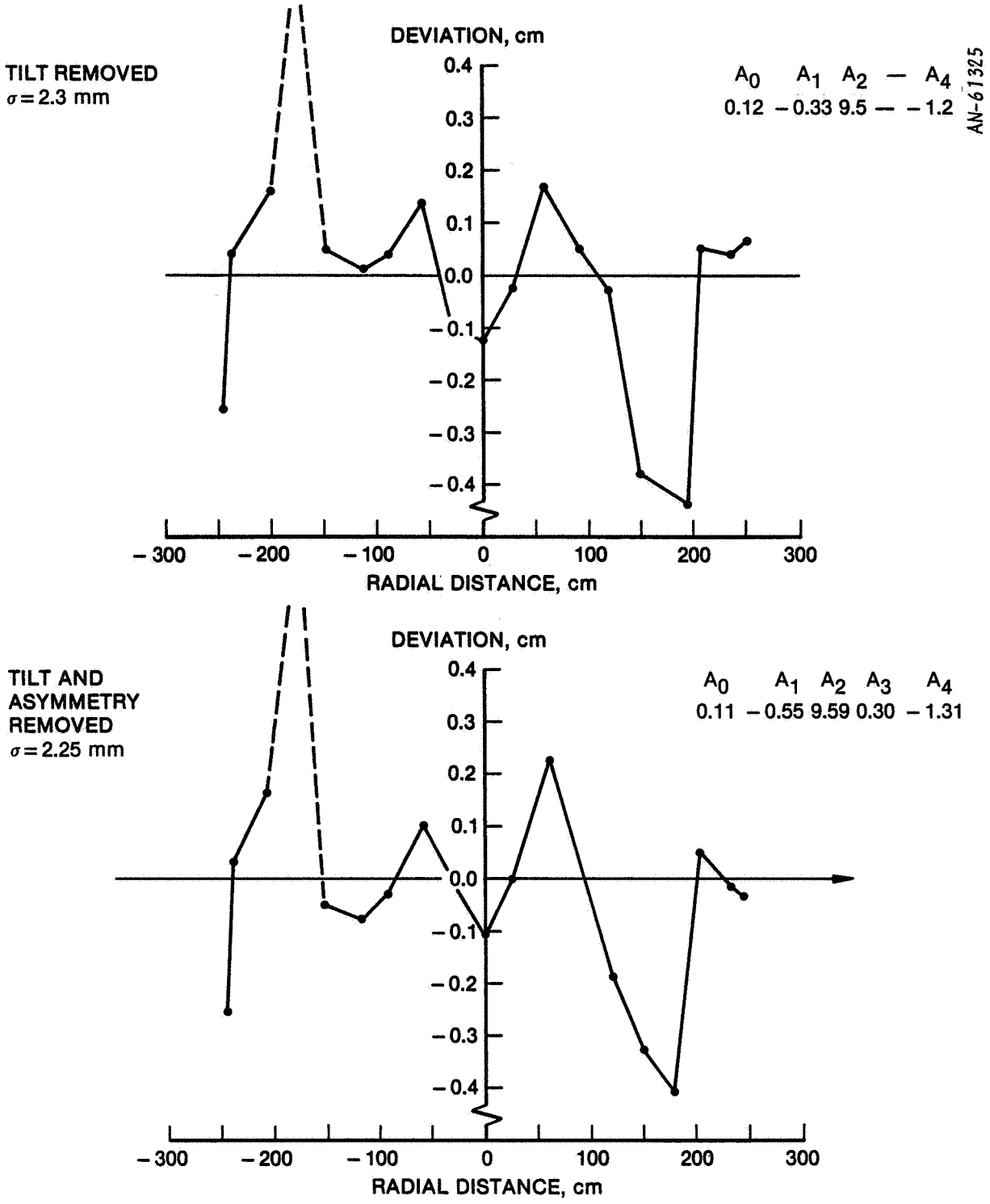

Figure 4.15. NASA Test 4-3, Line C (90°)

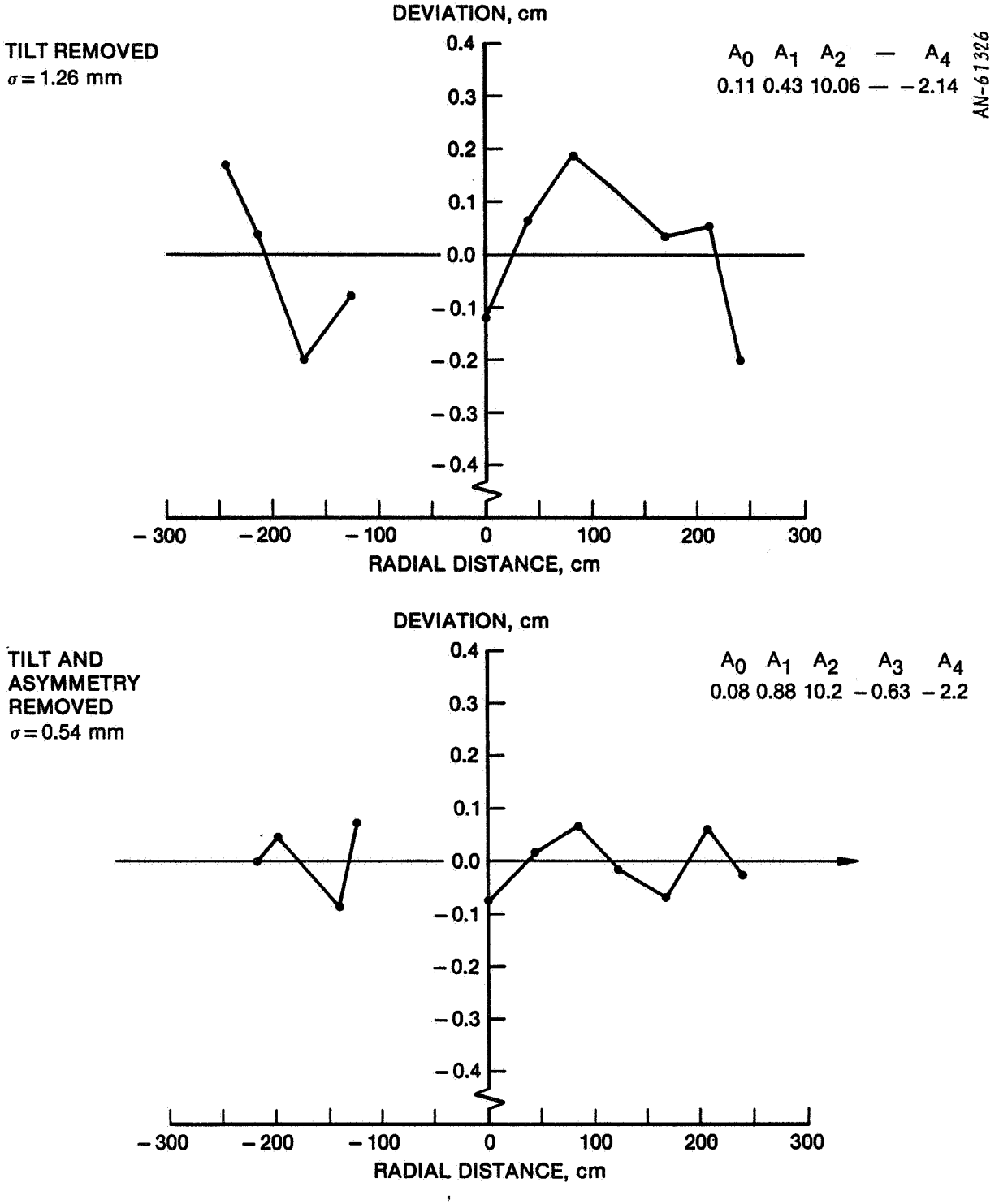

Figure 4.16. NASA Test 4-3, Line D (-45°)

5 3-D PLOTS

Displaying the membrane reflector quality and behavior has been aided considerably by 3-D projections of surface errors. The plots provide an indication of error sources and error propagation. Design improvements suggested and/or confirmed by these plots have substantially enhanced the surface quality. These improvements included:

- a flatter rim to which the membrane reflector is attached
- perimeter tension adjustments of the membrane
- elimination of tilt of the electrode surface with respect to the rim
- extension of the electrode surface area closer to the rim

The 3-D plots show views from several orientations. To aid in reading the plots, they are labeled with R (right), L (left), T (top), and B (bottom). R denotes the right side as observed when looking into the aperture (Fig. 5.1-a).[1] In the 3-D plots, it is not the reflector shape that is plotted but the residual between the reflector surface, $Z_{measured}$ and the ideal shape, Z_{ideal}. The measured shape, $Z_{measured}$, shown by the dashed line in Fig. 5.1-b corresponds to a positive residual. This lack of deflection near the rim would be shown as a symmetric upward (positive) bulge in the 3-D plots.

The following 3-D plots are annotated with engineering notes on the error shape distribution. The prior 2-D regression equations can be reviewed and correlated to the 3-D residual plots.

In all plots, the vertical scale is 100 times the horizontal scale (compare the 10 mm height of the reference frame in each plot with the diameter of the mirror, which is 4880 mm). Each plot is labeled with an average radius of curvature, ρ, and the voltages on the five electrodes.

[1] Figures 5.11-5.12 and 5.16-5.27 appear to be mirror-imaged compared with the other figures, because of the difference in sign of the out-of-plane viewing angle "Theta".

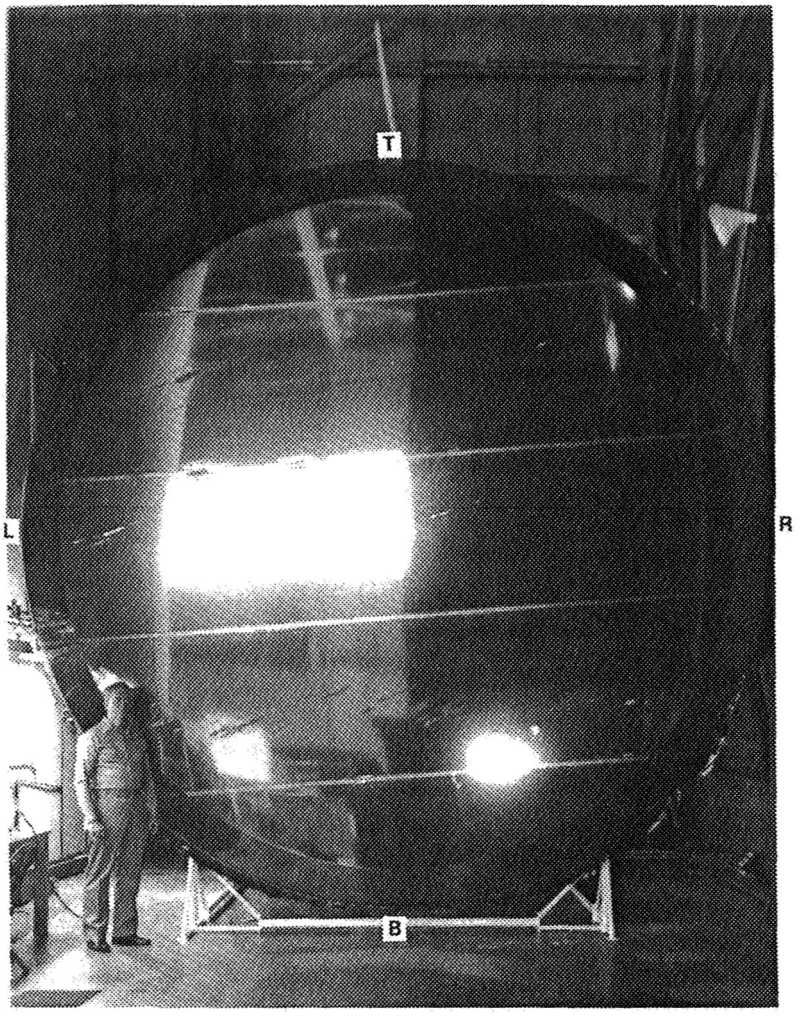

Figure 5.1-a. Rim Reference Locations

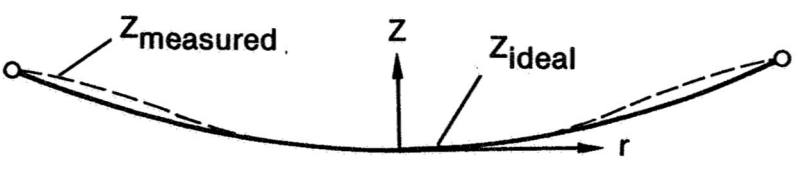

Figure 5.1-b. Coordinate Notation for Residual Error, $R = Z_{measured} - Z_{ideal}$

The overwhelming error is the periodic perimeter deformation that propagates over the aperture. This perimeter deformation will be seen in Tests 4-1 through 4-3. Subsequently, the rim flatness was improved, which mitigated this error distribution.

The seam/material irregularity over the central portion of the surface causes ridges in the left-right direction.

Along the rim, the plot exhibits a positive annular "bulge". All the subsequent plots will show this bulge. It is attributed particularly to the lack of electrode surface area near the rim and a consequent lack of pressure. The membrane reflector surface area is 27 percent larger than the electrodes. In most cases, the pressure near the rim could be made larger by increasing the voltage on the outermost electrodes.

Tests 4-1 through 4-3 used a 0.3 mil Kapton membrane aluminized on one side.

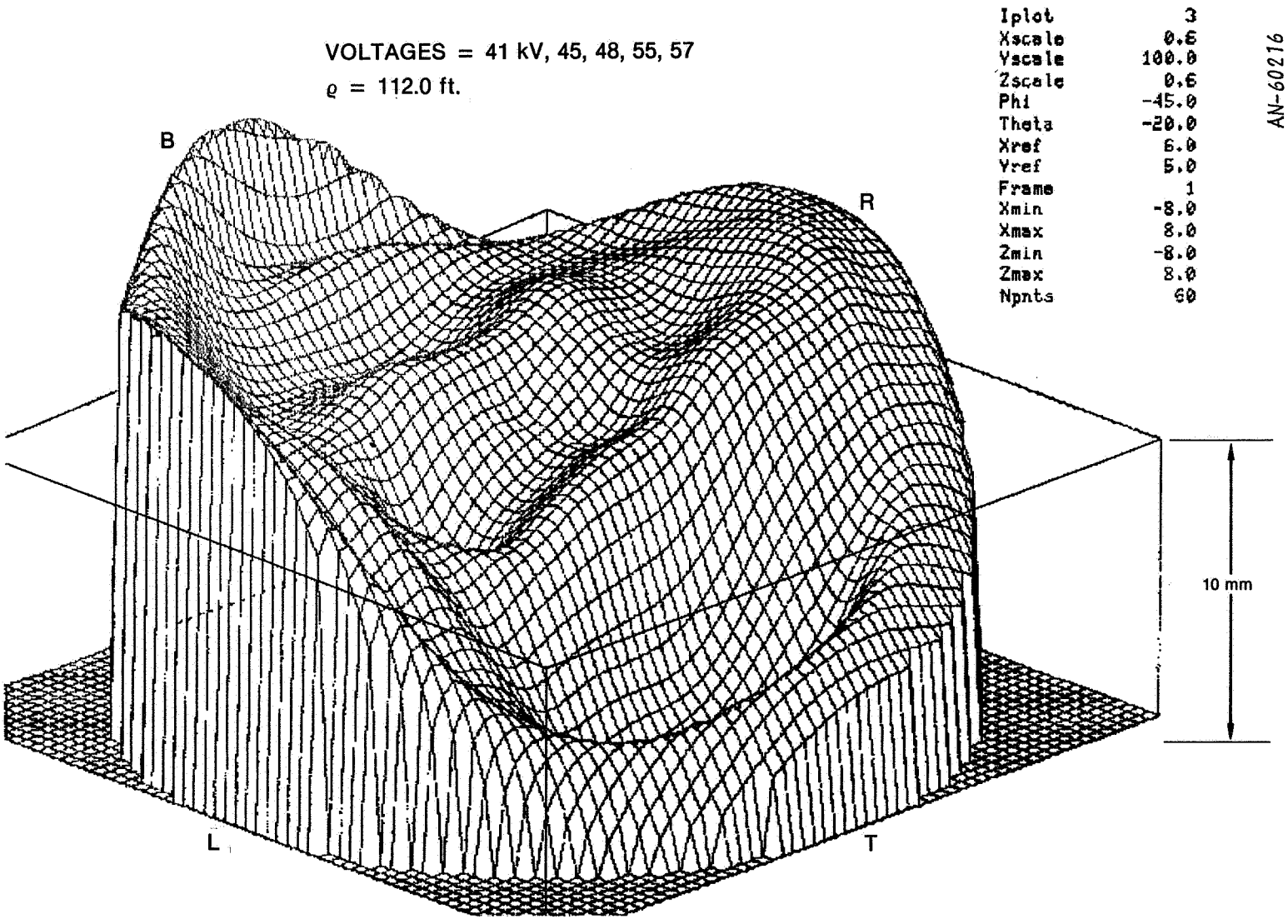

Figure 5.2. 3-D Plot, Test 4-1

The rim is shown alone. The viewing orientation is the same as in the previous figure for easy comparison.

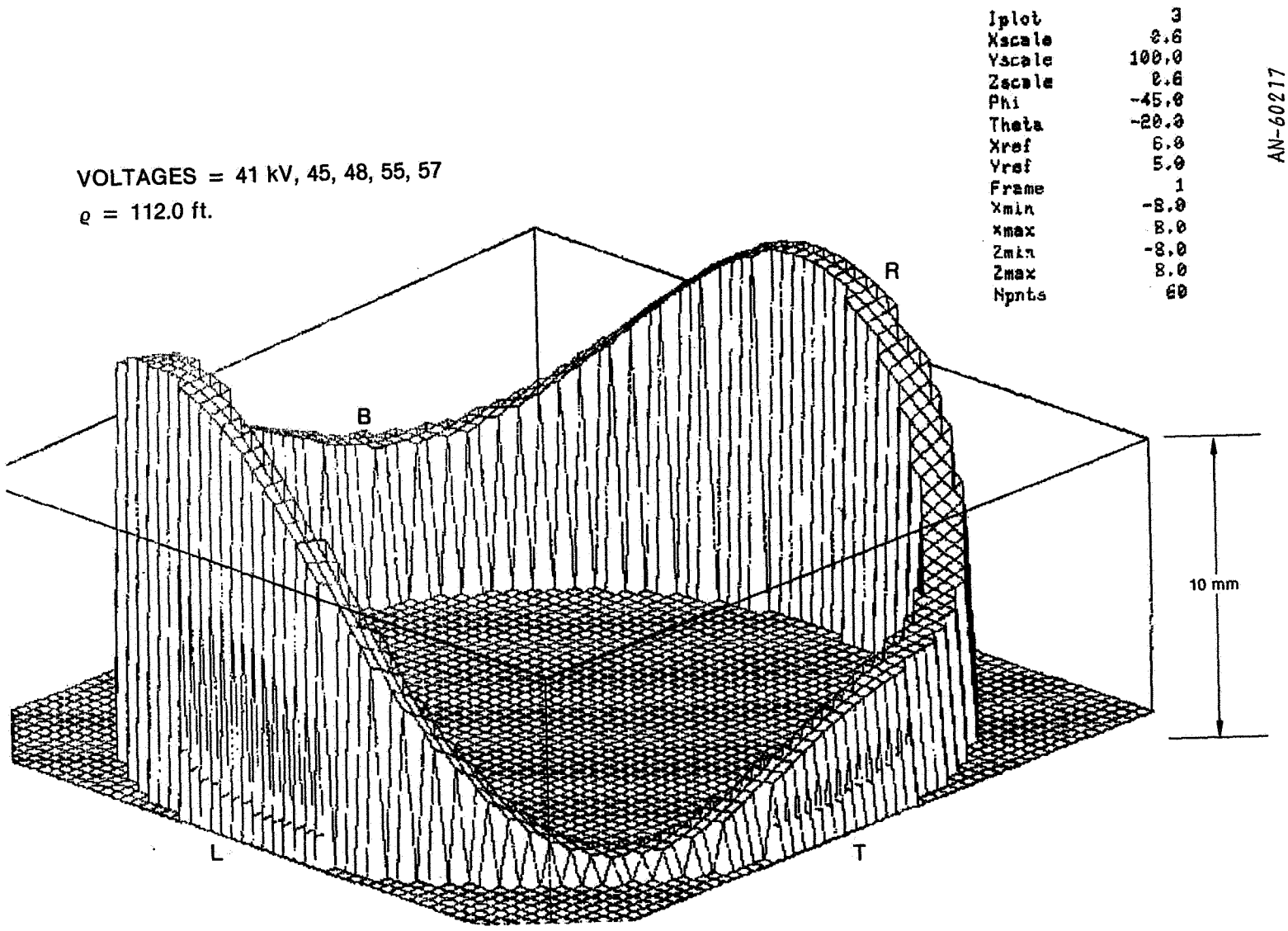

Figure 5.3. 3-D Plot, Test 4-1 (Rim Alone)

The error distribution is shown looking directly toward the edge of the rim. The zero error plane (identified) provides the proper reference for scaling error sources from this ideal reference. The largest error source is the rim deformation.

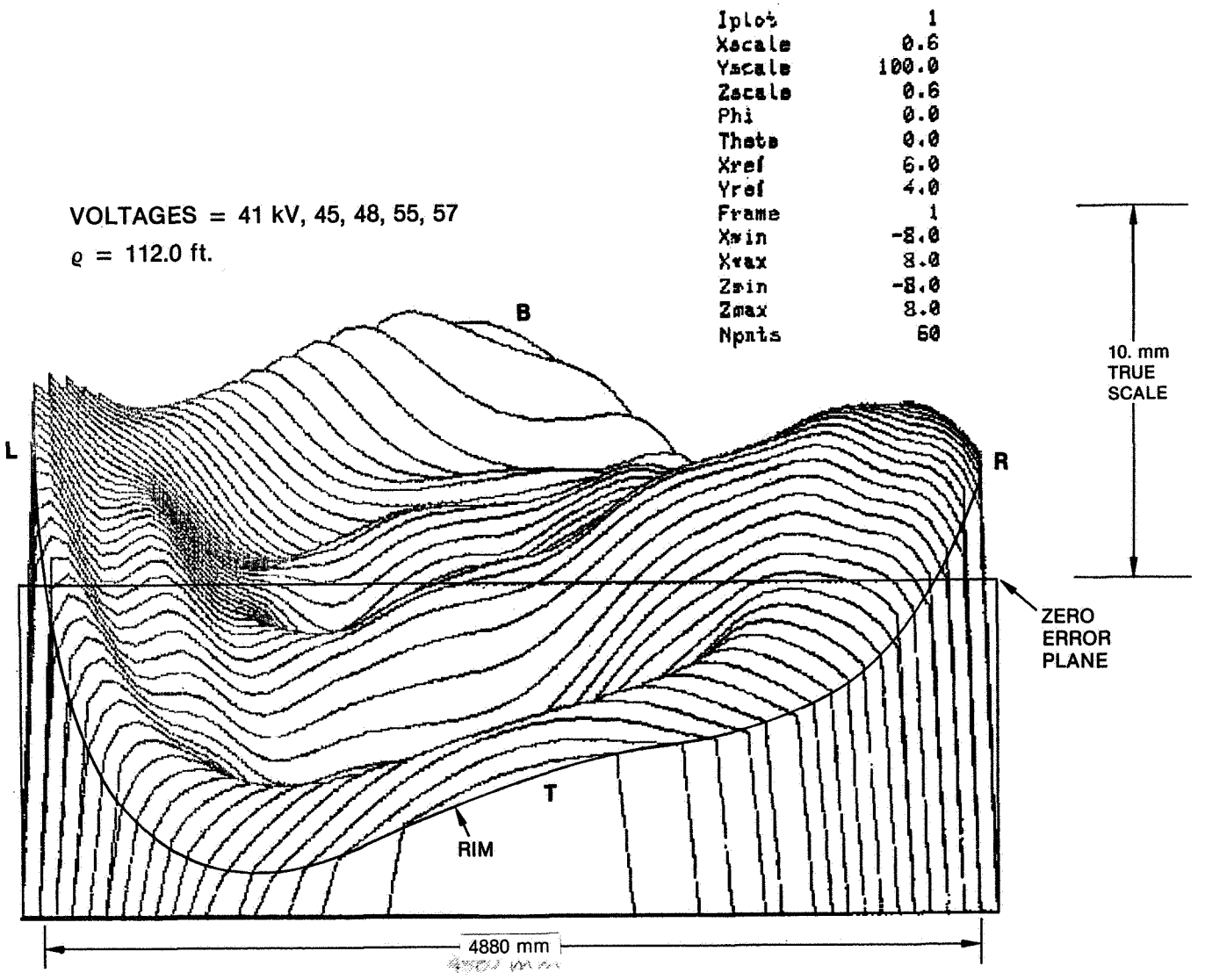

Figure 5.4. 3-D Plot, Test 4-1

The horizontal contour lines provide an indication of the surface waviness when traversing in the top-bottom direction. The seams are aligned from left to right.

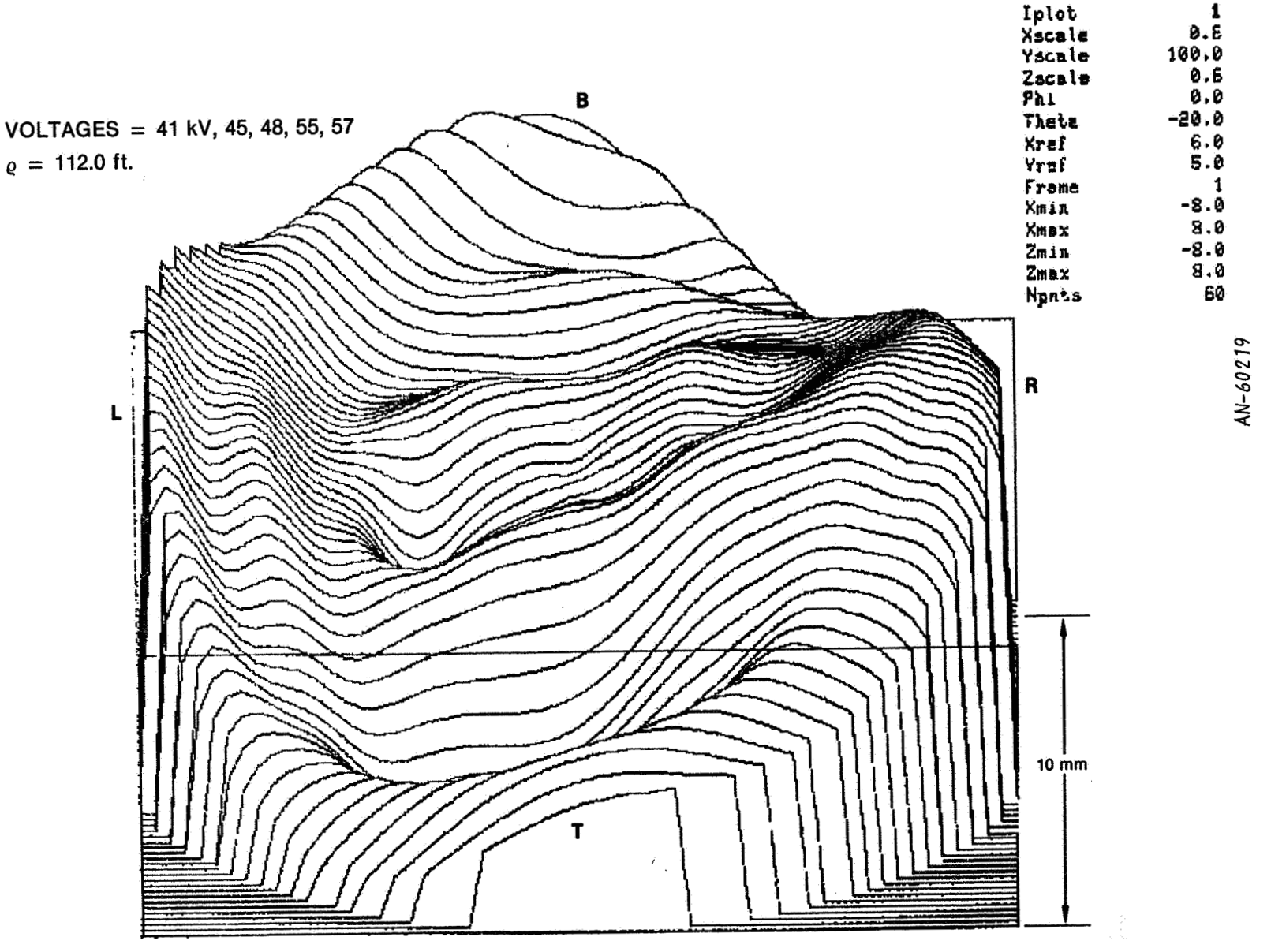

Figure 5.5. 3-D Plot, Test 4-1

A higher voltage distribution than the prior example results in larger deflections and stress. However, the same characteristic errors are evident. The annular "bulge" along the rim perimeter is somewhat reduced. The seam/material errors are apparent.

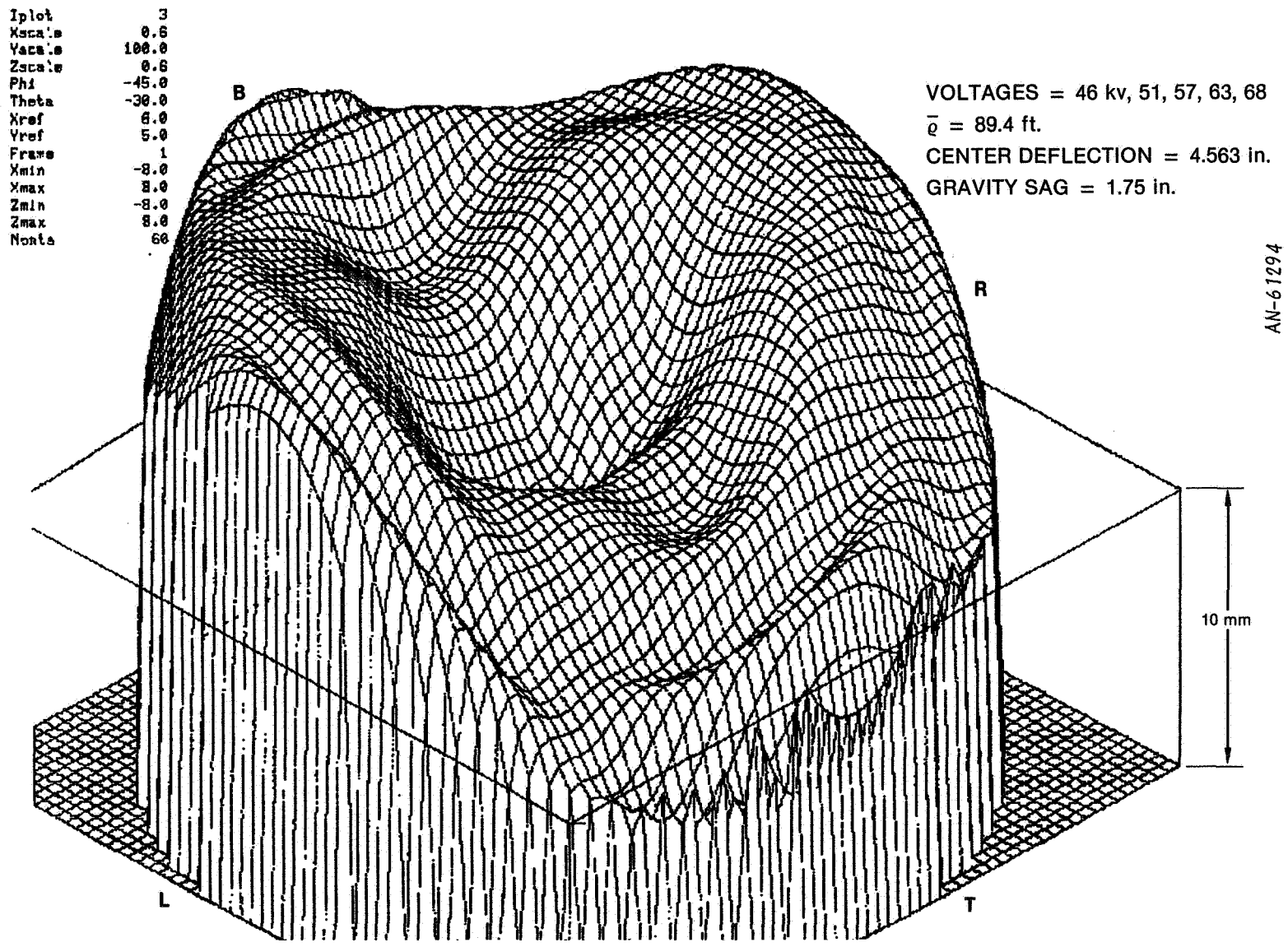

Figure 5.6. 3-D Plot, Test 4-2

A view from the top looking downward using horizontal contour lines defines the seam/material errors. The central deflection of 4.563 inches exceeded the design deflection of 3.43 inches with the specified voltage. The gravity sag deflection of 1.75 inches exceeded the design gravity deflection of 1.2 inches. Thus, the membrane was attached to the rim in a "loose" state possibly caused by humidity effects which led to the large central deflection.

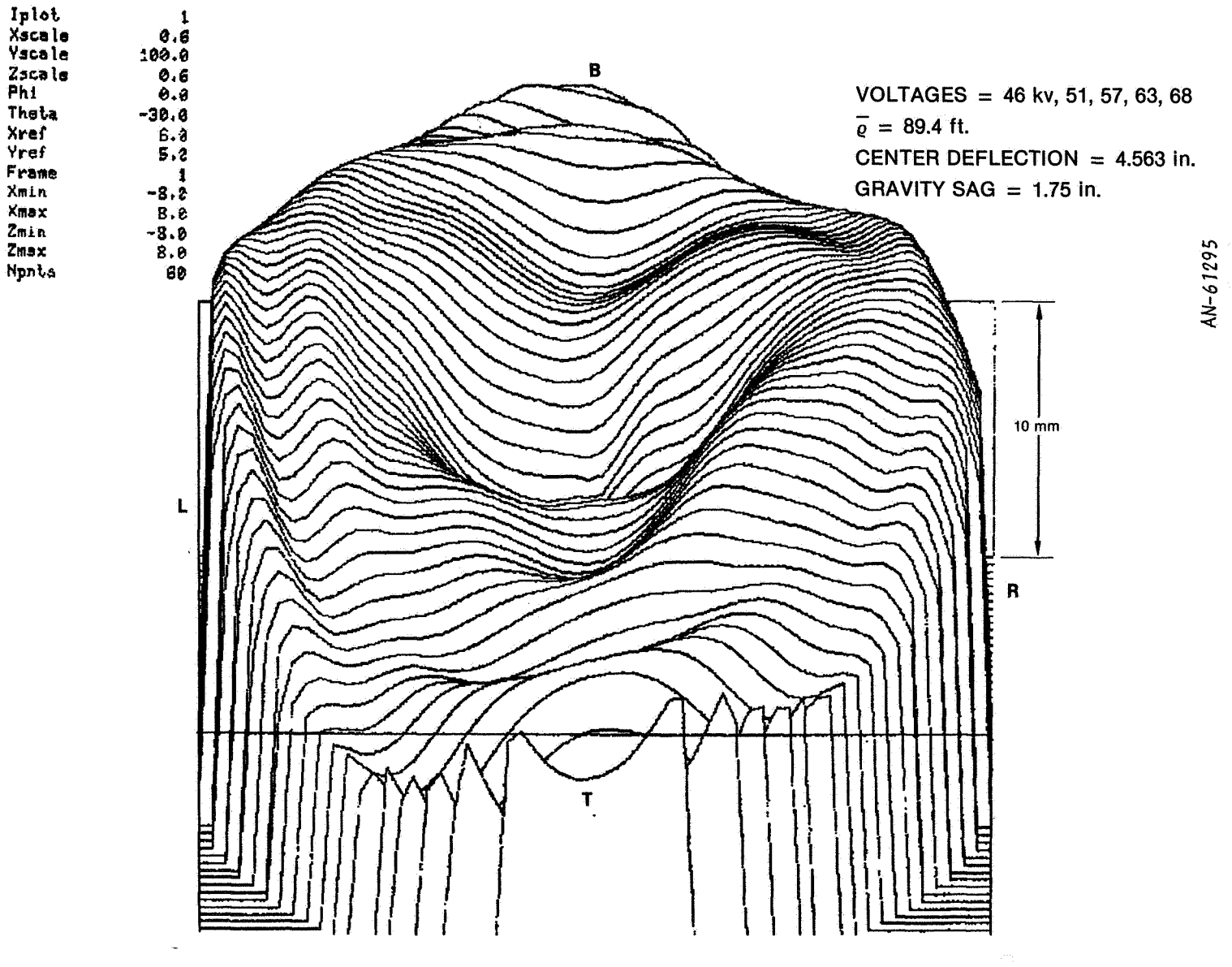

Figure 5.7. 3-D Plot, Test 4-2

The error distribution associated with a constant voltage, Test 4-3, does not appear much different than Tests 4-1 and 4-2. Again, the rim deformation dominates the error distribution.

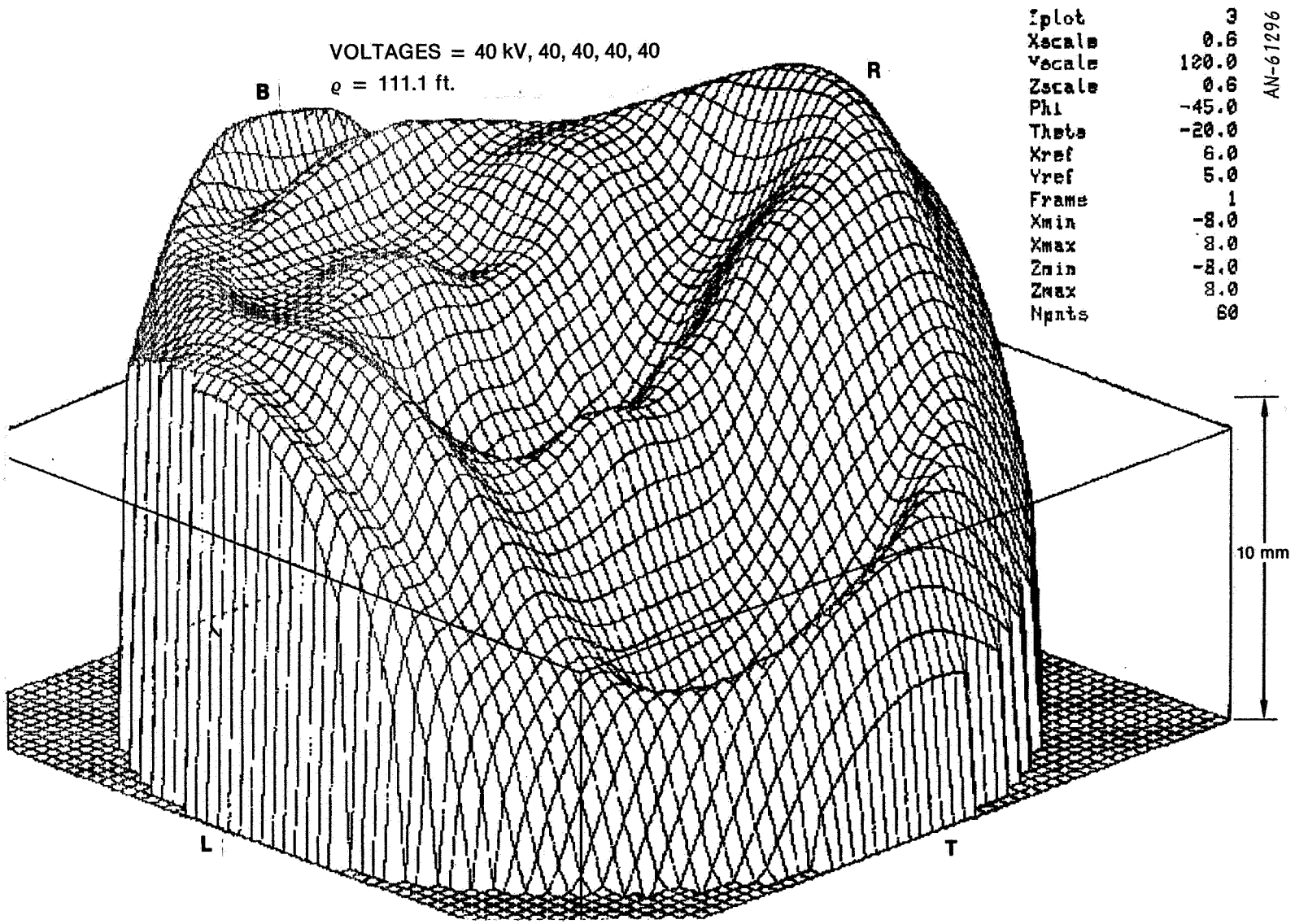

Figure 5.8. 3-D Plot, Test 4-3

The viewing angle is along the plane of the rim. The projected errors are in true scale. The largest error source is the rim. The next largest error source appears to be the annular deformation along the rim.

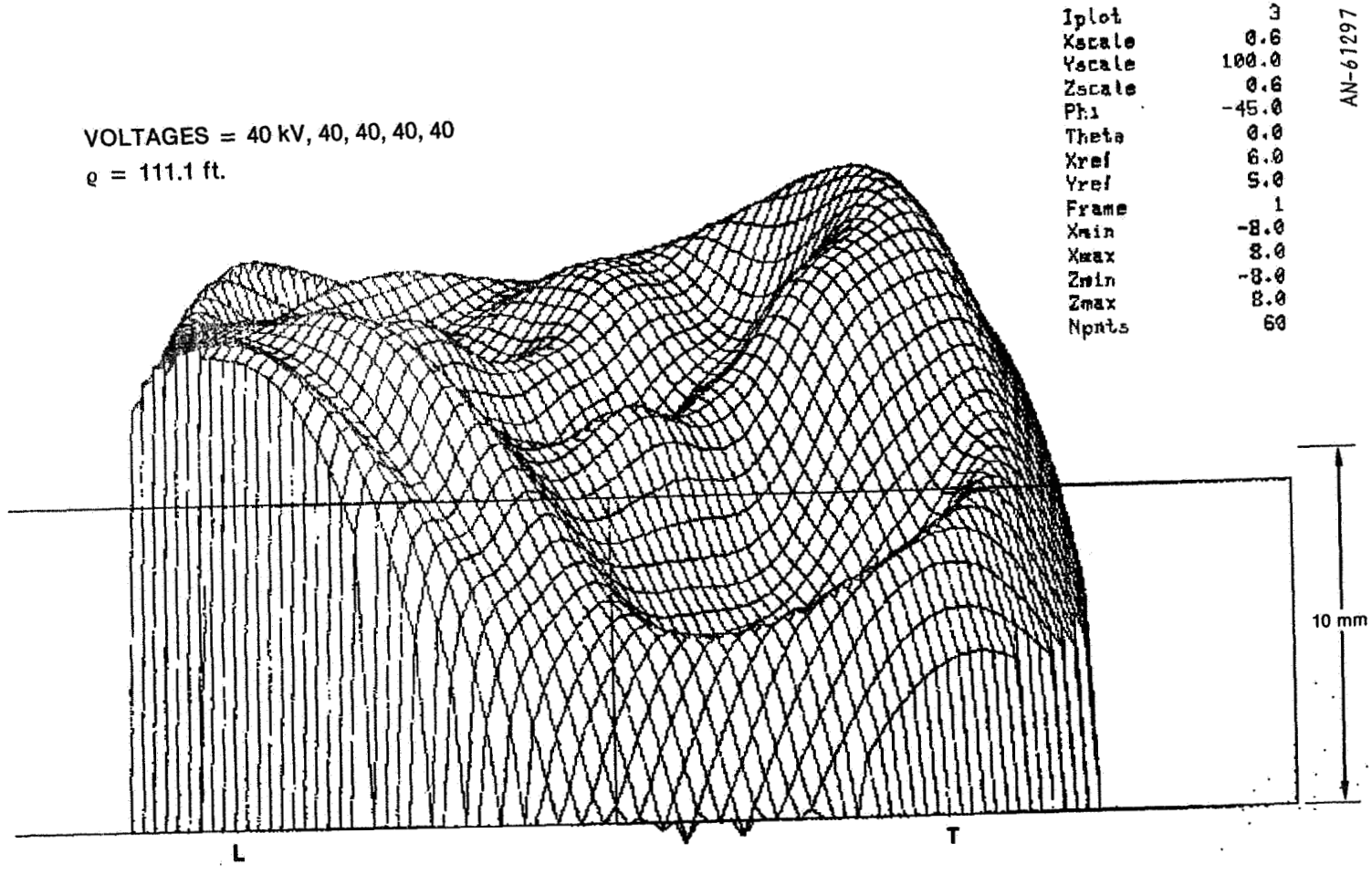

Figure 5.9. 3-D Plot, Test 4-3

Figure 5.10 compares the rim out-of-flatness errors, as obtained from the photogrammetry data. The low-frequency periodic errors that emanate from the rim cannot be compensated with this model, because no form of azimuthal control was provided in the electrode layout. Future models could provide azimuthal electrode segmentation (and voltage control) to attenuate the rim deformations. In subsequent tests, the rim was adjusted to minimize these perimeter errors.

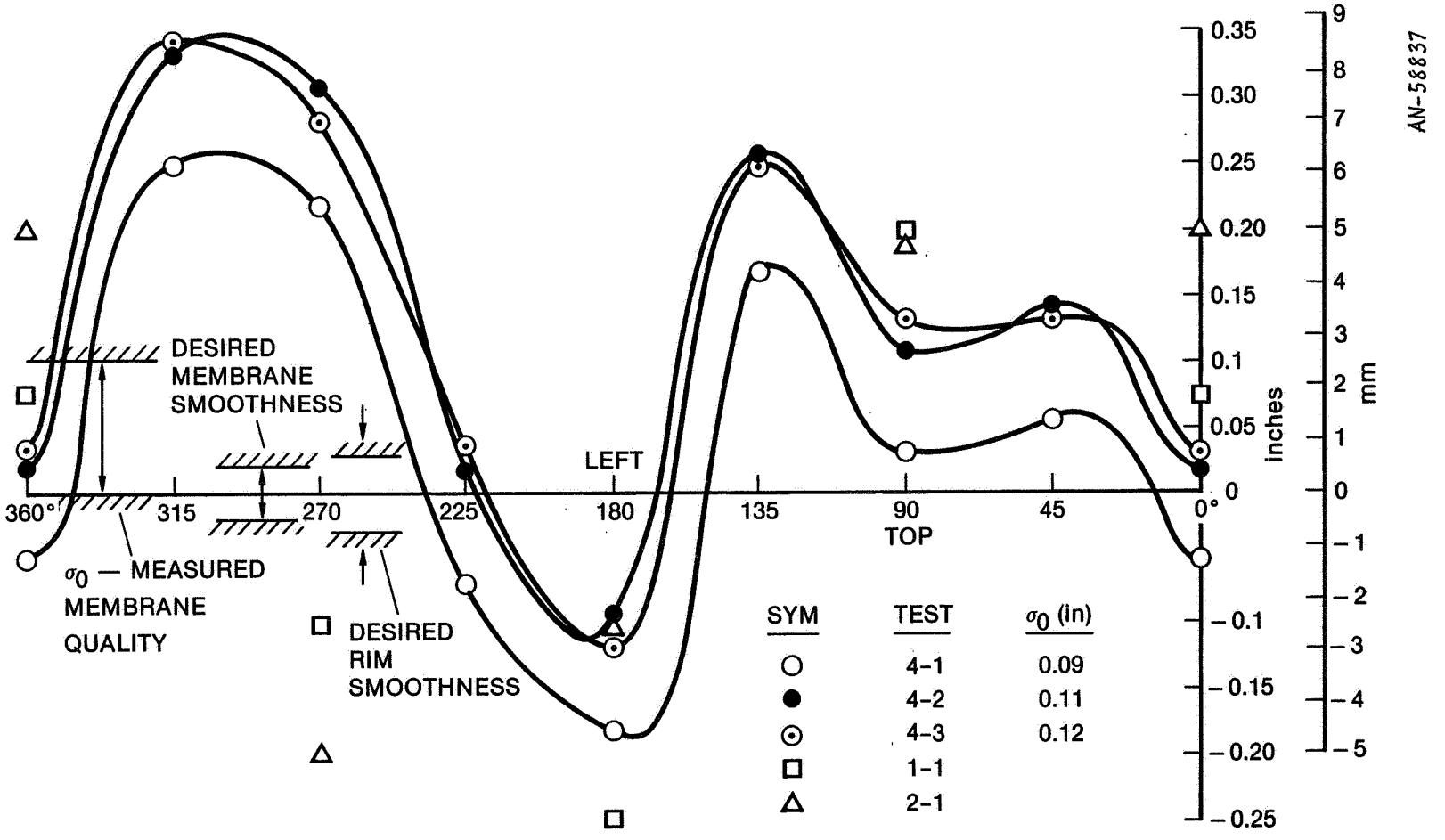

Figure 5.10. Flatness of Rim

Efforts at NASA were undertaken to eliminate the rim deformation. There was a substantial improvement as shown in the following figure. Tests 4-4 through 4-6 incorporated this rim.

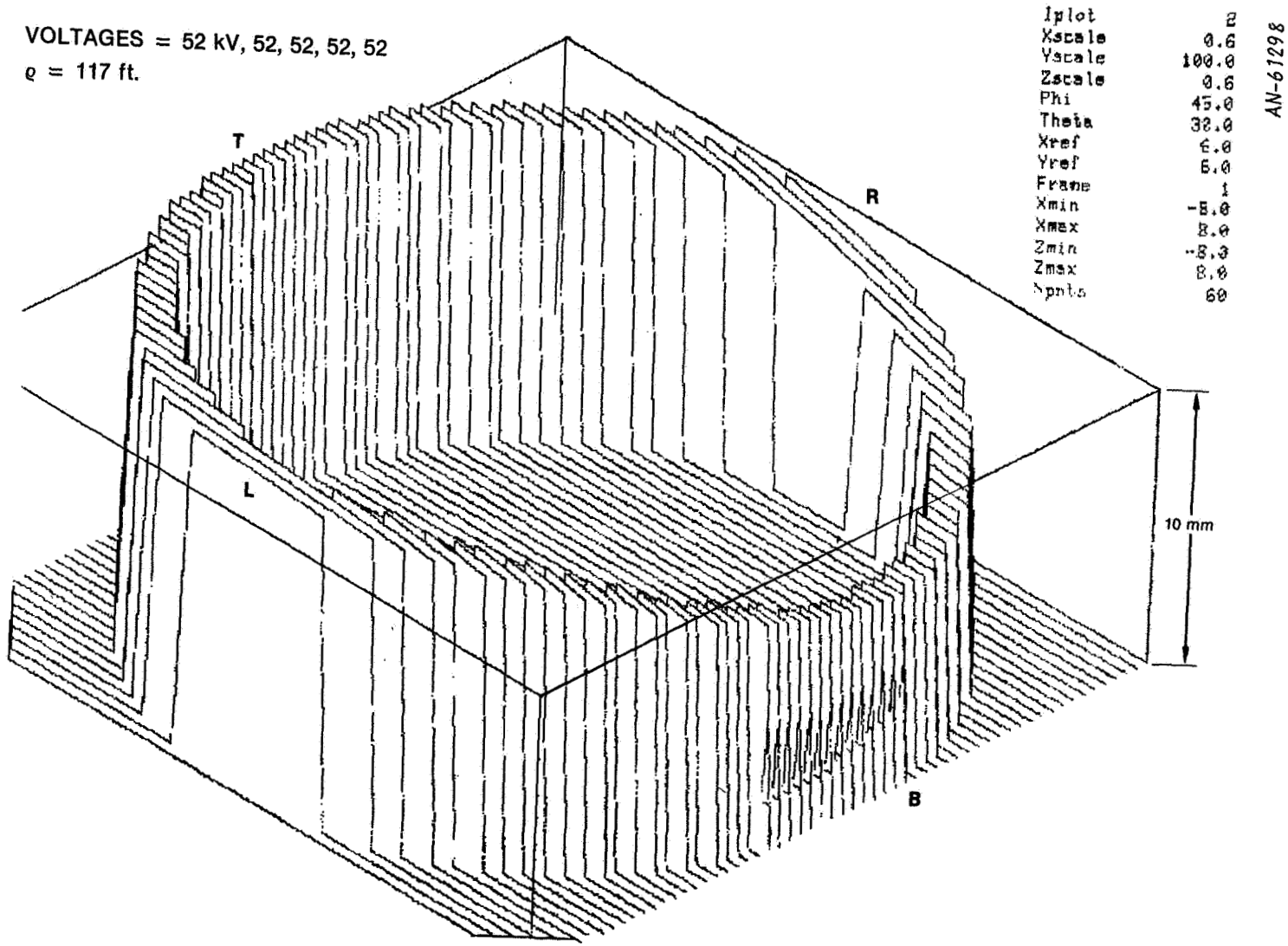

Figure 5.11. 3-D Plot, Test 4-4 (Rim Alone)

Tests 4-4 through 4-6 used a new 0.3-mil Kapton membrane with both sides aluminized. Humidity changes caused a problem between these tests by altering the membrane size.

Seam/material irregularity is not observed. The principal error appears as a non-symmetric low-frequency bulge from right to left. The right side has excessive deflection and the left side not enough. Tests 4-4 through 4-6 all have this trait. It was speculated, and confirmed, that the flat electrode surface was tilted with respect to the rim so that it was too close to the right side and too distant from the left side. This error was subsequently eliminated for test 5-1.

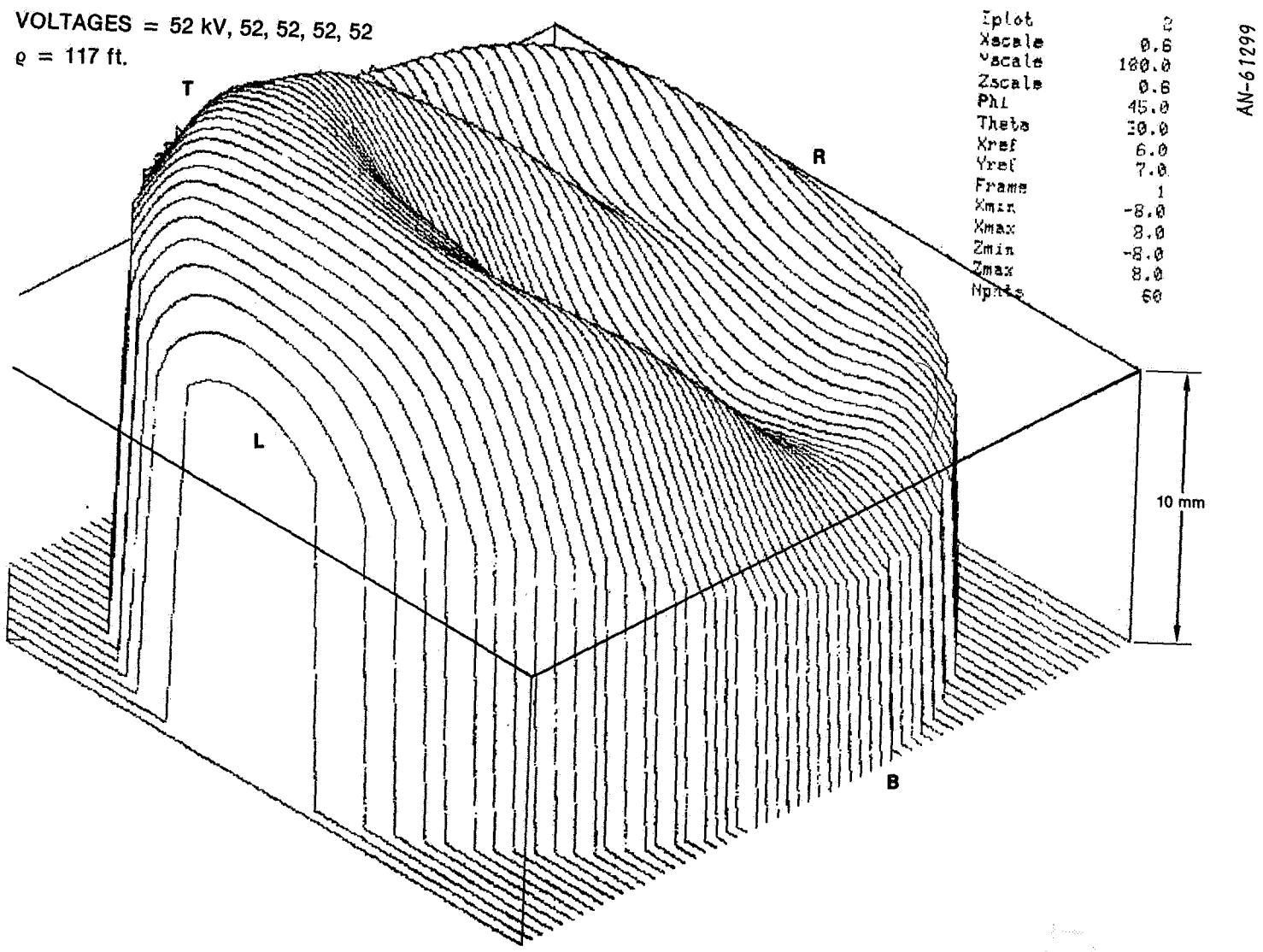

Figure 5.12. 3-D Plot, Test 4-4

This projection clearly displays the non-symmetry caused by tilt in the flat electrode surface.

Like prior cases, an annular bulge is present along the perimeter. The positive deflection is an indication that the membrane reflector did not deflect adequately near the rim. It indicates that electrostatic pressure is not adequate near the rim.

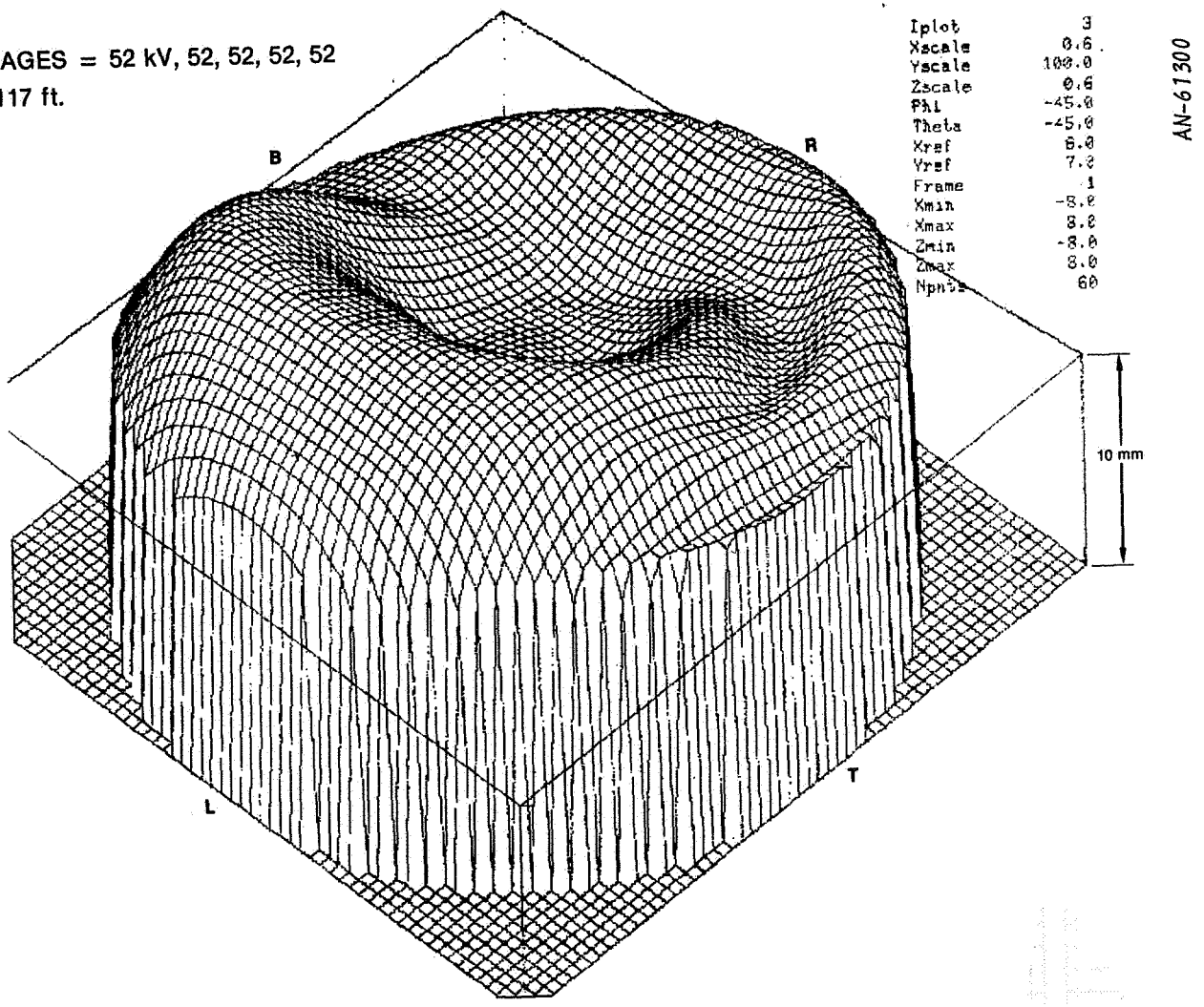

Figure 5.13. 3-D Plot, Test 4-4

Again, the excessive deflection on the right side is evident. The left side displays an under-deflection by several millimeters.

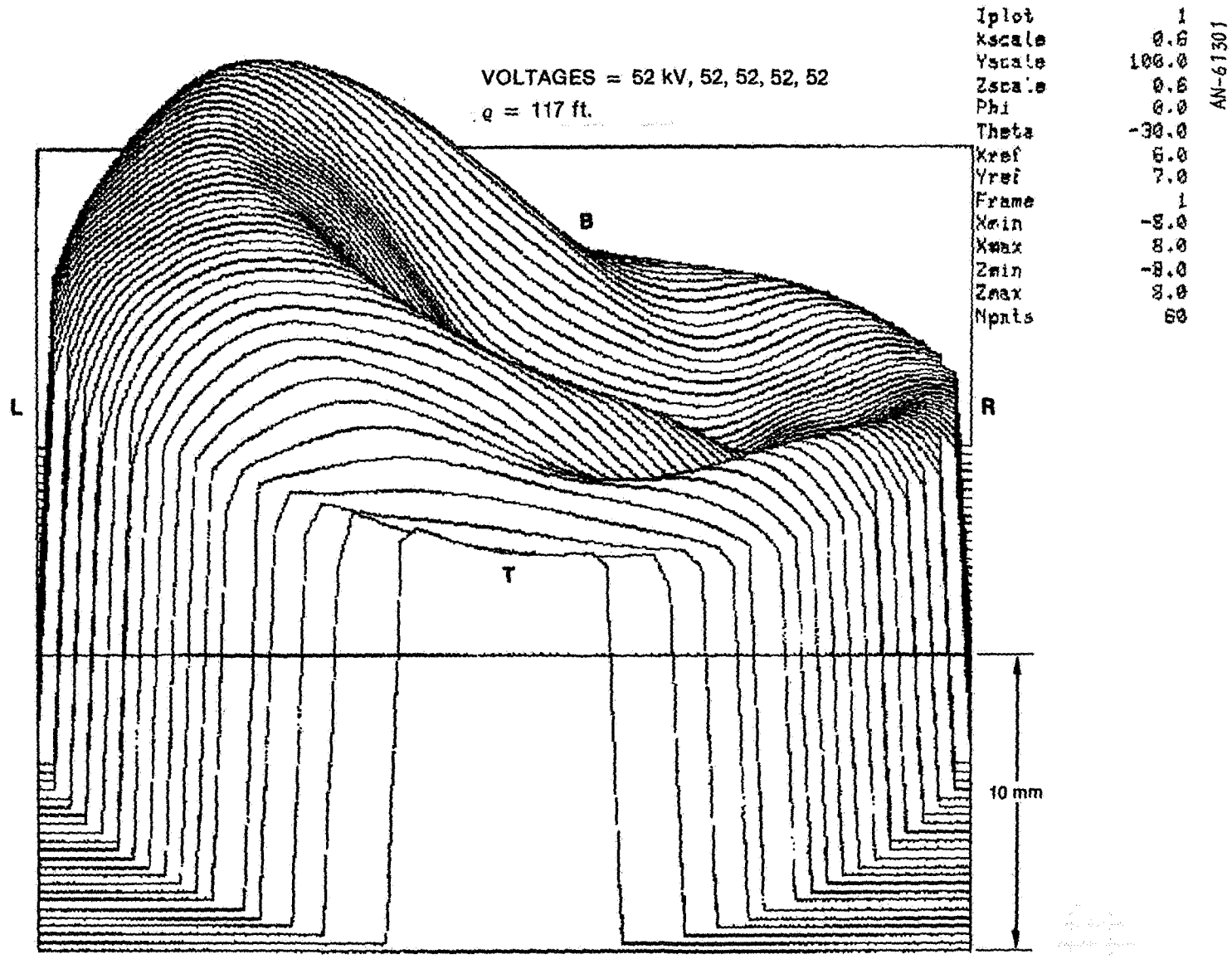

Figure 5.14. 3-D Plot, Test 4-4

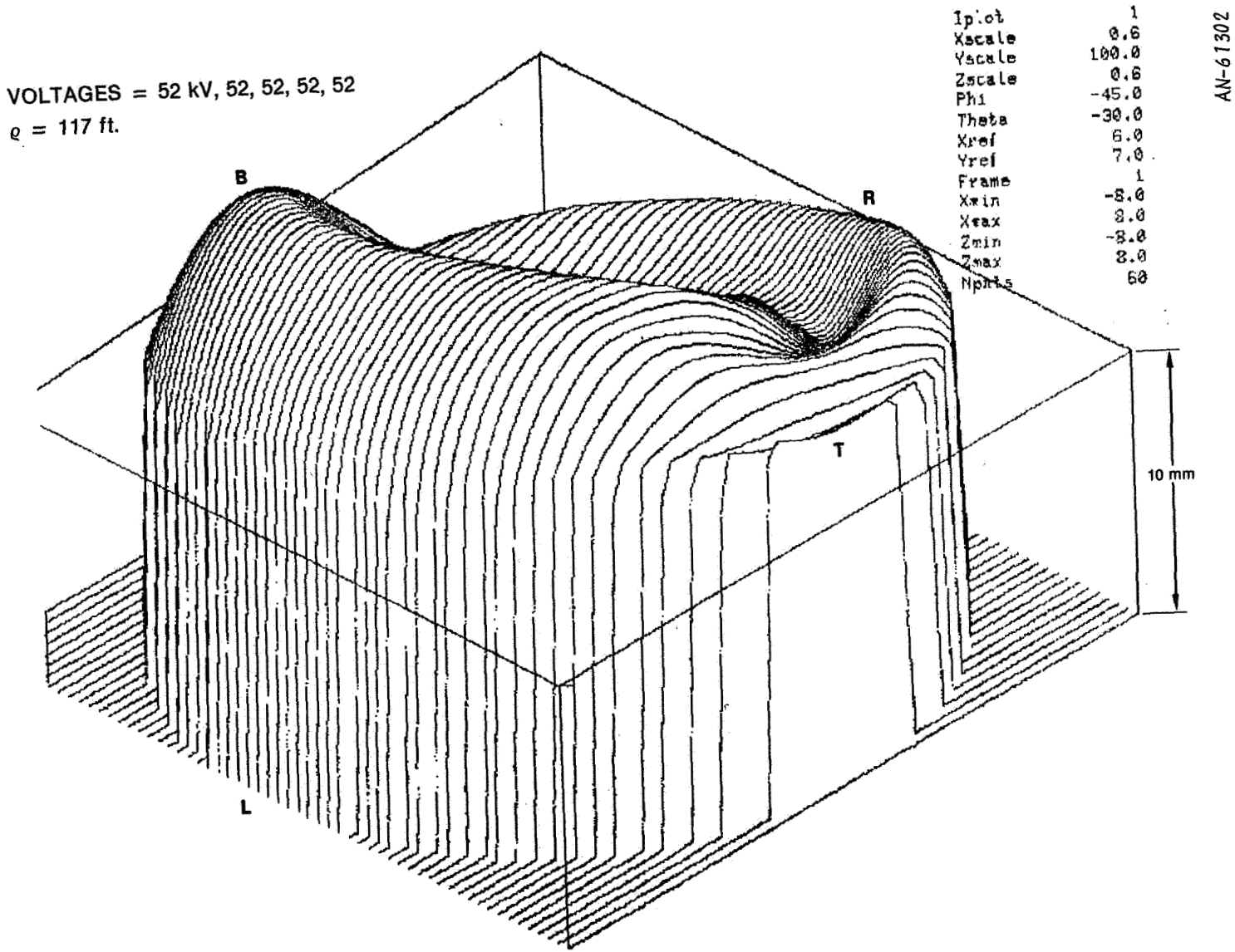

Figure 5.15. 3-D Plot, Test 4-4

In Test 4-5, the distribution of errors is quite similar to that in Test 4-4 despite the considerably different voltages.

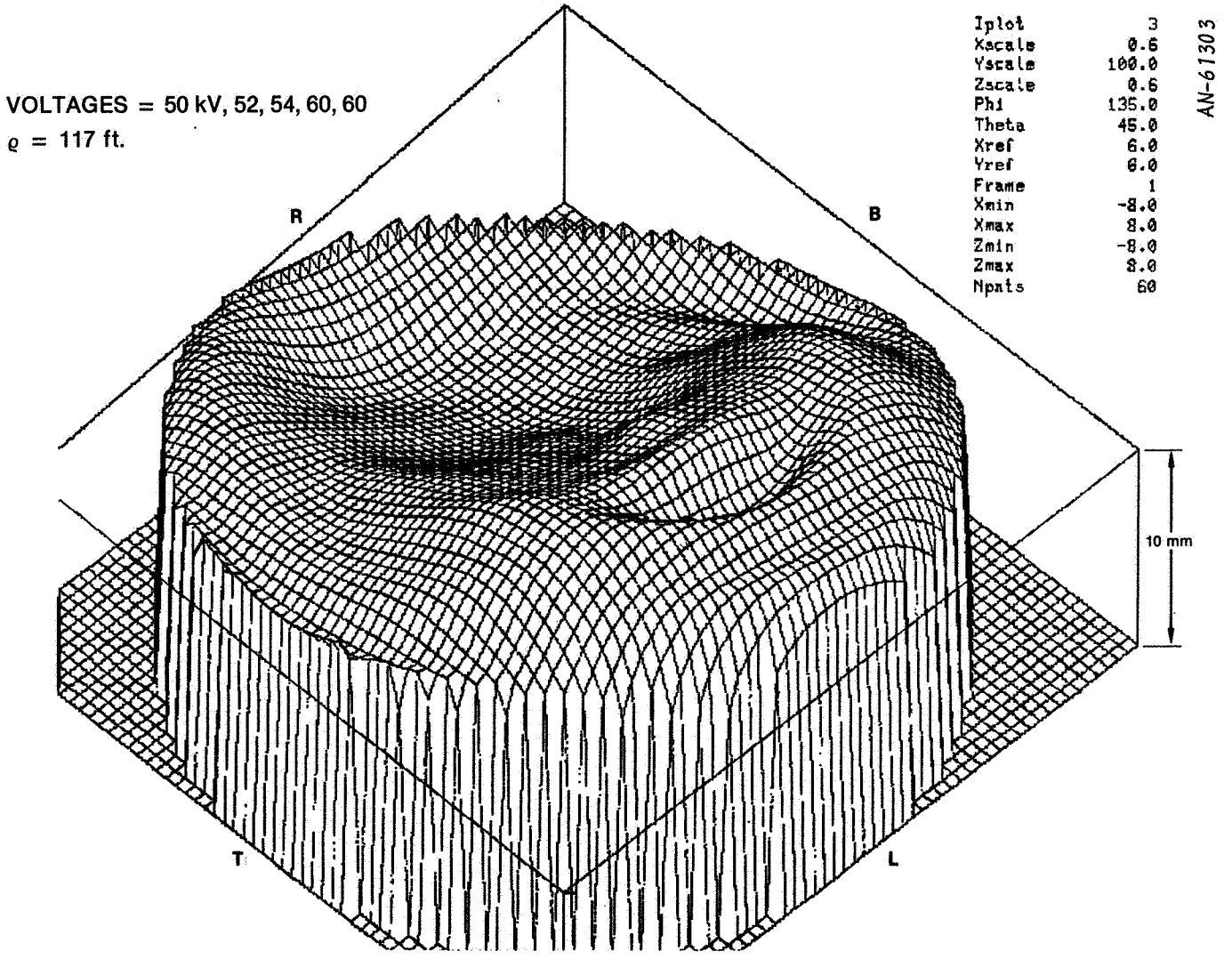

Figure 5.16. 3-D Plot, Test 4-5

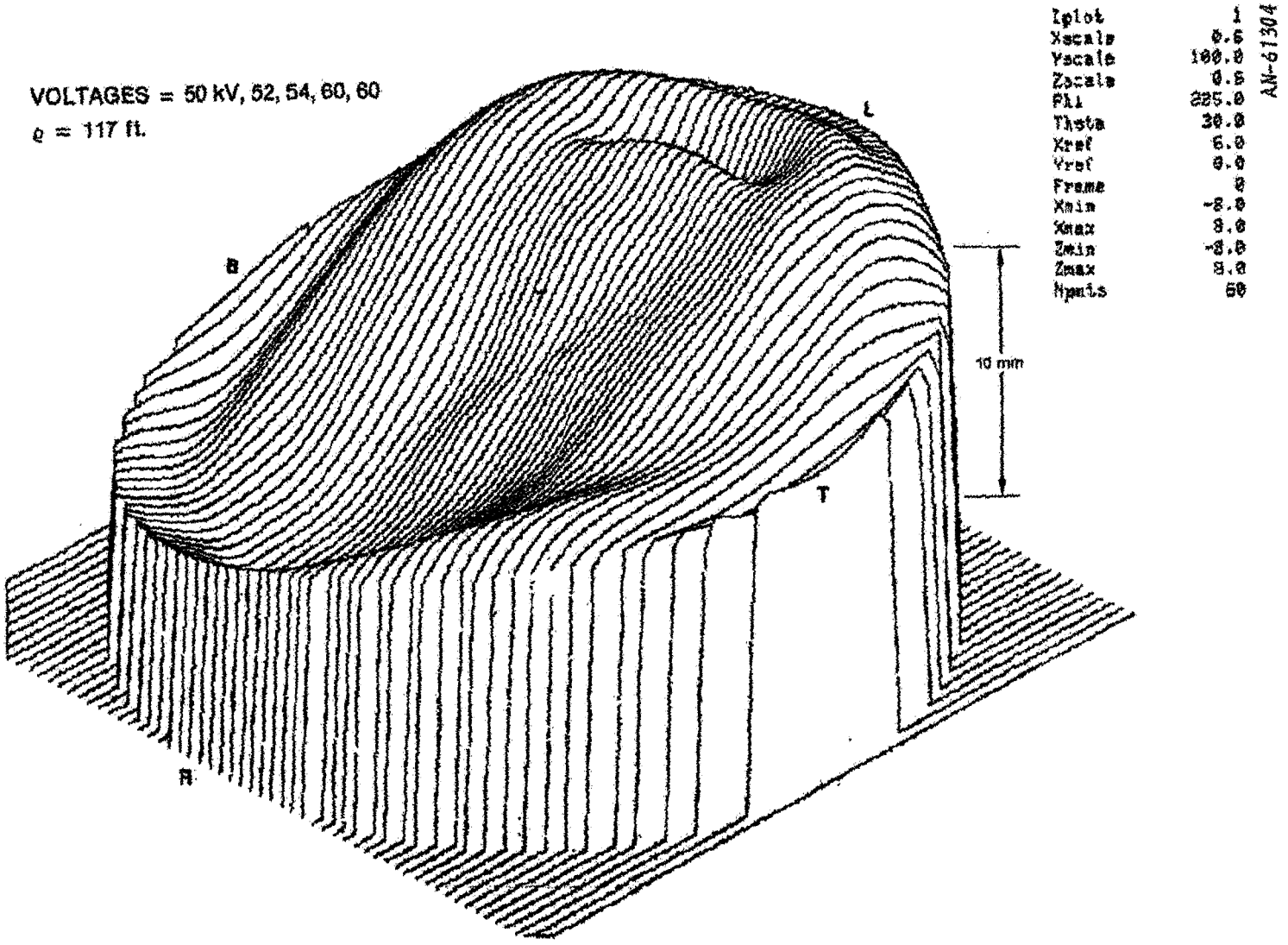

Figure 5.17. 3-D Plot, Test 4-5

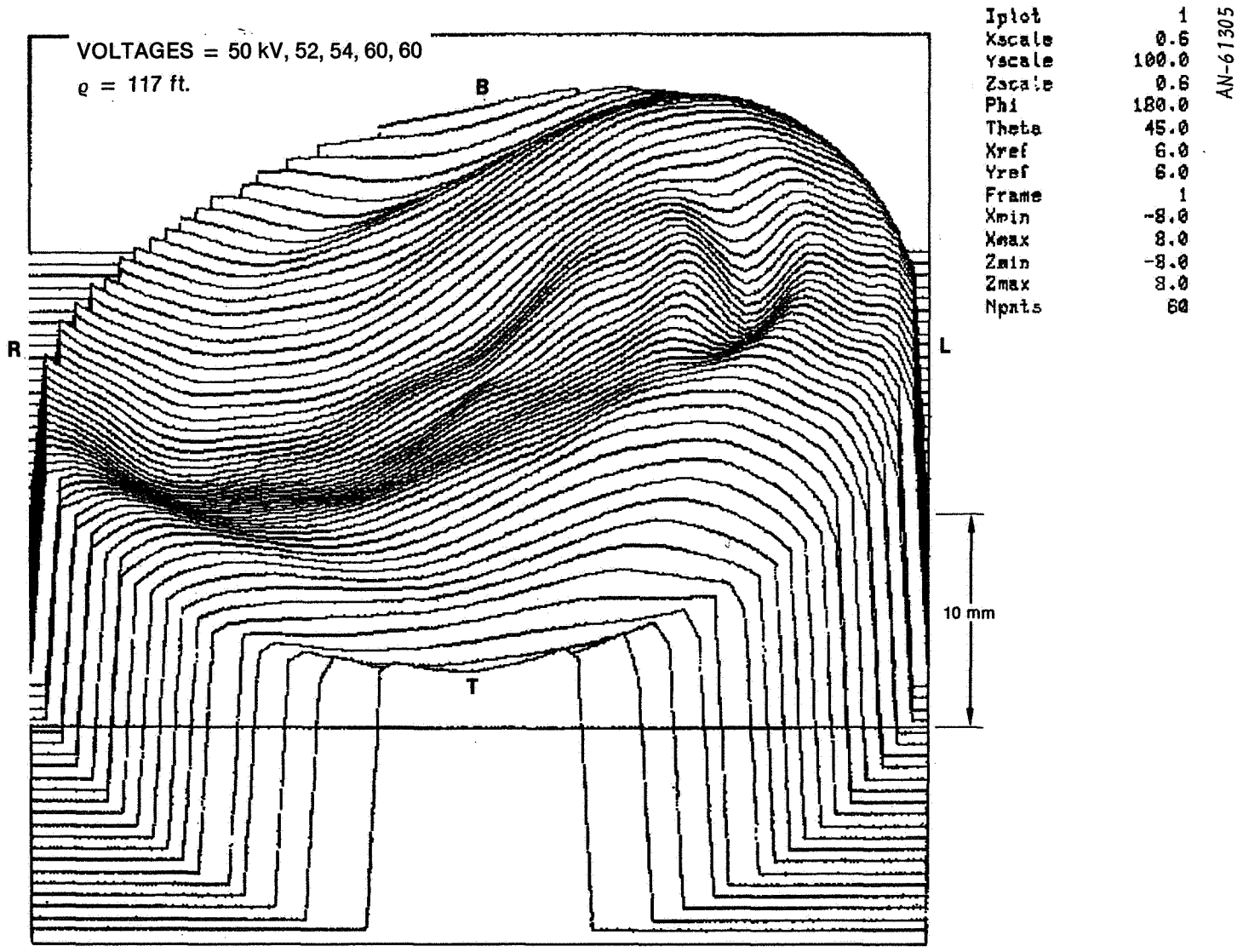

Figure 5.18. 3-D Plot, Test 4-5

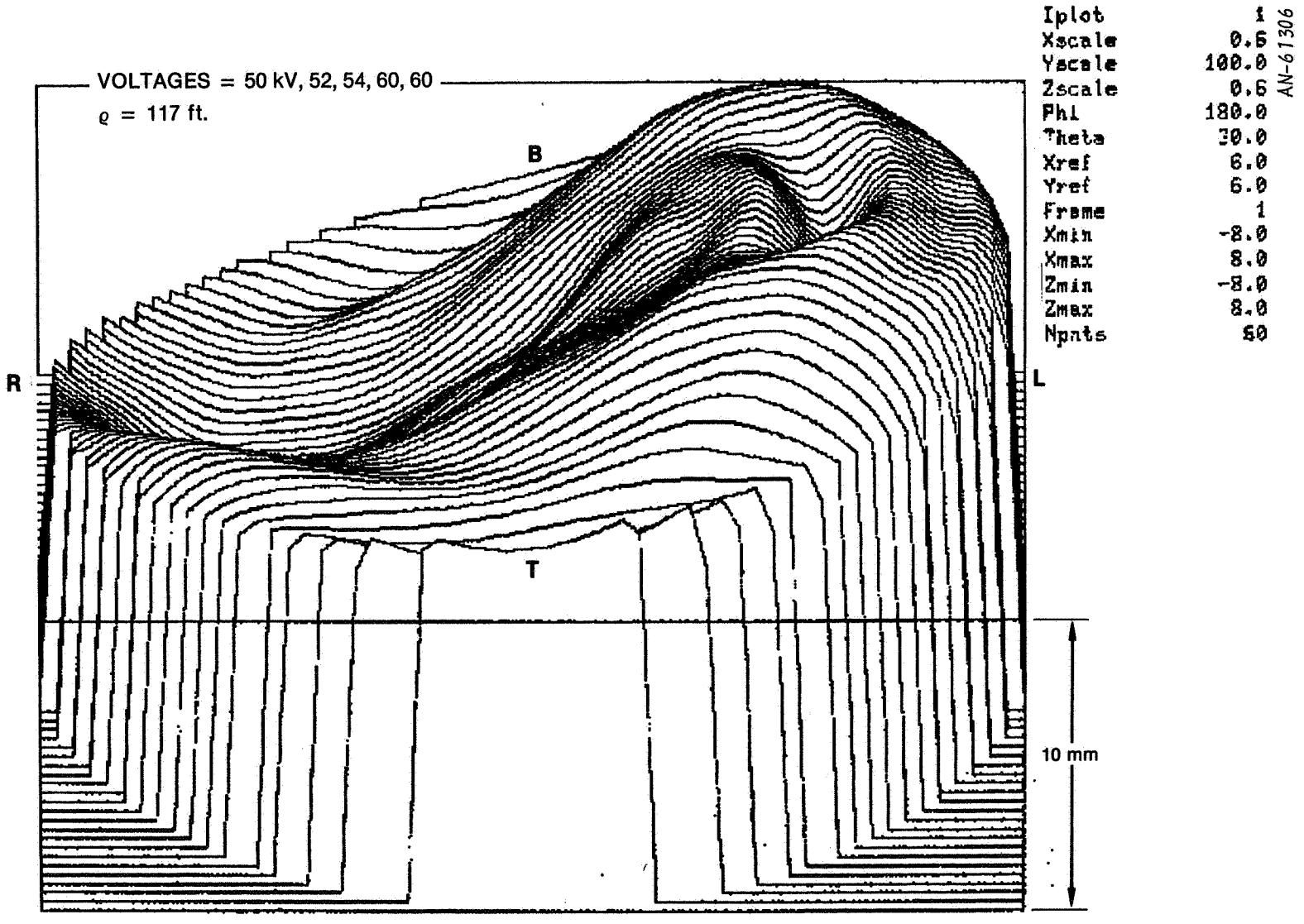

Figure 5.19. 3-D Plot, Test 4-5

This view of the errors is from the top looking directly down the plane of the rim. Errors shown are to scale. The positive error distribution near the left quadrant is approximately 4 mm. It was caused by an approximate $\pm$ 12 mm tilt of the back electrode surface.

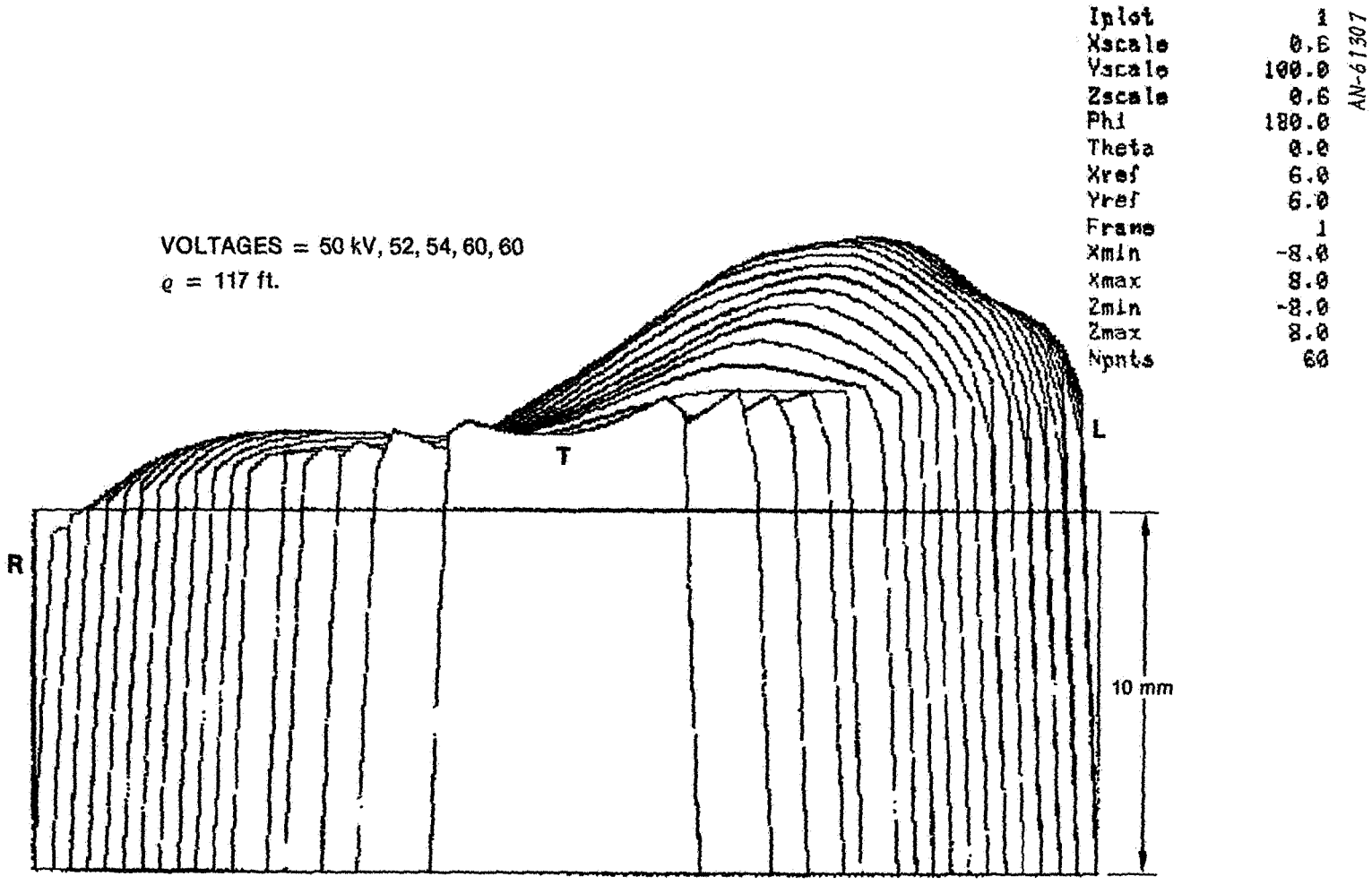

Figure 5.20. 3-D Plot, Test 4-5

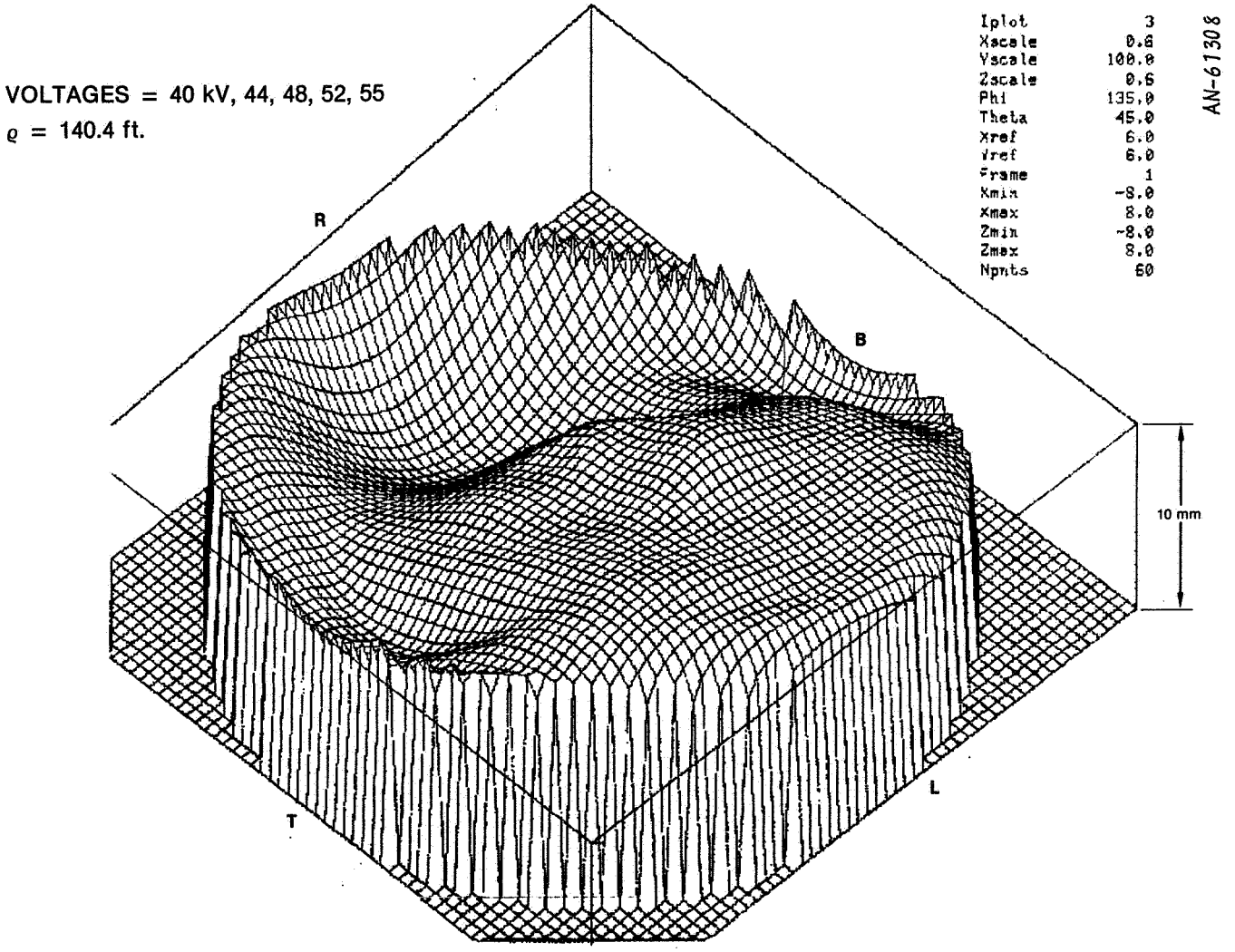

Figure 5.21. 3-D Plot, Test 4-6

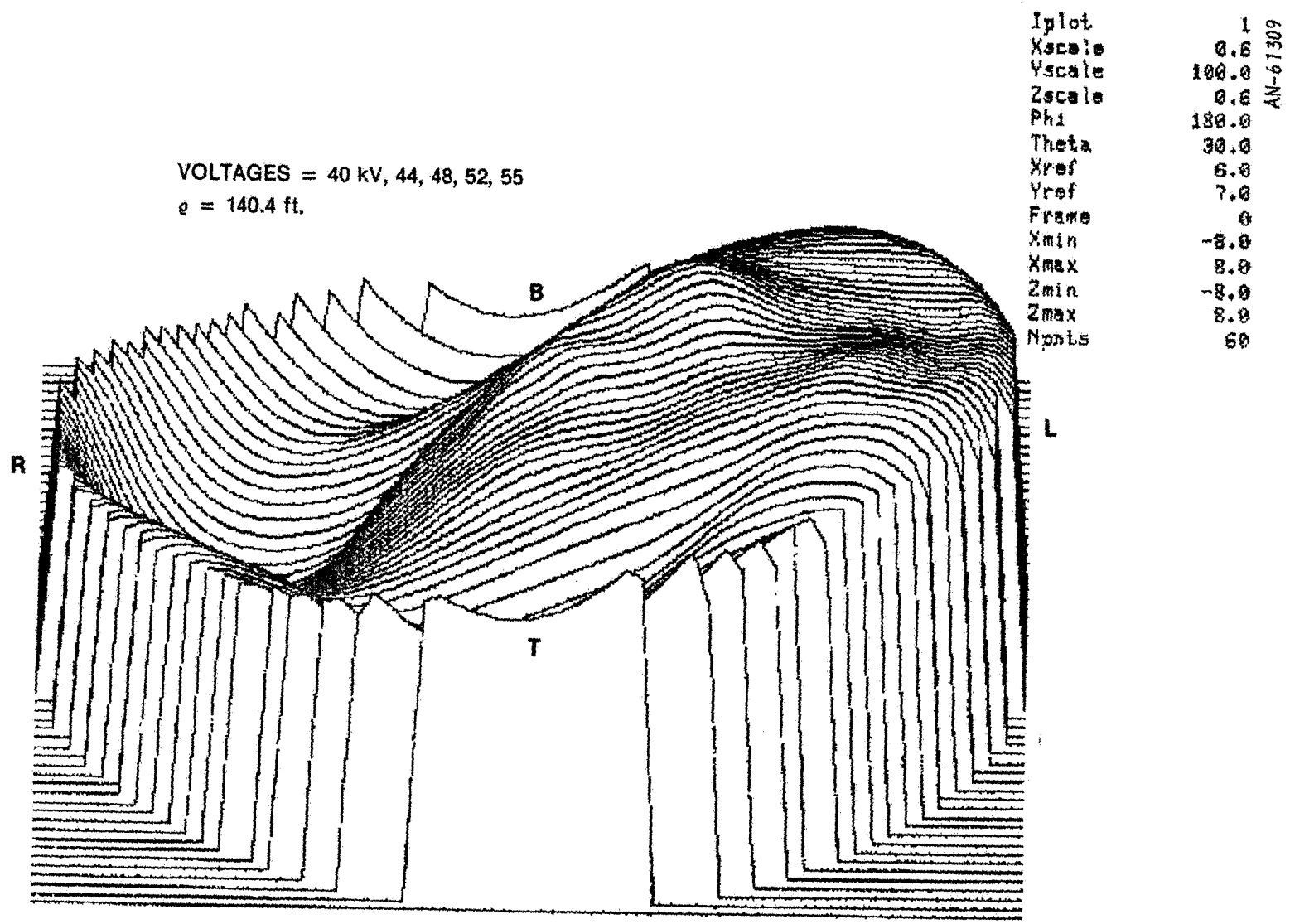

Figure 5.22. 3-D Plot, Test 4-6

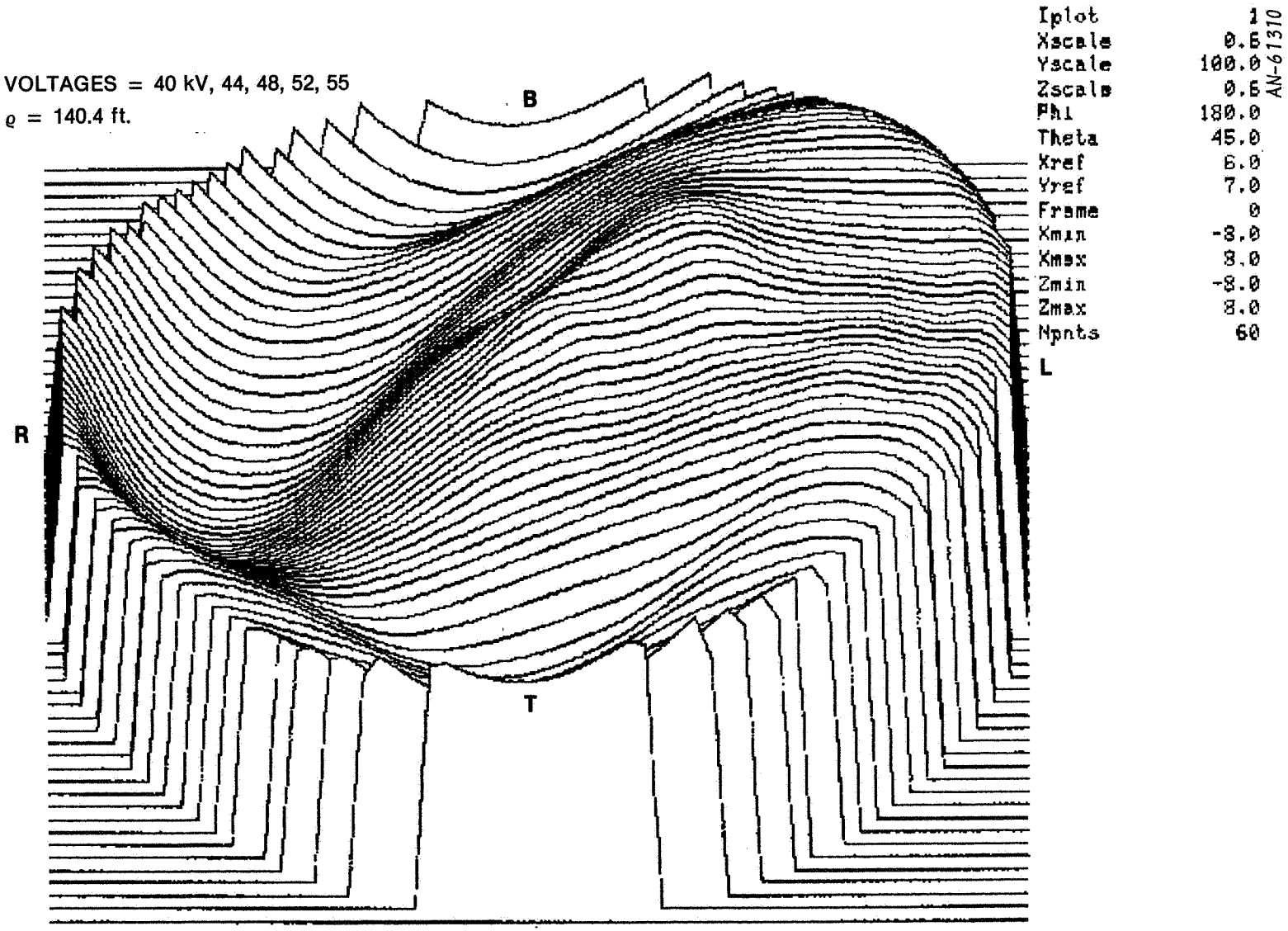

Figure 5.23. 3-D Plot, Test 4-6

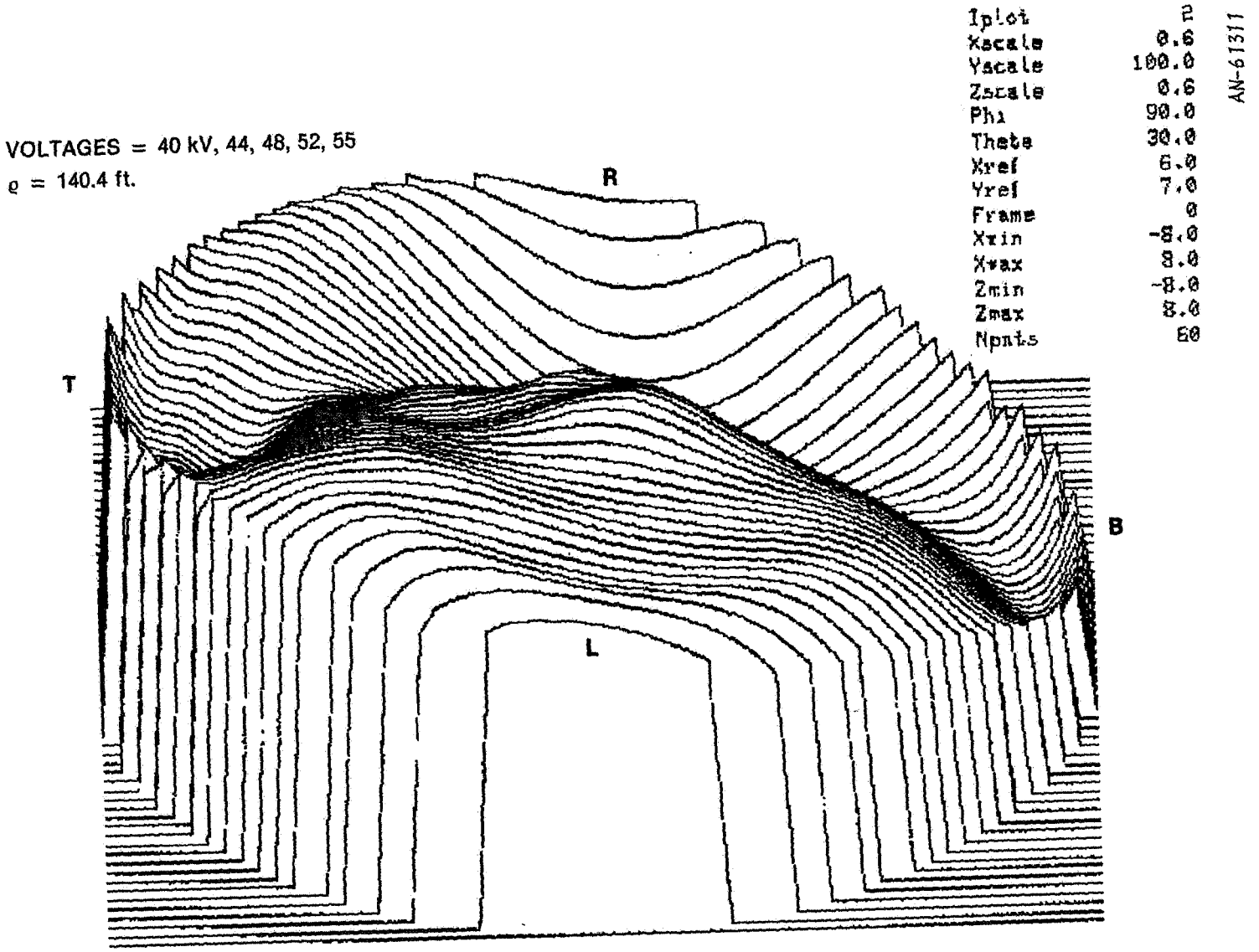

Figure 5.24. 3-D Plot, Test 4-6

This is the final test to be discussed. It was the best of the series that started in October 1980 (i.e., from Test 1-1 through Test 5-1).

The results are an order of magnitude better than Tests 4-1 through 4-3. This test used the same membrane reflector as Tests 4-4 through 4-6, but electrode tilt was removed. Time was not available to perform a 2-D regression analysis of the shape.

Seam errors are not evident. The rim appears quite flat. An excessive deflection appears near the top of the membrane reflector, which may have been caused by a low pre-tension in this area.

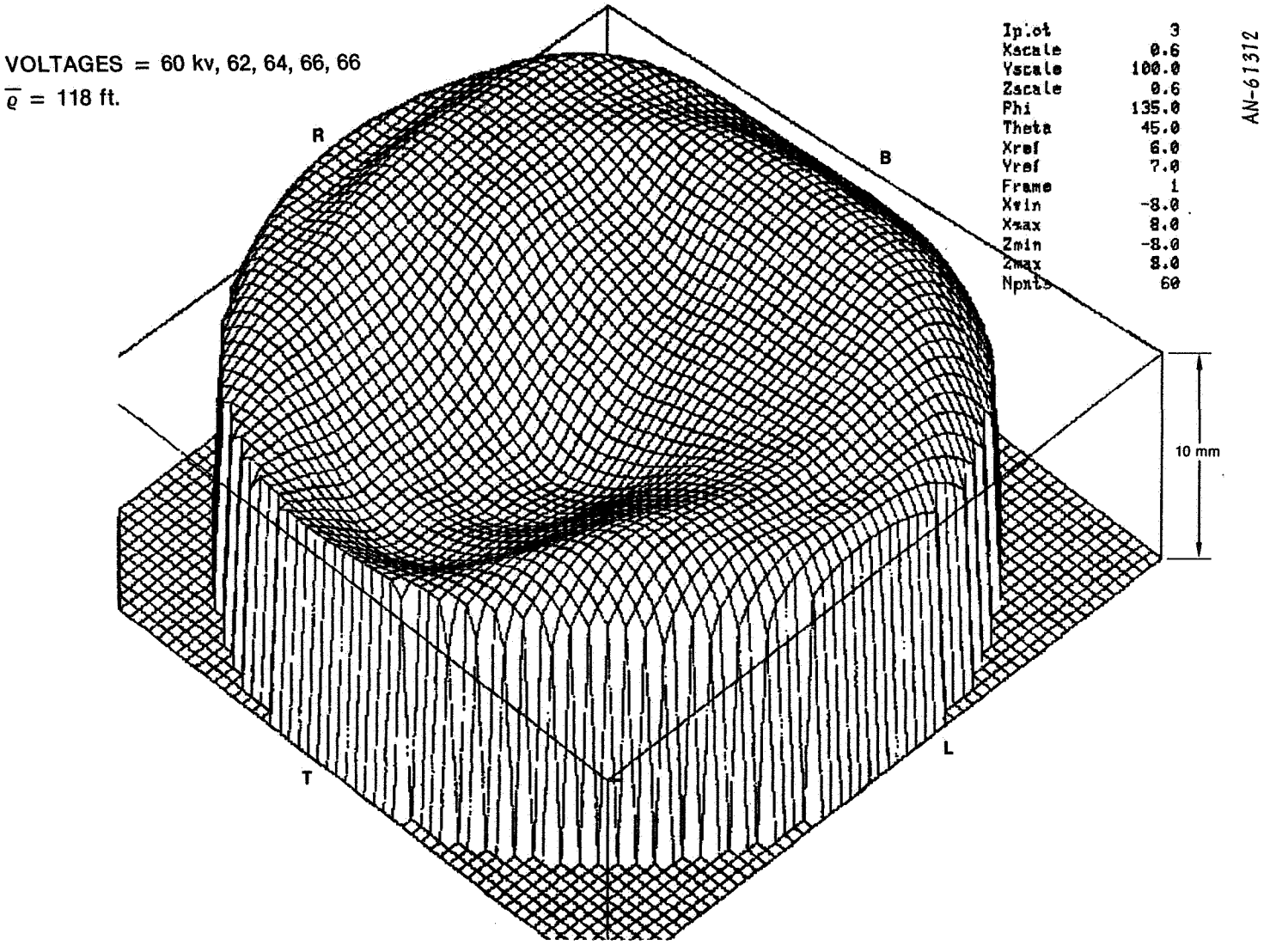

Figure 5.25. 3-D Plot, Test 5-1

From this view, the membrane reflector displays a high level of uniformity over the 4.88 m diameter.

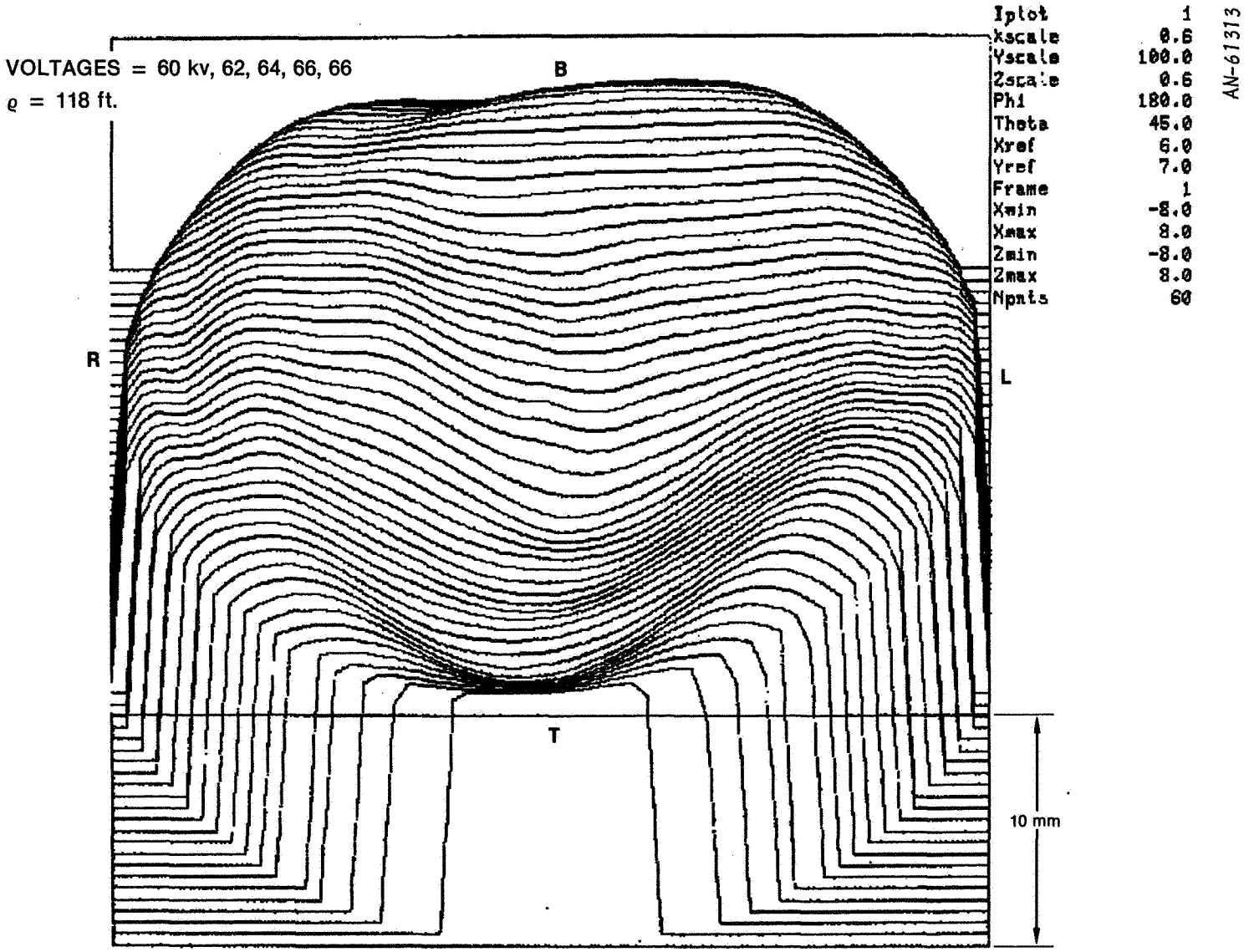

Figure 5.26. 3-D Plot, Test 5-1

The principal errors along the rim are quite symmetric in this edge-on view. Errors are shown to scale. The top straight line represents the zero error plane. It can be seen that the residual errors are principally around the rim. The membrane reflector does not exhibit an adequate deflection near the rim. The pressure and voltage are also inadequate near the rim.

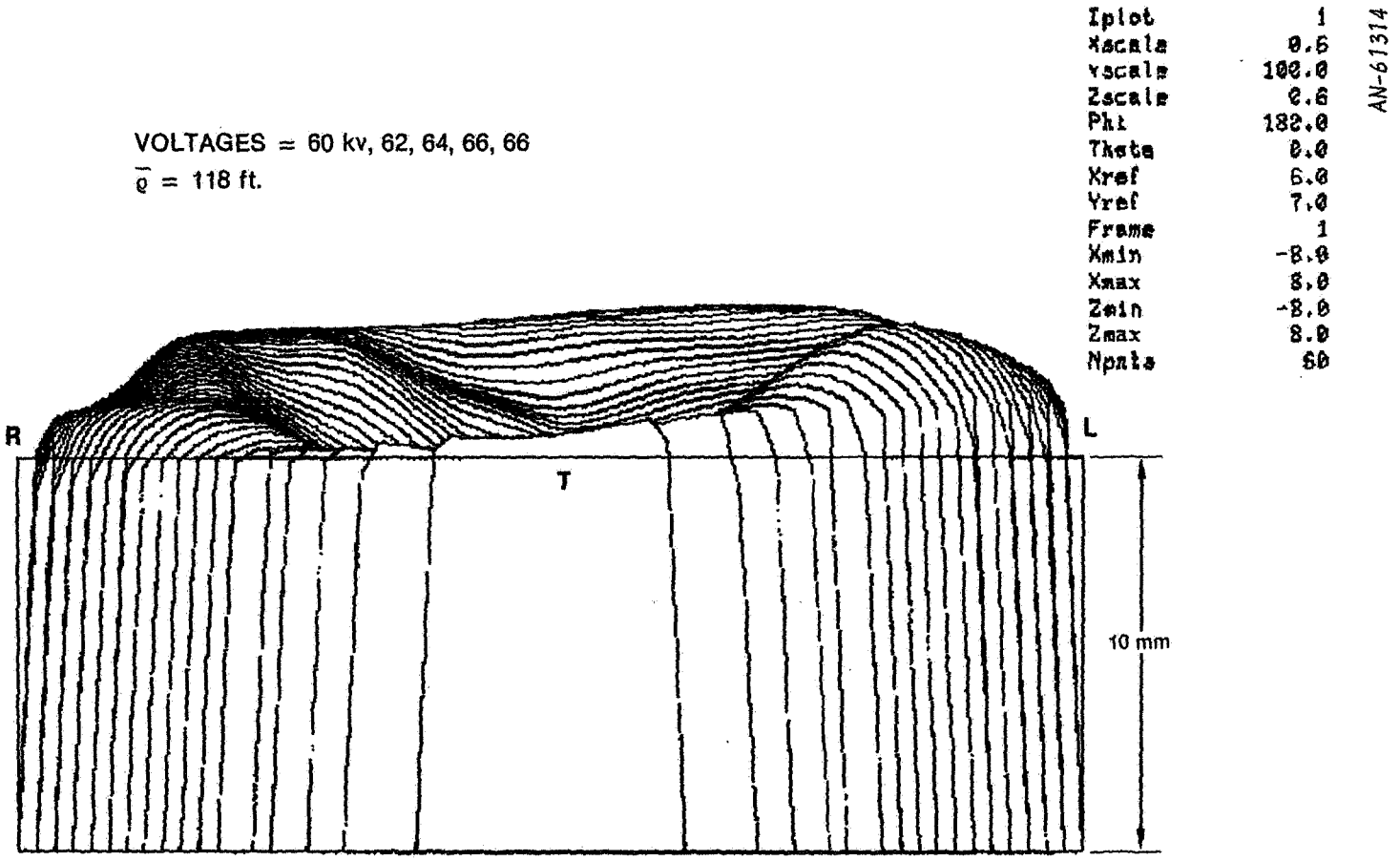

Figure 5.27. 3-D Plot, Test 5-1

1. Report No.	2. Government Accession No.	3. Recipient's Catalog No.
CR-165792		

4. Title and Subtitle	5. Report Date
Test Progress on the Electrostatic Membrane Reflector	June 29, 1981
	6. Performing Organization Code

7. Author(s)	8. Performing Organization Report No.
D. J. Mihora	CR-2-998
	10. Work Unit No.

9. Performing Organization Name and Address	11. Contract or Grant No.
General Research Corporation P.O. Box 6770 Santa Barbara, CA 93111	NAS1-16133
	13. Type of Report and Period Covered
12. Sponsoring Agency Name and Address	Contractor Report
National Aeronautics and Space Administration Langley Research Center Hampton, VA 23665	14. Sponsoring Agency Code NAS 1

15. Supplementary Notes

Langley designer/director of the experimental facility and technical monitor of this reported activity: J. W. Goslee

16. Abstract

An extremely lightweight type of precision reflector antenna is being developed for potential deployment from the Space Shuttle. This innovative antenna uses electrostatic forces to tension a thin membrane and form it into a concave reflector surface. The typical Shuttle-deployed antenna would have a diameter of 100 meters and an RMS surface smoothness of 10 to 1 mm for operation at 1 to 10 GHz. NASA Langley Research Center has built and is currently testing a subscale (16 foot diameter) model of the membrane reflector portion of such an antenna. Preliminary test results and principal factors affecting surface quality are addressed. Factors included are the effect of the perimeter boundary, splicing of the membrane, the long-scale smoothness of commercial membranes, and the spatial controllability of the membrane using voltage adjustments to alter the electrostatic pressure. Only readily available commercial membranes are considered in this test program.

17. Key Words (Suggested by Author(s))		18. Distribution Statement
Membranes	Active Control	Unclassified-Unlimited
Electrostatics	Precision	
Antennas	Structures	
Reflectors	Surface Sensors	

19. Security Classif. (of this report)	20. Security Classif. (of this page)	21. No. of Pages	22. Price
Unclassified	Unclassified	124	

For sale by the National Technical Information Service, Springfield, Virginia 22161